UNIVERSITÀ DEGLI STUDI DI MILANO

FACOLTÀ DI SCIENZE E TECNOLOGIE

Dipartimento di Fisica
Corso di Laurea Magistrale in Fisica

Nuclear energy functionals grounded in ab initio calculations

Relatore:
Prof. Gianluca Colò

Correlatori:
Prof. Xavier Roca-Maza
Prof. Francesco Pederiva

Candidato:
Francesco Marino

Matricola: **939987**

Anno accademico 2019-2020

Summary

Several complementary approaches have been developed to face the very complex nuclear many-body problem. Ab initio methods solve the Schrödinger equation employing realistic nuclear interactions that are fitted to reproduce two- and few-body observables. However, although very powerful and rapidly developing, due to their heavy computational load ab initio methods can currently deal with systems with only a limited number of nucleons. Self-consistent mean field methods based on the concept of nuclear energy density functionals (EDFs), on the other hand, allow to cover the whole nuclear chart with an overall good accuracy. Most of the current EDFs are phenomenological as they are fitted to finite nuclei observables. This constitutes a limitation when the EDFs are applied to systems for which few or no observations are available, such as nuclei close to the drip line, superheavy nuclei or neutron stars.
In order to further improve the predictive power of the EDFs, insights from ab initio nuclear theory can prove useful. In this thesis, inspired by a well-established method in condensed matter Density Functional Theory, we explore the possibility of deriving an EDF from first principle calculations by using the so called Local Density Approximation (LDA).
The method requires as input the equations of state (EoS) of symmetric and neutron matter for a given microscopic nuclear interaction. We have computed the EoS with the $AV4' + UIX_c$ interaction by means of the Auxiliary Field Diffusion Monte Carlo (AFDMC). Then, we have constructed EDFs from the $AV4' + UIX_c$ EoS, as well as from published results of the EoS derived with the $NNLO_{sat}$ interaction by using the Self-consistent Green's function method.
We have tested these EDFs on a set of finite nuclei and compared them with the experiment and with an existing nuclear EDF (SkP). The $NNLO_{sat}$-based EDF yields fair results, given the simplicity of the LDA scheme, especially in heavy nuclei, and thus constitutes a valid starting point for further improvements. On the other hand, in the case of the $AV4' + UIX_c$ potential, the results are much less satisfactory, as the LDA EDF predicts strongly overbound nuclei compared to AFDMC. A possible explanation (not explored in this thesis) is that the very different behaviour in the two cases may be due to the repulsive short-distance nature (hard core) of the $AV4'$ interactions which induces strong correlations in the many-nucleon wave function that cannot be mimicked by the LDA.
Finally, we state that, in order to obtain accurate EDFs, spin-orbit and surface contributions are mandatory and we suggest possible improvements based on ab initio calculations.

Contents

Acronyms **5**

Introduction **6**

1 Mean field methods and energy functionals **8**
1.1 Introduction 8
1.2 The Hartree-Fock method 9
1.3 Nuclear energy density functionals 10

2 Realistic nuclear interactions and ab initio methods **15**
2.1 Introduction 15
2.2 Realistic nuclear interactions 16
2.3 Quantum Monte Carlo 21
2.4 Self-consistent Green's function 27

3 Method **31**
3.1 Motivation 31
3.2 Infinite nuclear matter 33
3.3 Model equations of state 35
3.4 LDA energy functional 37

4 Energy functionals based on $NNLO_{sat}$ **39**
4.1 Introduction 39
4.2 Fitting the equations of state 40
4.3 Results in finite nuclei 44
4.4 Comparing SkP and (2,5,6) 46
4.5 Conclusion 52

5 Energy functionals based on $AV4' + UIX_c$ **53**
5.1 Introduction 53
5.2 Equations of state 54
5.3 Results in finite nuclei 57
5.4 Conclusions 61

6 Conclusions **62**

A Derivation of the Hartree-Fock equations **64**

B Relation to empirical parameters **67**
B.1 Thermodynamics 67
B.2 Calculation of the empirical parameters 68
B.3 From empirical parameters to the model EoS 70

C Mean field and rearrangement energy for the LDA functional **72**
C.1 Derivation of the mean field potential 72
C.2 Rearrangement energy 73
C.3 Test with a $t_0 - t_3$ Skyrme interaction 74

Bibliography **77**

Ringraziamenti **85**

Acronyms

3N Three-nucleon.

AFDMC Auxiliary Field Diffusion Monte Carlo.

DFT Density functional theory.

DMC Diffusion Monte Carlo.

EDF Energy density functional.

EFT Effective field theory.

EoS Equation of state.

g.s. Ground state.

GF Green's function.

GFMC Green's function Monte Carlo.

HEG Homogeneous electron gas.

HF Hartree-Fock.

L(S)DA Local (Spin) Density Approximation.

LEC Low-energy constant.

NM Neutron matter.

NN Nuclon-nucleon.

QCD Quantum chromodynamics.

QMC Quantum Monte Carlo.

s.p. Single-particle.

SCGF Self-consistent Green's function.

SM Symmetric matter.

VMC Variational Monte Carlo.

Introduction

Several complementary approaches have been developed to face the very complex nuclear many-body problem. Ab initio methods solve the many-nucleon Schrödinger equation in an exact or sistematically improvable way by using a realistic model for the nuclear interaction in the vacuum [1, 2]. Although they have witnessed many progresses in recent years, there are still limitations in the number of nucleons that ab initio methods can deal with [2–5]. The mean field methods based on the concept of nuclear energy density functionals (EDFs), on the other hand, allow to cover all the nuclear chart with an overall good accuracy [6, 7]. Besides the study of ground state properties, they are also widely used for the description of nuclear excitations [7–9]. The nuclear EDF approach is closely related to the Density Functional Theory (DFT) of condensed matter physics [10–12].
Most of the current EDFs are phenomenological as they are fitted to observable quantities, such as the radii and binding energies of a set of nuclei, or also to nuclear matter pseudo-observables, such as the saturation density and the saturation energy [13, 14]. This pragmatic approach has proved in general quite successful, but its dependence on empirical data, as well the absence of a guiding principle for systematically developing more accurate functionals, constitute a limitation to the reliability of EDFs for systems for which few or no observation are available, such as neutron stars, superheavy nuclei or nuclei close to the neutron drip lines [7, 15]. In order to further improve the nuclear EDFs, insights from ab initio theory can prove useful [15].
In condensed matter DFT, there exists a well-established methodology to construct EDFs based on first principles calculations of the homogeneous electron gas (HEG) [10]. This "reductionist" approach, pursued mostly by Perdew and collaborators [11, 16], aims at constructing a "ladder" of ever more accurate EDFs, relying as little as possible on fits to empirical quantities. Its main advantage over an "empiricist" approach is that the "ab initio" EDFs guarantee a more uniform accuracy in a wide range of systems [16]. The simplest EDFs are built using the so-called Local Density Approximation (LDA), which is then complemented by the introduction of gradient or surface terms.
The availability of ab initio equations of state (EoS) of infinite nuclear matter suggests that a similar approach may be explored in nuclear physics too [17, 18], although one must keep in mind that the nuclear EoS is still only partially known, as the results depend on the specific nuclear interaction and, to some extent, on the employed many-body method [19–22].
In this thesis, we construct and test LDA EDFs grounded in two different EoS, based on two different microscopic interactions and many-body methods: the $NNLO_{sat}$ chiral potential with the Self-consistent Green's function (SCGF) method [20, 23], and the phenomenological Argonne 4 nucleon-nucleon interaction plus the central part of the Urbana IX three-body potential ($AV4' + UIX_c$) with the Auxiliary Field Diffusion Monte Carlo (AFDMC) method [3, 24]. From the one hand, $NNLO_{sat}$ is the state of the art interaction for finite nuclei calculations, while at the same time it predicts an infinite matter

saturation point compatible with the empirical constraints [23, 25]. On the other hand, the $AV4' + UIX_c$ potential is a very simple interaction that, in spite of its simplicity, provides fair results in finite nuclei [24]. It is therefore interesting to test it in infinite matter too; also, its reduced computational weight allows to cover with the AFDMC method a wider range of densities than what is possible with more complicated interactions, in both neutron matter and in the more difficult (for AFDMC) symmetric matter.
The thesis is structured as follows. Chapter 1 introduces the nuclear mean field methods based on the EDF concept. Chapter 2 gives an overview of ab initio theory, with a focus on presenting the modern realistic interactions and on the principles of the SCGF and AFDMC methods. Chapter 3 describes the method followed to construct an EDF from a theoretical EoS by using the Local Density Approximation. This methodology is applied in Chapter 4, devoted to an analysis of the EDF based on the $NNLO_{sat}$ EoS, and in Chapter 5, in which we present a set of AFDMC results for the $AV4' + UIX_c$ interaction and then discuss the resulting EDF. Chapter 6 summarizes the work and suggests possible developments.

Chapter 1

Mean field methods and nuclear energy density functionals

Self-consistent mean field methods have enjoyed a great success in nuclear theory as they are the only class of methods that allows to cover the whole nuclear chart with good accuracy [7, 13, 15]. The physical picture behind mean field methods is that each nucleon can be thought of as an independent particle moving in an effective average potential generated by the interactions between all the other nucleons. In this Chapter, we focus on self-consistent methods based on the solution of Hartree-Fock (HF) equations. In Sec. 1.1, the general aspects of mean field methods are outlined. Then, Sec. 1.2 introduces the Hartree-Fock method. The subject of Sec. 1.3 is, after an introduction to Skyrme interactions, a discussion of the concept of local nuclear EDFs.

1.1 Introduction

The complexity of the nuclear many-body problem cannot be tamed by a single method alone and indeed over the decades several different approaches have been developed, each with its own strengths and weaknesses. Ab initio nuclear theory, for example, which is presented in Chapter 2, follows a microscopic approach, with the aim of solving the many-nucleon Schrödinger equation directly from the nuclear forces that govern the dynamics of the nucleons in the vacuum [2]. As the nuclear interaction has a rather complicated structure, such task is even more difficult than the corresponding one in the physics of electronic systems. The necessity to develop sophisticated methods to deal with the strongly correlated nuclear systems, as well as the very large computational resources required, have made the ab initio program viable only in relatively recent times. Nowadays, much work is devoted to first principle calculations and many successes have been obtained, although still only systems with a limited number of nucleons are within reach of ab initio methods.

A complementary approach is provided by mean field methods, such as the self-consistent mean field methods [6, 7, 13] described in this Chapter and the non-interacting shell model [26]. These methods are based on a single-particle description of the nucleus, where each nucleon is treated as an independent particle moving in an average potential. In the shell model a simple standard potential is used, while in self-consistent models the mean field is determined in an iterative, unprejudiced way, through the solution of the Hartree-Fock (HF) or, for open shell nuclei, the Hartree-Fock-Bogoliubov (HFB) equations [26]. The latter have the attractive feature that they are the only method able to cover the whole

nuclear chart with a good accuracy [27]. The key to the success of self-consistent mean field methods is the use of phenomenological, density-dependent interactions fitted on finite nuclei observables. These potential leave aside a strict connection with the bare nuclear interaction and must be instead thought of as effective interaction in the medium. Gradually, mean field methods have evolved into a framework close to that of the Density Functional Theory (DFT) [12] that is so successful in electronic systems, and the central problem has become the construction of accurate nuclear energy functionals (EDF), which are directly parametrized on nuclear observables without referring to an interaction potential.

1.2 The Hartree-Fock method

The core of the Hartree-Fock (HF) method lies in the independent-particle picture: one assumes that each particle of a system of A fermions can be described as an independent particle moving in an average potential generated by the interactions with all the other $A-1$ fermions. In nuclear physics, the success of the shell model in explaining qualitatively several properties of the nuclei suggests that an average potential does exist [26]. In the HF method, one starts from an interacting two-body (and eventually three-body) Hamiltonian from which the s.p. potential, or mean field, is derived self-consistently.
The starting point consists in considering an interacting system of A particles with Hamiltonian $H = T + V$, with V a two-body interaction, and assuming that the ground state can be approximated by a Slater determinant:

$$|HF\rangle = |\Phi(1...A)\rangle = \prod_{k=1}^{A} c_k^\dagger |0\rangle \tag{1.2.1}$$

where $|0\rangle$ is the vacuum state and $c_k^\dagger$ is the creation operator for an eigenstate k of the single-particle Hamiltonian h. The variational principle implies that the expectation value of H on the $|HF\rangle$ state:

$$E^{HF} = \langle HF| H |HF\rangle \tag{1.2.2}$$

is an upper limit to the true ground state energy of H. Then E^{HF} is minimized in order to determine a set of equations that define the s.p. Hamiltonian h and the s.p. orbitals $\phi_k(i)$. In coordinate space, the s.p. wave functions, $\phi_k(i) = \langle \mathbf{r}_i s_i t_i | k \rangle$, where s_i is the spin projection and t_i is equal to $\frac{1}{2}$ for neutrons and to $-\frac{1}{2}$ for protons, satisfy:

$$h(i)\phi_k(i) = \epsilon_k \phi_k(i) \qquad i = (\mathbf{r}_i, s_i, t_i) \tag{1.2.3}$$

The average one-body Hamiltonian is given by $H^{HF} = \sum_{i=1}^{A} h(i)$. The derivation roughly follows that of Ref. [26] and is also reported in detail in App. A.
In second quantization, the Hamiltonian operator looks like:

$$H = T + V = \sum_{12} t_{12} c_1^\dagger c_2 + \frac{1}{4} \sum_{1234} \bar{v}_{12,34} c_1^\dagger c_2^\dagger c_4 c_3 \tag{1.2.4}$$

where $t_{12} = \langle a| t |2\rangle$ and $\bar{v}_{12,34} = \langle 12| v |34\rangle - \langle 12| v |43\rangle$ are the antisymmetrized matrix elements of the potential. The sums are extended over a generic basis of single-particle states. It is useful to introduce the density matrix $\rho_{12} = \langle HF| c_2^\dagger c_1 |HF\rangle$. We assume in general that V is a density-dependent potential $V = V[\rho]$. Indeed, three-nucleon

interactions can be modelled in this way [28]. By requiring the vanishing of the variation of $\delta E^{HF}[\rho]$, one finds that the s.p. Hamiltonian is given by:

$$h_{ij} = \frac{\partial E^{HF}[\rho]}{\partial \rho_{ji}} = t_{ij} + \sum_{12} \bar{v}_{i1,j2}\rho_{21} + \langle HF| \frac{\delta v}{\delta \rho_{ji}} |HF\rangle \tag{1.2.5}$$

The eigenvalue equation 1.2.3 for the orbitals is solved in coordinate space or in a basis of harmonic oscillator or Woods-Saxon wave functions [26]. Its structure reminds the single particle Schrödinger equation, but is more involved, as the Hamiltonian h depends on the density, which itself is determined by the solution of the same equations. As a consequence, the HF equations must be solved with an iterative procedure: one starts from an Hamiltonian with a known potential, for example the Woods-Saxon, solves the resulting equation, then plugs the orbitals inside the definition of h and solves the new equations, and so on until the convergence is reached. Also, one should be aware that the eigenfunctions ϕ_k and eigenvalues ϵ_k, do not have a physical meaning per se, although they can be used to construct observable quantities. The only exception is the highest eigenvalue in a finite system, which is equal to minus the nucleon separation energy, or the ionization energy in electronic systems [10]. At the end of the procedure, the total energy is easily computed with the following formula:

$$E = \frac{1}{2}\left(T + \sum_k \epsilon_k\right) + E_{rea} \tag{1.2.6}$$

where E_{rea} is called rearrangement energy:

$$E_{rea} = -\frac{1}{2}\sum_{ij} \langle HF| \frac{\delta v}{\delta \rho_{ji}} |HF\rangle \rho_{ij} \tag{1.2.7}$$

E_{rea} is non-vanishing only for density-dependent potentials. See also App. A.

1.3 Nuclear energy density functionals

The choice of the two-body interaction $V[\rho]$ is critical to the success of mean field calculations. In nuclear physics, the Hartree-Fock method became widespread when the connection to the bare interactions in the vacuum was abandoned and *phenomenological* interactions tailored for the use in these methods were introduced: in a pioneering work [28], Brink and Vautherin interpreted the Skyrme interaction, that had been initially proposed as a model of the nuclear interactions in the vacuum, as an effective in-medium potential and parametrized it directly on observables of finite nuclei. The Skyrme interaction is a density-dependent zero-range potential, mimicking the short-range character of the nuclear force, and contains spin-, isospin- and momentum-dependent terms. It reads [6]:

$$\begin{aligned} V(\mathbf{r}_1,\mathbf{r}_2) = t_0\left(1+x_0P_\sigma\right)\delta(\mathbf{r}) + \frac{t_1}{2}\left(1+x_1P_\sigma\right)\left[\mathbf{k}^{\dagger 2}\delta(\mathbf{r}) + \delta(\mathbf{r})\mathbf{k}^2\right] + t_2\left(1+x_2P_\sigma\right)\mathbf{k}^\dagger\delta(\mathbf{r})\mathbf{k} + \\ + \frac{t_3}{6}\left(1+x_3P_\sigma\right)\left[\rho(\mathbf{R})\right]^\alpha\delta(\mathbf{r}) + iW_0\,\sigma\cdot\left[\mathbf{k}^\dagger\times\delta(\mathbf{r})\mathbf{k}\right] \end{aligned} \tag{1.3.1}$$

P_σ is the spin-exchange term $\frac{1}{2}(1+\sigma_1\cdot\sigma_2)$, $\mathbf{r}=\mathbf{r}_1-\mathbf{r}_2$, $\mathbf{R}=\frac{\mathbf{r}_1+\mathbf{r}_2}{2}$, $\mathbf{k}=-\frac{i}{2}(\nabla_1-\nabla_2)$ is the relative momentum operator and $\sigma=\sigma_1+\sigma_2$ is the total spin. It has 10 parameters

(including α).
Other effective interactions, based on different Ansätze, have been introduced, such as the finite-range Gogny potential and the relativistic mean field models [6]. All share, though, the two following fundamental properties. First, they are phenomenological interactions: they contain a set of free parameters that are fitted on observable quantities of infinite or semi-infinite matter and finite nuclei, for example the saturation point of infinite matter and the binding energies and radii of a few selected magic nuclei [13]; once they have been parametrized, they can be used in mean field calculations all over the nuclear chart. Second, it has proved necessary for their success that such interactions include density-dependent terms [7]. However, a density-dependent Hamiltonian $H[\rho]$ poses conceptual problems, unless one considers it merely as a tool to generate the energy expectation value [13]:

$$E[\rho] = \langle HF| H[\rho] |HF\rangle \tag{1.3.2}$$

The total energy is a functional of the density and is a well-behaved object, whose minimization can be safely carried out. $E[\rho]$ is called the nuclear *energy-density functional* (EDF). The Skyrme interaction, due to the delta function entering its definition, leads to energy functionals that can be written as the space integral of an energy density, $E = \int d\mathbf{r}\, \mathcal{E}(\mathbf{r})$ [1]. The original Skyrme functional for even-even nuclei is for example [28]:

$$\begin{aligned}\mathcal{E}_{pot}(\mathbf{r}) = \frac{t_0}{2}\left[\left(1+\frac{x_0}{2}\right)\rho^2 - (x_0+\frac{1}{2})(\rho_n^2+\rho_p^2)\right] + \frac{1}{4}(t_1+t_2)\rho\tau + \frac{1}{8}(t_2-t_1)(\rho_n\tau_n+\rho_p\tau_p) + \\ \frac{1}{16}(t_2-3t_1)\rho\Delta\rho + \frac{1}{32}(3t_1+t_2)(\rho_n\Delta\rho_n+\rho_p\Delta\rho_p) + \frac{1}{16}(t_1-t_2)(\mathbf{J}_n^2+\mathbf{J}_p^2) + \frac{1}{4}t_3\rho_n\rho_p\rho \\ -\frac{W_0}{2}\left(\rho\nabla\cdot\mathbf{J} + \rho_n\nabla\cdot\mathbf{J}_n + \rho_p\nabla\cdot\mathbf{J}_p\right)\end{aligned} \tag{1.3.3}$$

ρ_q, τ_q and $\mathbf{J}_q$ are called respectively number density, kinetic energy density and spin-orbit density and will be better described below.

The central role played by the EDF has progressively led to directly propose new energy functionals, without resorting to an underlying interaction $V[\rho]$ [7]. This shift has made nuclear mean field methods close to the spirit of the Density Functional Theory (DFT), originally proposed for electronic systems [12].
The general structure of a nuclear energy functional is the following [13]:

$$E = E_{kin} + E_{pot} + E_{Coul} + E_{pair} \tag{1.3.4}$$

It is given by the sum of kinetic, potential, Coulomb and pairing terms. E_{kin} is the kinetic energy of a system of independent particles:

$$E_{kin} = \int d\mathbf{r}\, \mathcal{E}_{kin}(\mathbf{r}) = \int d\mathbf{r}\, \frac{\hbar^2}{2m}\tau(\mathbf{r}) \tag{1.3.5}$$

The Coulomb energy can be written as the sum of direct and exchange terms, $E_{Coul} = E_{dir} + E_{ex}$. The direct or Hartree term is a functional of the local densities alone and is treated exactly. On the other hand, since the Coulomb potential has a finite range, the exchange term is a functional of the non-local densities. In Skyrme and other local

[1] Skyrme functionals are (quasi) local functionals [13]

functionals, E_{Coul} is often treated in Slater approximation [13]:

$$\begin{aligned} E_{dir} &= \frac{e^2}{2}\int d\mathbf{r}\int d\mathbf{r}'\,\frac{\rho_p(\mathbf{r})\rho_p(\mathbf{r}')}{|\mathbf{r}-\mathbf{r}'|} \\ E_{ex} &= -\frac{3e^2}{4}\left(\frac{3}{\pi}\right)^{1/3}\int d\mathbf{r}\,\rho_p^{4/3}(\mathbf{r}) \end{aligned} \tag{1.3.6}$$

In the so-called local EDFs, the potential energy term depend on the densities evaluated at the same point $\mathbf{r}$ and thus can be expressed as the integral of an energy density:

$$E_{pot}[\rho] = \int d\mathbf{r}\,\mathcal{E}_{pot}(\mathbf{r}) \tag{1.3.7}$$

Skyrme functionals are a prominent example of local EDFs, but several models that go beyond the original EDF have been developed [13]. Indeed, the most general local functional $\mathcal{E}_{pot}$ is a combination of all possible local densities, which can be built in a systematic way from the full density matrix $\rho(\mathbf{r},s,t;\mathbf{r}',s',t')$ and its derivatives [7, 13], that satisfies Galilean, parity and time-reversal invariances. In most cases, one also requires that it be made of terms bilinear in the densities and that contain a limited number of gradient operators, in general up to two [13, 29] [2].
From the full density operator $\rho(\mathbf{r},s,t;\mathbf{r}',s',t')$, six densities and currents for protons and neutrons each ($q=p,n$) can be determined up to second order in the derivatives [6]: number density $\rho_q(\mathbf{r})$, spin density $\mathbf{s}(\mathbf{r})$, number current $\mathbf{j}_q(\mathbf{r})$, spin-current tensor $\mathcal{J}(\mathbf{r})$, kinetic density $\tau_q(\mathbf{r})$ and kinetic spin density $\mathbf{T}_q(\mathbf{r})$. The spin-current tensor is usually approximated by the spin orbit current, to which it reduces in spherically symmetric nuclei:

$$\mathbf{J}_i = \sum_{jk}\epsilon_{ijk}\mathcal{J}_{jk} \tag{1.3.8}$$

Neutron and proton densities are often recoupled into the isoscalar ($t=0$) and isovector ($t=1$) channels: isoscalar densities are total densities (e.g. $\rho_0=\rho_n+\rho_p$), while isovector densities account for proton-neutron differences (e.g. $\rho_1=\rho_n-\rho_p$) [6]. The potential term $\mathcal{E}_{pot}$ reads:

$$\mathcal{E}_{pot}(\mathbf{r}) = \sum_{t=0,1}\left(\mathcal{E}_t^{even}(\mathbf{r})+\mathcal{E}_t^{odd}(\mathbf{r})\right) \tag{1.3.9}$$

where $t=0,1$ label the isoscalar and isovector terms respectively, $\mathcal{E}_t^{even}$ contains only time-even densities and $\mathcal{E}_t^{odd}$ only time-odd time densities. The time-even EDF is given by:

$$\mathcal{E}_t^{even} = C_t^{\rho}\rho_t^2 + C_t^{\Delta\rho}\rho_t\Delta\rho_t + C_t^{\tau}\rho_t\tau_t + C_t^{J}\mathbf{J}^2 + C_t^{\nabla J}\rho_t\nabla\cdot\mathbf{J}_t \tag{1.3.10}$$

while the time-odd energy density reads:

$$\mathcal{E}_t^{odd} = C_t^{s}\mathbf{s}_t^2 + C_t^{\Delta s}\mathbf{s}_t\cdot\Delta\mathbf{s}_t + C_t^{sT}\mathbf{s}_t\cdot\mathbf{T}_t + C_t^{\nabla s}\left(\nabla\cdot\mathbf{s}_t\right)^2 + C_t^{j}\mathbf{j}_t^2 + C_t^{\nabla j}\,\mathbf{s}_t\cdot\nabla\times\mathbf{j}_t \tag{1.3.11}$$

The coefficients cannot be determined by symmetry arguments and in principle may all depend on the densities, but in most applications, only the C_t^{ρ} and C_t^{s} have a density-dependence, often in the form $C_t^{\rho}=a+b\rho^{\alpha}$, α being in many functionals equal to 1/6, while the others are constants. These choices are motivated by experience. The presence of fractional powers of the density ρ, in particular, has been shown to be very important

[2] Actually, also some higher-order energy functionals, which contain a higher number of derivative operators, have been proposed [15].

to achieve a proper saturation point in symmetric matter [30]. Other dependencies on the number densities have been proposed, though, for example in Ref. [18, 31], and a different parametrization of the nuclear EDF will be a major theme of this work. We mention that the Skyrme functionals are often written with the $t-x$ notation of Ref. [14, 28] and Eq. 1.3.1. The algebraic relations relating the two different notation ($t-x$ and C) are reported e.g. in Ref. [29].

From now on, we concentrate on even-even nuclei, which are simpler to study. Then, the local EDF is a functional of the time-even densities $\rho_q(\mathbf{r})$, $\tau_q(\mathbf{r})$ and $\mathbf{J}_q(\mathbf{r})$ only [6], which are related to single particle orbitals by [26]:

$$\begin{aligned} \rho_q(\mathbf{r}) &= \sum_{ks} |\phi_k(\mathbf{r},s,t)|^2 \\ \tau(\mathbf{r}) &= \sum_{ks} |\nabla\phi_k(\mathbf{r},s,t)|^2 \\ \mathbf{J}_q(\mathbf{r}) &= (-i)\sum_{kss'} \phi_k^*(\mathbf{r},s,t)\left[\nabla\phi_k(\mathbf{r},s',t)\times\sigma_{ss'}\right] \end{aligned} \tag{1.3.12}$$

Also, we neglect the pairing energy; this approximation limits us to the study of closed shell nuclei, or to nuclei where there is a significant energy gap between the last fully occupied level and the first empty one. Then the total energy is:

$$E = E_{kin} + E_{pot} + E_{Coul} \tag{1.3.13}$$

where

$$\begin{aligned} E_{pot} &= \int d\mathbf{r}\, \mathcal{E}_{pot}(\mathbf{r}) \\ \mathcal{E}_{pot} &= \sum_{t=0,1} \mathcal{E}_t^{even} \\ E_{kin} &= \int d\mathbf{r}\, \mathcal{E}_{kin}(\mathbf{r}) = \int d\mathbf{r}\, \frac{\hbar^2}{2m}\tau(\mathbf{r}) \end{aligned} \tag{1.3.14}$$

The Coulomb energy is given by Eq. 1.3.6.
The mean field equations are determined by minimizing the total energy by the variational principle:

$$\delta\left(E - \sum_k \epsilon_k |\phi_k(\mathbf{r}|^2 d\mathbf{r}\right) = 0 \tag{1.3.15}$$

determines the single-particle Hamiltonian [6, 26]:

$$h_q = -\nabla\cdot\frac{\hbar^2}{2m_q^*(\mathbf{r})}\nabla + U_q(\mathbf{r}) + U_{Coul}(\mathbf{r})\delta_{q,p} + \mathbf{W}_q(\mathbf{r})\cdot(-i)\,(\nabla\times\sigma) \tag{1.3.16}$$

where:

$$U_q = \frac{\delta E}{\delta\rho_q} \qquad \frac{\hbar^2}{2m_q^*(\mathbf{r})} = \frac{\delta E}{\delta\tau_q} \qquad \mathbf{W}_q = \frac{\delta E}{\delta\mathbf{J}_q} \tag{1.3.17}$$

and the Coulomb potential in Slater approximation is given by [32]:

$$U_{Coul}(\mathbf{r}) = \frac{\delta E_{Coul}}{\delta\rho_p(\mathbf{r})} = \frac{e^2}{2}\left[\int d\mathbf{r}'\,\frac{\rho_p(\mathbf{r}')}{|\mathbf{r}-\mathbf{r}'|} - \left(\frac{3}{\pi}\rho_p(\mathbf{r})\right)^{\frac{1}{3}}\right] \tag{1.3.18}$$

$m_q^*(\mathbf{r})$ is called the effective mass, $U_q(\mathbf{r})$ represents an average field and $\mathbf{W}(\mathbf{r})$ is a one-body spin-orbit potential. The mean field equations for even-even nuclei are then [26]:

$$\left[-\nabla \cdot \frac{\hbar^2}{2m_q^*(\mathbf{r})}\nabla + U_q(\mathbf{r}) + U_{Coul}(\mathbf{r})\delta_{q,p} + \mathbf{W}_q(\mathbf{r}) \cdot (-i)\,(\nabla \times \sigma)\right] \phi_j(\mathbf{r}) = \epsilon_j \phi_j(\mathbf{r}) \tag{1.3.19}$$

We can see that they are local equations; the computational burden of the non-local exchange (Fock) term is avoided. Still, the mean field equations must be solved self-consistently, since the potential terms are themselves functions of the density.
Once the single-particle orbitals have been determined, the total energy can be computed in two ways:

- as the space integral of the Skyrme EDF evaluated on the ground state densities:

$$E = \int d\mathbf{r}\, \mathcal{E}(\mathbf{r}) \tag{1.3.20}$$

- with the HF formula for a density-dependent Hamiltonian 1.2.6:

$$E = \frac{1}{2}\left(T + \sum_k \epsilon_k\right) + E_{rea} \tag{1.3.21}$$

The equality of these two expressions constitutes a non-trivial check on the correctness of the implementation of a HF code and of its convergence.

In nuclear matter, i.e. a system made of an infinite numbers of neutrons and protons interacting through the nuclear interaction only Sec. 3.2, translational invariance implies that the orbitals are plane waves and that the number densities are uniform [3]. As a consequence, the kinetic density τ_q is likewise uniform and is not an independent quantity, but it is related to the number density by [26]:

$$\tau_q = \frac{3}{5} k_{F,q}\, \rho_q = \frac{3}{5}\left(3\pi^2\right) \rho_q^{5/3} \tag{1.3.22}$$

Moreover, the spin-orbit density $\mathbf{J}_q$ vanishes, as well the derivatives of the density ($\nabla\rho_q = \Delta\rho_q = 0$). As a consequence, to the nuclear matter energy only do the ρ and $\rho\tau$ terms of Eq. 1.3.10 contribute, while the gradient ($\rho\Delta\rho$), spin-orbit ($\rho\nabla\cdot\mathbf{J}$) and tensor ($\mathbf{J}^2$) terms are non-vanishing only in non-uniform systems, such as nuclei, neutron drops or semi-infinite matter. These considerations suggest regrouping the EDF $\mathcal{E}_{pot}$ for a generic nuclear system as:

$$\mathcal{E}_{pot} = \mathcal{E}_{loc} + \mathcal{E}_{non-loc} \tag{1.3.23}$$

where

$$\mathcal{E}_{loc} = \sum_{t=0,1}\left(C_t^\rho \rho_t^2 + C_t^\tau \rho_t \tau_t\right) \tag{1.3.24}$$

$$\mathcal{E}_{non-loc} = \sum_{t=0,1}\left(C_t^{\Delta\rho} \rho_t \Delta\rho_t + C_t^J \mathbf{J}_t^2 + C_t^{\nabla J} \rho_t \nabla\cdot\mathbf{J}_t\right) \tag{1.3.25}$$

We call these local and non-local contributions. $\mathcal{E}_{loc}$ reflects the bulk nuclear properties, while $\mathcal{E}_{non-loc}$ accounts for the surface effects. Infinite matter probes only the bulk contributions.

[3] We consider here isospin-asymmetric, but spin-symmetric nuclear matter. Time-odd densities vanish.

Chapter 2

Realistic nuclear interactions and ab initio methods

The purpose of ab initio methods is to solve the Schrödinger equation for a system of interacting nucleons, taking as input a realistic model for the nuclear interaction in the vacuum [2]. In this Chapter, after an introduction to ab initio nuclear theory (Sec. 2.1), we give a brief description of realistic microscopic interactions [4, 33] (Sec. 2.2) and present an overview of two classes of many-body methods: Quantum Monte Carlo [3, 34] (Sec. 2.3) and Self-consistent Green's function [5, 35] (Sec. 2.4).

2.1 Introduction

The goal of ab initio or first principle calculations is to solve the Schrödinger equation for a system of interacting particles in an exact or sistematically improvable way, starting from the base interaction in the vacuum between the constituents of the system [1, 2]. This is indeed a very challenging task and requires advanced theoretical and computational methods. On the one hand, a direct numerical solution of the Schrödinger equation is not feasible and clever techniques and approximations are required. On the other hand, nuclear theory studies are made more difficult by the complicated structure of the bare nuclear interaction in the vacuum, as well as by the fact that nuclear forces are still not completely understood.

The first ab initio studies in nuclear physics date back to the 1950's, with the introduction of Brückner G-matrix [36]. However, they obtained a limited success, while phenomenological models, such as the shell model, lead to breakthroughs in the comprehension of nuclear systems [26] (Ch. 1). The interest in first principle calculations has started to revive in the 1980s, due to the introduction of new sophisticated many-body methods, the development of accurate microscopic nuclear interactions and the availability of increased computational power [2].
Ab initio methods take as input two- and three-nucleon potentials that have been constrained to accurately reproduce few-body observables, such as nucleon-nucleon scattering data or the binding energies of the deuteron and the triton [33, 37]. Additional quantities can also be included in the fit protocol, for example the saturation point of symmetric matter [4, 38]. Then, the Schrödinger equation for the many-nucleon system is solved numerically with a suitable many-body method. Several different techniques have been developed: examples are Quantum Monte Carlo (QMC) [3, 4, 34], Self-consistent Green's

function (SCGF) [5, 35, 39], Coupled-cluster [2, 40], Brückner–Hartree–Fock (BHF) [26, 36], Fermi hypernetted chain/single-operator chain [22], Many-body perturbation theory (MBPT) [41, 42], as well as few-body methods such as the Hyperspherical Harmonics [1, 2].
While the problem of determining the nuclear interaction is still open, there do exist realistic models of two- and three-nucleon forces, (Sec. 2.2). Alongside phenomenological interactions [4, 37], to some extent inspired by meson exchange theories, a great deal of attention has been attracted by chiral potentials [33, 38], which are rooted in a low-energy description of Quantum Chromodynamics (QCD) in terms of nucleons and pions, called chiral effective field theory (EFT). Although attempts to directly derive nuclear physics from QCD are in their infancy [43], due to the heavy load of lattice QCD simulations, chiral EFT is a powerful tool to ground the nuclear problem on the symmetries of the underlying theory.
Ab initio theory has found wide applications in the study of finite nuclei [5, 34], infinite matter [3, 39] and neutron stars [19, 44], and beta decay rates [45]. Current limitations are inherent to the computational cost of full-scale calculations that still precludes the study of heavy nuclei, as well as to the partially unsettled problem of finding a universally valid microscopic interaction. Indeed, there exist several realistic potentials, i.e. that reproduce phase shifts well, but a single interaction that, when used in many-body calculations, allows to accurately describe both finite nuclei and infinite matter is not available yet [21].

2.2 Realistic nuclear interactions

Nucleons are not elementary particles, but bound state of quarks and gluons. Hence, the most fundamental description of nuclear systems should be grounded on Quantum Chromodynamics (QCD). However, the success of QCD-based approaches is still limited, due to the heavy cost of non-perturbative lattice field theory calculations [4, 43]. Instead, an effective description of nuclear systems assumes the nucleons as degrees of freedom and models their interactions through a non-relativistic Hamiltonian, which include two- and three-nucleon (and possibly many-nucleon) potential terms:

$$H = T + \sum_{i<j} V_{ij}^{NN} + \sum_{i<j<k} V_{ijk}^{3N} + ... \tag{2.2.1}$$

In the above equation, NN stands for nucleon-nucleon interactions, $3N$ for three-nucleons interactions and the dots refer to higher order terms, which will be neglected in this context. The problem of determining the nuclear interaction is very tough and, although a universally accepted solution has not been found yet, over the years several realistic models of nuclear forces have been devised, some taking a phenomenological approach, for example the Argonne family [37], some others trying to stick closer to QCD and making use of effective field theory (EFT) techniques, chiral interactions being a prominent example [38]. In this Section, we present the main elements of realistic nuclear forces.

Phenomenological NN interactions are often inspired by meson-exchange model [4]; for example, the one-pion exchange (OPE) potential is often used to describe the long-range component of the interaction. The widely employed phenomenological Argonne interactions [37, 46] explicitly includes the OPE and complement it with a set of intermediate- and short-range terms that model the two-pion exchange and the short-range behaviour

[4]. The sophisticated AV18 [37] interaction can be expressed as a sum of 18 operators:

$$V_{ij} = \sum_{p=1}^{18} v^p(r_{ij}) O_{ij}^p \tag{2.2.2}$$

where:

$$\begin{aligned} O_{ij}^{1...8} &= [1, \sigma_i \cdot \sigma_j, S_{ij}, \mathbf{L} \cdot \mathbf{S}] \otimes [1, \tau_i \cdot \tau_j] \\ O_{ij}^{9...14} &= \left[\mathbf{L}^2, \mathbf{L}^2 \sigma_i \cdot \sigma_j, (\mathbf{L} \cdot \mathbf{S})^2\right] \otimes [1, \tau_i \cdot \tau_j] \\ O_{ij}^{15...18} &= \left[T_{ij}, \sigma_i \cdot \sigma_j T_{ij}, S_{ij} T_{ij}, \tau_i^z + \tau_j^z\right] \end{aligned} \tag{2.2.3}$$

where $r_{ij} = |\mathbf{r}_i - \mathbf{r}_j|$, $\mathbf{L}$ is the relative angular moment of the pair of nucleons, $\mathbf{S}$ is the total spin, $S_{ij} = 3\sigma_i \cdot \hat{\mathbf{r}_{ij}} \sigma_j \cdot \hat{\mathbf{r}_{ij}} - \sigma_i \cdot \sigma_j$ is the tensor operator in coordinate space and $T_{ij} = 3\tau_i^z \tau_j^z - \tau_i \cdot \tau_j$ is the isotensor operator. The first 14 operators are associated to the spin, isospin, tensor, spin-orbit and quadratic spin-orbit components of the nuclear force; the last 4 operators, involving T_{ij}, break charge independence. The radial functions $v^p(r_{ij})$ are fitted in order to reproduce the Nijmegen database of NN elastic scattering phase shifts (up to energies of about 350 MeV) [47] with a $\chi^2/datum \approx 1$, as well as to reproduce properties of the deuteron. We remind that symmetry arguments allow to constrain the operator structure of NN interactions, but not the expression of the radial functions [26].

$AV18$ is a rather complex potential and computationally demanding and not all many-body methods can deal with all the 18 operators properly. A set of simplified Argonne potential [48], $AV_n^{'}$, with contain a restricted set of operators, have been proposed. These interactions are not simply truncation of the full AV18, but are refitted in order to reproduce as many nucleon-nucleon properties as possible. The $AV_8^{'}$ includes the first 8 operators of 2.2.3, i.e. up to the spin-orbit term. The $AV_6^{'}$ force lacks the spin-orbit term, while $AV_4^{'}$ has the very simple structure $[1, \sigma_i \cdot \sigma_j] \otimes [1, \tau_i \cdot \tau_j]$, which lacks also the tensor term. See also Sec. 5.1.

In addition to NN forces, phenomenological three-nucleons interactions have been developed. It is well known, in fact, that if only NN forces are included in the Hamiltonian, then light nuclei are underbound and the equilibrium density of nuclear matter is overestimated [34, 46]. In order to provide the missing contribution to the binding energies, it has proved necessary to introduce three-nucleon potentials. The popular Urbana IX (UIX) [49], for example, consists of two terms: an attractive two-pion exchange P-wave term (Fujita-Miyazawa) and a phenomenological short-range repulsive central term [4, 50], see Sec. 5.1 and Ref. [51]. The Fujita-Miyazawa interaction, whose diagrammatic representation is shown in Fig. 2.1, describes a process in which two pions are exchanged among the three nucleons and a Δ resonance is excited in the intermediate state [50] and provides the missing binding energy in light nuclei. The central term is purely phenomenological and prevents nuclear matter from being overbound at large density [51]. The UIX interaction contains two parameters ($A_{2\pi}$, U_0) which are fit to reproduce the ground state energies of ^{3}H and ^{4}He ($A_{2\pi}$) and the saturation point of symmetric nuclear matter (U_0) in combination with a given NN potential, tipically $AV18$. Another popular three-body potential is the Illinois 7 (IL7) [4, 52], having a slightly richer structure than UIX. The prediction the Green's function Monte Carlo ground and excited state energies of light nuclei for the $AV18$ and $AV18 + IL7$ Hamiltonian are shown in Fig. 2.2.

Although in many regards successful, phenomenological potentials suffer from some drawbacks: since they are constructed in an empirical way, there is not a systematic method to improve them and it is not possible to estimate the uncertainties associated with the

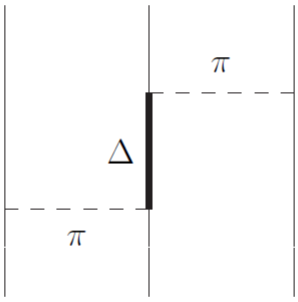

Figure 2.1: Feynman diagram associated with Fujita Miyazawa 3N interaction. Taken from Ref. [50].

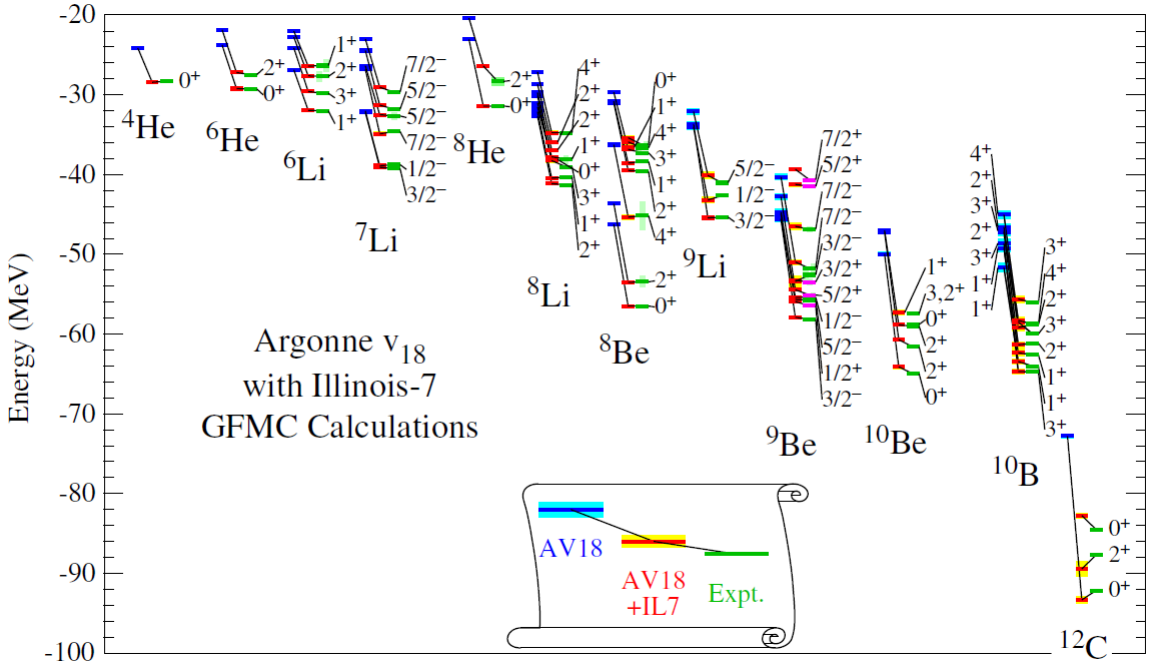

Figure 2.2: Green's function Monte Carlo energies of light nuclear ground and excited states for the $AV18$ and $AV18 + IL7$ Hamiltonians compared to experiment. Taken from Ref. [34].

interactions [4]. Moreover, the three-nucleon interaction is still somewhat problematic, as it is difficult to obtain a NN+3N interaction that simultaneously reproduces well both nuclei and the saturation point of symmetric matter [21] (Sec. 3.2). For example, the Argonne NN interaction plus the Illinois 7 (IL7) 3N force yield equations that are too soft, while UIX forces are better suited for nuclear matter studies, but perform worse in finite nuclei [34].

The framework of effective field theories (EFTs) allows one to overcome some limitation of phenomenological interactions. Chiral EFT, in particular, allow to construct nuclear forces in a systematic way consistent with the symmetries of QCD [38, 43, 53]. The principle of chiral EFT is to build a low-energy field theory of QCD in terms not of quarks and gluons, but of the degrees of freedom relevant to the low-energy nuclear physics regime. In practice, one writes down the most general Lagrangian, function of nucleon, pion and eventually Δ isobar fields and their derivatives, which is consistent with the symmetries of QCD. An important role is played by the chiral symmmetry [38]: if we take into account only the light up and down quarks, then the QCD Lagrangian satisfies an approximate $SU(2)_L \times SU(2)_R$ (or $SU(2)_V \times SU(2)_A$) symmetry, only slightly violated by the small quark masses. Such symmetry is however spontaneously broken to $SU(2)_V$, as the vacuum is not invariant under the axial group $SU(2)_A$. If the underlying symmetry were realized in the vacuum, in fact, mesons should come in pairs of opposite parity [38], which is not observed. As stated in Goldstone theorem, the spontaneous breaking of the chiral symmetry implies the existence of a triplet of pseudo scalar bosons: the pions [1]. Pions are therefore a fundamental ingredient of nuclear physics. Indeed, the exchange of pions is the main mechanism responsible of the interaction between nucleons.
The framework outlined above is valid at low energies, but it breaks down at a scale $\Lambda_\chi \approx m_\rho \approx 800\, MeV$, at which the vector ρ mesons appears. Λ_χ is called the hard scale of the effective theory, while the pion mass identifies the soft scale $Q \approx m_\pi$. Now, the most general EFT Lagrangian contains an infinite number of terms: a principle is needed to organize the Feynman diagrams that can be evaluated from it. In chiral perturbation theory, the diagrams are ordered in powers of the ratio of the external momenta over the hard scale $(Q/\Lambda_\chi)^\nu$, where a so-called power counting scheme is used to determine the power ν for each term. Then, the effective Lagrangian together with a power counting allow to determine the effective nuclear potential at each order ν, as shown in Fig. 2.3.
The nuclear potential can thus be constructed from the Lagrangian according to a systematic, order by order expansion; this provides a meaningful way to estimate the uncertainties associated with the truncation of the expansion. The interaction contains both pion exchange and contact terms; the latter, which determine the short-range behaviour of the interaction, are defined in terms of a set of coupling constants or low-energy constants (LECs) [33, 54]. In principle, the LECs can be determined directly from QCD by matching EFT and lattice QCD predictions, but are usually fit to experimental data due to the challenging non-perturbative nature of low-energy QCD [43]. In principle, the LECs can be determined by matching EFT and lattice QCD predictions [43], but in practice this program is in its infancy Several fit protocols do exist, contributing to the existence of a large number of chiral potentials [21, 55].
Another interesting feature of chiral interactions is that many-body forces arise naturally

[1] Goldstone theorem states that the spontaneous breaking of a global continuous symmetry of the Lagrangian implies the existence of a multiplet of *massless* scalar bosons. Since the chiral symmetry of QCD is only approximate, the resulting Goldtone bosons, the pions, are not exactly massless; however, they are much lighter than the nucleons and the other mesons.

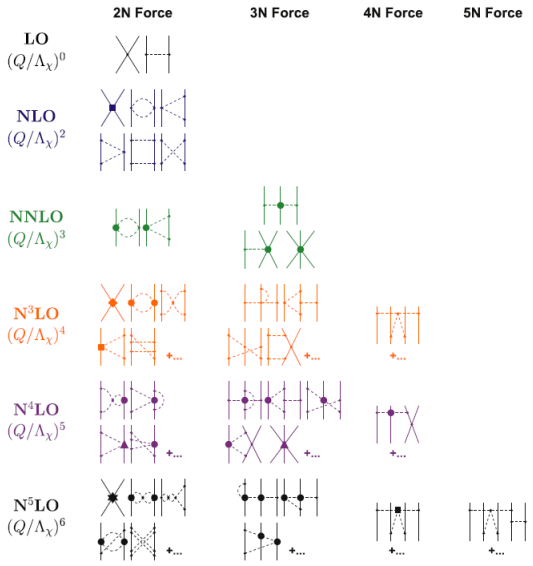

Figure 2.3: Hierarchy of nuclear forces in chiral perturbation theory. Solid lines represent nucleons and dashed lines pions. Taken from Ref. [53].

at sufficiently high orders. This allows, for example, to give a theoretical justification to three-body forces, that were previously introduced on a purely phenomenological basis. At the leading order (LO), $\nu = 0$, only momentum-independent contact terms and the one-pion exchange (OPE) diagram contribute. At next-to-leading-order (NLO), two-pion exchange appears. At $NNLO$, three-body forces show up. Up to $NNLO$, the operator structure is the same as that of phenomenological potentials. Going up in the hierarchy, ever more complicated many-nucleon forces appear [53]. Moreover, by taking into account only low-energy degrees of freedom, chiral potential have generally a "softer" character than phenomenological forces, i.e. they have a much smaller associated cutoff [5, 33, 56]; as a consequence, they are easier to be dealt with by many-body methods.
Chiral EFTs are not
The promise of a systematic expansion of the nuclear potential has attracted a lot of attention to chiral EFT and several interactions have been developed at different orders in the chiral expansion, with different fit protocols and cut-offs. As an example, we mention the $NNLO_{sat}$ interaction by Ekström *et al.* [23] (Sec. 4.1) , that has been optimized simultaneously in its two- and three-nucleon components; the data set includes two-nucleon properties, as well as binding energies and radii of a few selected nuclei belonging to the oxygen and carbon chains. This choice, which constitute a sort of violation of the strict EFT paradigm, as information on many-body systems is used to constrain the microscopic forces, has allowed to reach a good agreement up to medium-mass nuclei, while at the same time the saturation properties of symmetric matter are compatible with the empirical constraints [20]. The $NNLO_{sat}$, in particular, is perhaps the only chiral potential that predicts both binding energies and charge radii in agreement with experiment, even in nuclei heavier than those used in the fitting protocol [25, 57] (Fig. 2.4). Other chiral interactions are discussed in e.g. Ref. [25, 33, 42, 58]. Also, we mention that quite recently local chiral interactions have been formulated in coordinate space, allowing them to be used in Quantum Monte Carlo methods [3, 54, 59] (Sec. 2.3).
Unfortunately, chiral interactions are not immune from some of the issues that afflict phenomenological forces. First of all, the LECs are free parameters and different parameter sets and optimization protocols yield different results when the interactions are used in

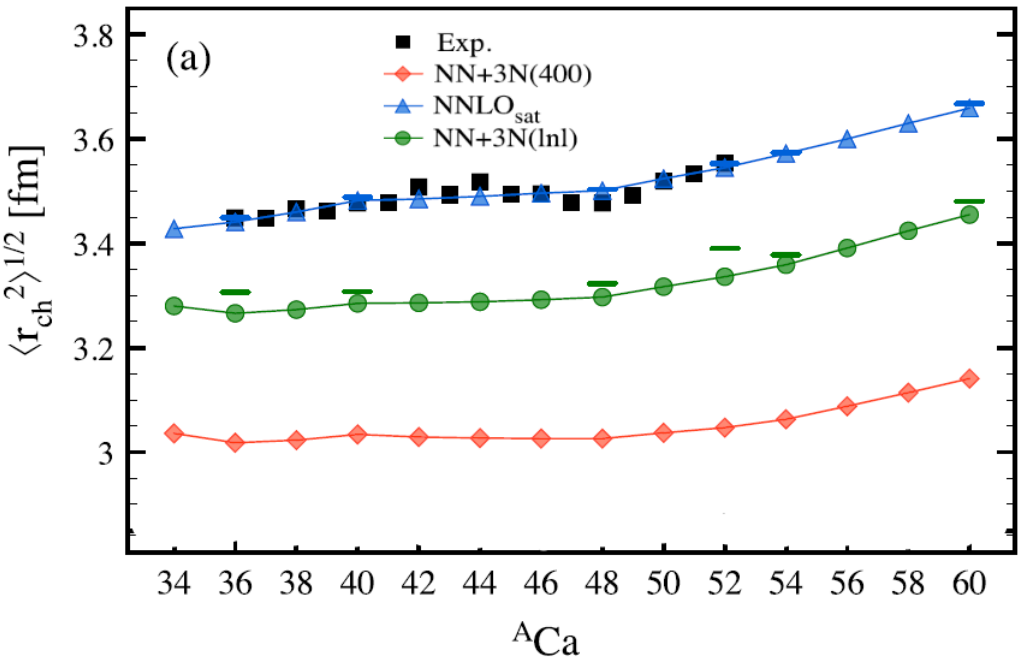

Figure 2.4: Rms charge radii of calcium isotopes computed within the ADC(2) approximation with the $NN+3N(400)$, $NN+3N(lnl)$, and $NNLO_{sat}$ interactions. The available experimental radii are also shown. Adapted from Ref. [25], Fig. 12.

many-body calculations. The choice of the cut-offs and the regulators also contribute to a proliferation of available chiral potentials. Moreover, a well known limitation is that it has not been possible up to now to find a single interaction that achieves completely satisfying results in both infinite matter and finite nuclei [21, 43]. A recent work [58], for example, compares the interactions proposed by Drischler *et al.* [42] and Hüther *et al.* [60] respectively, and shows the first one works well in infinite matter, on which it was fitted, but underbinds medium-mass nuclei, while the second one is accurate for nuclei, but it is excessively attractive in symmetric matter. These issues show that the quest for the nuclear interaction is still open and chiral interaction still need to be improved. Nonetheless, it is generally believed that chiral forces constitute a definite progress with respect to the older phenomenological models [33].

2.3 Quantum Monte Carlo

Quantum Monte Carlo (QMC) methods are powerful tools to study strongly interacting many-body systems [3, 4, 34, 61]. While Variational Monte Carlo (VMC) is a variational method that exploits Monte Carlo integration techniques to determine an upper bound to the ground state energy, the more sophisticated Diffusion Monte Carlo (DMC) methods provide in principle an exact solution to the Schrödinger equation, which is solved by means of a stochastic imaginary time evolution. All Monte Carlo methods allow to estimate the statistical error on any given observable. These feature have made QMC, especially the DMC, very popular in different areas of physics. A classic example in condensed matter is the calculation of the HEG correlation energy [62] (Sec. 3.1).
In nuclear physics, QMC is among the state of the art methods for the study of finite nuclei [3, 4] and neutron matter [19, 22, 63]. Symmetric matter is more cumbersome and

a limited number of full scale calculations has been performed [59, 64]. Also, QMC methods have no difficulties in treating hard nuclear interactions, but, on the other hand, are limited to nearly local potentials [3]. Recently chiral interactions have been formulated in coordinate space [3, 54], so that now both chiral and phenomenological interactions are accessible to Monte Carlo techniques.
Two different implementations of the DMC algorithm applied to the nuclear many-body problem have been developed: the Green's Function Monte Carlo (GFMC) and the Auxiliary Field Diffusion Monte Carlo (AFDMC) methods These two methods differ in the way they treat the spin and isospin degrees of freedom [3, 4, 65]. GFMC is somewhat more accurate, but, since its computational cost scale exponentially with the number of nucleons, is limited to small systems [34]. The AFDMC, on the other hand, thanks to its cost scaling polynomially with the number of nucleons ($\sim A^3$), allows to study infinite matter and medium-mass nuclei [4]. Indeed, the bottleneck of the powerful diffusion methods is the very large computational workload that is necessary for full-fledged calculations. Another limitation is the infamous sign problem that complicates the application of QMC to fermions [3]. In this Section, we introduce the VMC, DMC, and AFDMC methods and discuss briefly the sign problem.

Variational Monte Carlo The variational principle states that, given a Hamiltonian H and a trial state $|\Psi_T\rangle$, the expectation value of H on $|\Psi_T\rangle$ is an upper bound to the g.s. energy E_0:

$$E_T = \frac{\langle\Psi_T| H |\Psi_T\rangle}{\langle\Psi_T|\Psi_T\rangle} \geqslant E_0 \tag{2.3.1}$$

The equality holds if and only if the trial state is the true ground state of the Hamiltonian. The Variational Monte Carlo (VMC) [66] exploits the variational principle to solve the many-body Schrödinger equation. Once a coordinate space trial wave function $\Psi_T(R\sigma\tau) = \langle R\sigma\tau|\Psi_T\rangle$, is chosen, where R,σ and τ stand for the positions, spins and isospins of all the particles, the energy expectation value E_T reads

$$E_T = \frac{\sum_{\sigma\tau}\int dR\,|\Psi_T(R\sigma\tau)|^2 \frac{H\Psi_T(R\sigma\tau)}{\Psi_T(R\sigma\tau)}}{\sum_{\sigma\tau}\int dR\,|\Psi_T(R\sigma\tau)|^2} \tag{2.3.2}$$

Computing E_T involves integrals of very high dimensionality. This would require a prohibitive cost with traditional integration methods, such as Simpson's rule, and the solution comes in the use of Monte Carlo techniques. The rationale is that, if one manages to sample *independent* random space configurations R, distributed according to a suitable probability density $P(R)$, then integrals of the form $\int dR\,P(R)f(R)$ can be approximated as a finite sum [61]:

$$\int dR\,P(R)f(R) \approx \frac{1}{N}\sum_{i=1}^{N} f(R_i) \tag{2.3.3}$$

where N is the number of samples. In Eq. 2.3.2, the probability distribution is $|\Psi_T(R\sigma\tau)|^2$. The central limit theorem then implies that the standard error on the integral scales like $1/\sqrt{N}$, independently of the dimensionality [61]. This constitutes a great progress when the method is applied to large systems. The Metropolis algorithm is often employed to sample the configurations with distribution $P(R)$ [66].
The structure of the trial wave functions is chosen a priori and is critical to obtain a good estimate of the ground state energy. The wave function depends on a set of variational parameters α and the solution of the variational problem is equivalent to minimizing the

trial energy E_T with respect to the variational parameters, i.e. $\frac{\partial E_T(\alpha)}{\partial \alpha_k} = 0$ [66].
In nuclear physics, the trial state Ψ_T is usually assumed to factorize as the product of a state Φ and a correlation operator $\mathcal{F}$ [34]:

$$|\Psi_T\rangle = \mathcal{F}\,|\Phi\rangle \tag{2.3.4}$$

where $|\Phi\rangle$ describes the quantum numbers and the long-range behaviour of the many-body wave function. Common choices are a combination of Slater determinants or BCS states with the desired total angular momentum and parity for nuclei [3], or plane waves for nuclear matter [59]. The operator $\mathcal{F}$ models the short-range correlations induced by the nuclear interaction. It is often written as a generalization of the Jastrow ansatz [61, 66]:

$$\mathcal{F} = \mathcal{S}\prod_{i<j}\sum_{p} f_{ij}^{(p)} O_{ij}^{(p)} \tag{2.3.5}$$

The sum runs the same operators that appear in the Hamiltonian ($\sigma_i \cdot \sigma_j$, $\tau_i \cdot \tau_j$, S_{ij}...), while $f_{ij}^{(p)}$ are radial Jastrow functions. The symmetrization operator $\mathcal{S}$ is needed to enforce the antisymmetry of the wave function.
The main drawbacks of the VMC method are that the computational time scales exponentially with the number of particles and that the goodness of the result entirely depends on the accuracy of the trial wave function [50]. In nuclear physics, the VMC method is used as a first step to provide accurate trial wave functions for the more powerful Diffusion Monte Carlo methods.

Diffusion Monte Carlo The principle of Diffusion Monte Carlo (DMC) is to project an initial wave function $|\psi_T\rangle$ into the ground state by means of an imaginary time evolution [61, 66]. The time-dependent Schrödinger equation:

$$i\hbar\frac{\partial\,|\psi(t)\rangle}{\partial t} = (H - E_T)\,|\psi(t)\rangle \tag{2.3.6}$$

where E_T is an energy offset, admits the solution [2]:

$$|\psi(t+\delta t)\rangle = e^{-i(H-E_T)\delta t/\hbar}\,|\psi(t)\rangle \tag{2.3.7}$$

We now Wick-rotate to imaginary time by setting $\tau = it/\hbar$ (or $t = -i\hbar\tau$). With this choice, the real variable τ has the dimensions of the inverse of an energy. Then:

$$|\psi(\tau+\delta)\rangle = e^{-(H-E_T)\delta\tau}\,|\psi(\tau)\rangle \tag{2.3.8}$$

If we expand the initial state $|\psi\rangle$ on the basis of the eigenstates of H, $H\,|n\rangle = E_n\,|n\rangle$, then:

$$\begin{gathered} |\psi\rangle = \sum_{n=0}^{+\infty} c_n\,|n\rangle \implies \\ |\psi(\tau)\rangle = \sum_{n=0}^{+\infty} c_n e^{-(E_n-E_T)\tau}\,|n\rangle = e^{-(E_0-E_T)\tau}\left[c_0\,|0\rangle + \sum_{n=1}^{+\infty} c_n e^{-(E_n-E_0)\tau}\,|n\rangle\right]. \end{gathered} \tag{2.3.9}$$

Thus the excited states are exponentially damped with respect to the g.s. component and in the limit of large times $\tau \longrightarrow +\infty$, $|\psi(\tau)\rangle \propto |0\rangle$. The initial wave function $|\psi(\tau=0)\rangle =$

[2] We assume the Hamiltonian does not explicitly depend on time.

$|\psi_T\rangle$ and an estimate of the ground state energy (E_T) are usually obtained with VMC calculations.
The imaginary-time evolution is conveniently expressed in integral form as:

$$\psi(R, \tau + \delta\tau) = \int dR'\, G(R, R', \delta\tau)\psi(R', \tau) \tag{2.3.10}$$

where $\psi(R, \tau) = \langle R|\psi(\tau)\rangle$ is the coordinate space wave function and

$$G(R, R', \delta\tau) = \langle R|\, e^{-(H-E_T)\delta\tau}\, |R'\rangle \tag{2.3.11}$$

is the imaginary-time propagator or Green's function. For small time steps the calculations of the propagator is feasible, since the Trotter-Suzuki formula implies that $G(R, R', \delta\tau)$ can be split as the product $G(R, R', \delta\tau) = G_0(R, R', \delta\tau) \cdot G_V(R, R', \delta\tau)$, where [65]:

$$\begin{aligned} G_0(R, R', \delta\tau) = \langle R|\, e^{-T\delta\tau}\, |R'\rangle = \frac{1}{(4\pi D\, \delta\tau)^{\frac{3A}{2}}}\, e^{-\frac{(R-R')^2}{4D\delta\tau}} \\ G_V(R, R', \delta\tau) = e^{-\left(\frac{V(R)+V(R')}{2} - E_T\right)\delta\tau} \end{aligned} \tag{2.3.12}$$

and $D = \frac{\hbar^2}{2m}$ is a diffusion constant.
The Schrödinger equation for A non-interacting particles ($H = T$), with Green's function G_0, is formally identical to the diffusion equation, in a $3A$-dimensional space, of a set of A Brownian particles in random motion. This analogy suggests that the wave function $\psi(R, \tau)$ can be interpreted as a probability density for the configuration R, called in this context a walker, and the propagator $G_0(R, R', \delta\tau)$ as a transition matrix [3]. The analogy with Brownian motion also suggest that the wave function $\psi(R, \tau)$ can be represented by a set of discrete points R_k:

$$\psi(R, \tau) = \sum_k \delta(R - R_k) \tag{2.3.13}$$

In practice, the imaginary-time evolution 2.3.10 is realized in the following way. The trial wave $\psi_T(R)$ is used to samples a set of $10^2 - 10^3$ walkers R', called a population, then each walker is evolved independently by diffusing its coordinate by a Brownian motion:

$$R = R' + \xi \tag{2.3.14}$$

ξ is sampled from the distribution $G_0(R, R', \delta\tau)$, i.e. a Gaussian centered in the origin with width $\sigma^2 = 2D\delta\tau$.
If we now consider the interacting Hamiltonian again ($H = T+V$), the factor $G_V(R, R', \delta\tau)$ in the full propagator acts as a time-dependent normalization factor. An efficient way to implement it is to use a branching or birth/death algorithm [61]: each walker is assigned a weight $w_k = G_V(R, R', \delta\tau)$, then a new population is generated, made of n_k copies of each walker, where:

$$n_k = [w_k + \eta_k] \tag{2.3.15}$$

η_k is a random number uniformly distributed in the interval $[0, 1]$, while $[x]$ is the integer part of x. After a sufficient number of steps, the walker population is distributed according to the ground state wave function of the interacting system (Fig. 2.5). Then, one can

[3] The *wave function* $\psi(R, \tau)$ is interpreted as a probability distribution, *not* its square modulus! This interpretation is valid provided that the wave function is positive-definite. We will come back to this when discussing the fermion sign problem.

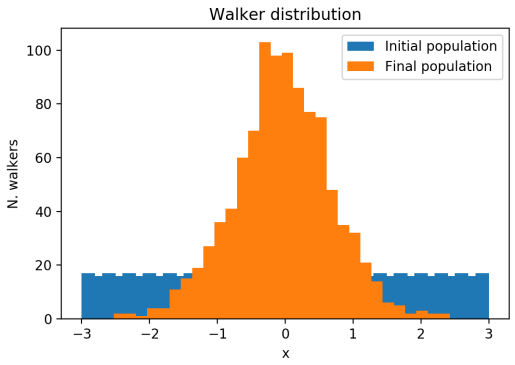

Figure 2.5: Walker evolution in Diffusion Monte Carlo. The histogram displays the initial population of walkers, distributed uniformly, and the final population after several thousand time steps, for a one-dimensional problem of one particle confined in a harmonic potential $V(x) = \frac{1}{2}x^2$. The final population is very close to a Gaussian, that indeed is the g.s. wave function of the problem.

begin accumulating the observables of interest.
In the DMC method, one gets access to a discrete representation of the ground state wave function in coordinate space through the walkers distribution. Thus, it is possible to estimate the expectation value in the g.s. of all operators: all the contribution to the total energy, the one-body density, the momentum distribution... [66]. The statistical error on any average scale like $1/\sqrt{N}$, where N is the number of samples.
The algorithm we have described is the simplest form of Diffusion Monte Carlo and has several limitations. It is very inefficient, mostly because the population may fluctuate significantly from step to step. Moreover, as the Brownian motion has no information about the potential, two walkers may find themselves very close to each other, even if the interaction is repulsive at short distances. This can cause e.g. the Coulomb potential to diverge, leading to severe numerical problems. The solution comes in the form of the *importance sampling* technique, where essentially a trial wave function is used to guide the diffusion process [61, 65, 66]. Another issues is that the DMC algorithm as outlined here is not apt for studying fermionic systems, due to the sign problem [61].

Sign problem A necessary condition that had to be imposed in the DMC algorithm is that wave function be positive everywhere, in order to allow the interpretation of $\psi(R, \tau)$ as the density of walkers. This means that the method outlined above can work for systems of boson, but not for fermions, since the wave function of a system of fermions is antisymmetric with respect to the exchange of a pair of particles. This implies that fermion wave functions must take both positive and negative values. An extension of DMC is thus required to deal with fermions [4]. This issue, called the *fermion sign problem*, plagues all DMC methods and has not found a completely satisfying remedy yet. However, some approximate solutions exist.
In condensed matter, the Hamiltonian is time-reversal invariant, thus one can work with real wave functions. In nuclear physics, on the other hand, the Hamiltonians in general

[4] An equivalent statement is the following: the imaginary time evolution project an initial state onto the *mathematical* ground state of the Hamiltonian. Such state is a positive and nodeless function [4]. However, fermion wave functions must change sign due to antisymmetry and thus must have at least one node. The *physical* ground state of a system of fermions is actually an excited state of the Hamiltonian.

are not time-reversal invariant. Hence, nuclear wave functions are complex. In the former case, a popular method is the fixed-node approximation [61, 65], that satisfies a variational principle and thus provides upper bounds to the true g.s. energy. In the latter case, other methods, such as the fixed-phase approximation [65] and the constrained path approximation [3], must be employed with the complex wave functions; however, they do not necessarily provide an upper bound to the g.s. energy.
In the fixed-node approximation, the nodal surface, defined as the set of points where the trial wave function vanishes, is used to split the configuration space in regions where the trial state does not change sign. Then the DMC algorithm is run in each of these regions. If the nodal surface is exact, one finds the true ground state energy; otherwise, an upper estimate of the g.s. energy is obtained [61].

Auxiliary Field Diffusion Monte Carlo In nuclear physics, the diffusion algorithm must be generalized to deal with the spin and isospin degrees of freedom. In the Green's Function Monte Carlo (GFMC) [34, 65], each of the spin-isospin configuration of the many-body wave function is propagated in imaginary time. The wave function $|\psi\rangle$ is a vector in the spin-isospin space having components $a_\alpha = \langle\alpha|\psi\rangle$ for each state $|\alpha\rangle = |\sigma_1,\tau_1\rangle\otimes ...\otimes|\sigma_A,\tau_A\rangle$. For example, the spin part of a three-particle systems is described by an 8-component spinor [65]:

$$|\psi\rangle_{A=3} = \begin{pmatrix} a_{\uparrow\uparrow\uparrow} \\ a_{\uparrow\uparrow\downarrow} \\ a_{\uparrow\uparrow\downarrow} \\ a_{\uparrow\downarrow\downarrow} \\ a_{\downarrow\uparrow\uparrow} \\ a_{\downarrow\downarrow\uparrow} \\ a_{\downarrow\uparrow\downarrow} \\ a_{\downarrow\downarrow\downarrow} \end{pmatrix} \qquad a_{\uparrow\uparrow\downarrow} = \langle\uparrow\uparrow\downarrow|\psi\rangle_{A=3} \tag{2.3.16}$$

The Green's function 2.3.11 is generalized to a matrix in spin-isospin space:

$$G_{\alpha\beta}\left(R,R',\delta\tau\right) = \langle R,\alpha|\, e^{-(H-E_T)\delta\tau}\,|R',\beta\rangle \tag{2.3.17}$$

Each component $a_\alpha(R,\tau)$ evolves according to:

$$a_\alpha(R,\tau+\delta\tau) = \sum_\beta \int dR'\, G_{\alpha\beta}\left(R,R',\delta\tau\right)\alpha_\beta(R',\tau) \tag{2.3.18}$$

Although accurate, GFMC is limited to small nuclei (up to 12 nucleons), since the full summations over the spin and isospin states implies a computational cost that scales exponentially with number of particles [34]. An alternative is provided by the Auxiliary Field Diffusion Monte Carlo (AFDMC) method [4, 65], which ensures a polynomial scaling $\sim A^3$ by sampling the spin and isospin states, instead of considering all of them explicitly. The main idea is to use wave functions that are tensor product of *single-particle* states. For example, the spin part of a $A = 3$ system is:

$$|\psi\rangle_{A=3} = \begin{pmatrix} a_{1\uparrow} \\ a_{1\downarrow} \end{pmatrix}_1 \otimes \begin{pmatrix} a_{2\uparrow} \\ a_{2\downarrow} \end{pmatrix}_2 \otimes \begin{pmatrix} a_{3\uparrow} \\ a_{3\downarrow} \end{pmatrix}_3 \qquad a_{k\uparrow} =_k \langle\uparrow|\psi\rangle_{A=3} \tag{2.3.19}$$

In general, the dimension of the vector describing a system of A nucleons scales as $4A$, while in GFMC the number of components has factorial growth with A. However, while one-body operators do preserve such single-particle representation, the latter is not closed under the action of quadratic spin/isospin operators [4]: a quadratic operator, e.g. $\sigma_i \cdot \sigma_j$, when acting on a product state generates a combination of single-particle wave functions, so that the number of states grows very quickly during the imaginary time propagation and any computational advantage over GFMC would be lost.
In order to conserve the single-particle representation, quadratic operators are linearized by making use of the Hubbard-Stratonovich transformation [66]:

$$e^{\frac{\lambda}{2}O^2} = \frac{1}{\sqrt{2\pi}} \int dx\, e^{-\frac{x^2}{2}+\sqrt{-\lambda}xO} \tag{2.3.20}$$

An integration over a new variable x, called auxiliary field, is introduced. Thus, in AFDMC not only the spatial coordinates, but also the spin and isospin states are diffused: the latter are sampled through the auxiliary fields [4].
The AFDMC method allows to simulate larger systems than GFMC. It is currently limited, though, to somewhat simplified interactions; also, simpler trial wave functions must be used, in compliance with the requisite that they have a single-particle representation [3, 34]. For these reasons, it is slightly less accurate than the GFMC method. See Ref. [3, 4, 59] for recent progresses.

2.4 Self-consistent Green's function

The Self-consistent Green's function (SCGF) method [5, 35, 39] provides a non-perturbative and systematically improvable solution to the Schrödinger equation for a system of A interacting fermions that is rooted on the concept of many-body propagators or Green's functions (GF) [67]. The one-particle propagator $g_{\alpha\beta}(\omega)$, in particular, provides access to all one-body observables and to the ground state energy; moreover, it gives information on the neighbouring $A \pm 1$ nuclei, for example on the one-nucleon addition and removal energies [25].
The interest in SCGF lies in the wealth of information that can be accessed in a single stage, as well as in its computational cost scaling polinomially with the number of particles, allowing it to compare favourably with respect to other exact methods, whose cost scales exponentially [35]. It is nonetheless a demanding method and for now converged results are available for mass numbers up to $A \approx 60 - 70$ and for nuclear matter [5], although in a recent study [68] charge radii and charge density distributions have been computed in heavy nuclei up to $A = 138$.
SCGF works best with "soft" interactions, i.e. with a low momentum cutoff, such as the chiral forces [25]. Hard, phenomenological potentials can also be dealt with, see e.g. Ref. [56] for symmetric matter calculations with the $AV18$ potential, but require sophisticated resummation techniques [69] that hinder applications in medium-mass nuclei .
In SCGF, the dressed Green's function is determined by solving the Dyson equation (or the Gorkov equations if one deals with open shell nuclei [70]) suitably written in a form that does not depend on any reference function, but only on $g(\omega)$ itself. Thus, once an approximate expression for the irreducible self-energy $\Sigma^*(\omega)$ (Fig. 2.6) is given, the Dyson equation 2.4.2 can be solved in an iterative fashion, where the propagator is fed back into Σ^* until convergence is reached.

The very basic elements of the standard (Dyson) SCGF are the following. The dressed one-particle propagator is defined as [5]:

$$ig_{\alpha\beta}(t_\alpha, t_\beta) = \left\langle \Psi_0^A \right| T \left[a_\alpha(t_\alpha) a_\beta^\dagger(t_\beta) \right] \left| \Psi_0^A \right\rangle \tag{2.4.1}$$

i.e. as the expectation value on the the A-particles ground state of the time ordered product of the annihilation and creation operators $a_\alpha(t_\alpha)$, $a_\beta^\dagger(t_\beta)$, where Greek letters denote states in the one-particle Hilbert space. One usually works with the Fourier transform of 2.4.1, $g_{\alpha\beta}(\omega)$, and writes down the equations in the frequency domain. The knowledge of the one-particle propagator allows one to compute the expectation value on $\left|\Psi_0^A\right\rangle$ of any one-body operator, as well as the ground state energy through the Koltun sum rule, if the Hamiltonian of the system contains only one- and two-particle operators [35]. In order to exactly compute the g.s. energy for a system comprising three-nucleon interactions, the two-body Green's function is needed; however, a good approximation can be obtained with $g(\omega)$ alone with a modified sum rule [5].

A step towards the solution of the very hard task of determining the dressed propagator is the use of perturbation theory in the form of Feynman diagrams [67]. Once a reference state is chosen, e.g. the g.s. of a non-interacting Hamiltonian $H_0 = T + U$, with U a suitable one-body potential, then the dressed propagator can be expanded as a perturbation series on top of the reference Green's function $g^0_{\alpha\beta}(\omega)$. The expansion, that contains an infinite number of Feynman diagrams, is conveniently reorganized into the Dyson equation:

$$g_{\alpha\beta}(\omega) = g^0_{\alpha\beta}(\omega) + \sum_{\gamma\delta} g^0_{\alpha\gamma}(\omega) \Sigma^*_{\gamma\delta}(\omega) g_{\delta\beta}(\omega) \tag{2.4.2}$$

where the irreducible self-energy operator $\Sigma^*_{\gamma\delta}(\omega)$ has been implicitly defined. Fig. 2.6 shows the diagrammatic representation of the Dyson equation and of the first terms of the self-energy. Eq. 2.4.2 is in principle exact, although in practice the self-energy, which itself contains an infinite number of terms, must be somehow approximated. The power of the Dyson equations, however, lies in the fact that any finite number of contributions to $\Sigma^*(\omega)$ corresponds to including an *infinite* number of terms in the expansion of the dressed Green's function $g_{\alpha\beta}(\omega)$: thus the Dyson equation effectively resums an infinite set of diagrams [67].

Actually, SCGF employs a different formulation of the Dyson equation, detailed in Ref. [35], where the reference propagator $g^0(\omega)$ is replaced by the dressed Green's function $g(\omega)$ and inside $\Sigma^*(\omega)$ a subset of the irreducible diagrams, called skeleton diagrams, is included. Such skeletons are themselves expressed in terms of $g(\omega)$, so that $\Sigma^*(\omega) = \Sigma^*\left[g(\omega)\right]$ and everything depends on the dressed propagator, without any reference to unperturbed states. Thus, a truly self-consistent equation is found and is solved recursively, until the convergence between one iteration and the next is reached.

As anticipated, in practical applications the self-energy must be somehow truncated, keeping a finite or infinite subset of diagrams. There are different options for the truncation. The ladder approximation, for example, is well suited for dealing with the strong short-range repulsive cores of nuclear interactions and it allows to perform fully self-consistent calculation in infinite matter [35, 39] [6]. The algebraic diagrammatic construction at order

[5] We closely follow the notation of Ref. [5].

[6] In nuclear matter the finite temperature SCGF method is commonly employed [35, 72]. The main advantage of the finite-T formalism is that it allows to perform fully self-consistent and thermodynamically consistent calculations.

(a) Diagrammatic expansion of the irreducible self-energy for a two-body interaction.

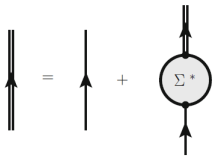

(b) Diagrammatic representation of the Dyson equation 2.4.2. Double lines: dressed propagators $g(\omega)$. Single lines: bare Green's functions $g^0(\omega)$. Taken from Ref. [35].

Figure 2.6

Figure 2.7: Skeleton contribution to the self-energy up to second order in the hypothesis of two-body forces only. Taken from Ref. [71].

n (ADC(n)) [35] approximation, which is based on enforcing the correct analytic properties of the self-energy, is systematically improvable, since, as the order n is increased, one gets closer to the exact answer, that would be recovered in the limit $n = +\infty$ (Fig. 2.8). The ADC(n) is the state of the art method for finite nuclei [5].
The non-perturbative and iterative character of the method makes it difficult to directly estimate the accuracy of a given approximation scheme, which is an important feature of many-body methods such as QMC [34] or perturbation theory (MBPT) [41]. One then resorts to comparing the predictions for the observables such as energies or radii at successive orders in the ADC(n) expansion (Fig. 2.8), in finite nuclei [5], or to comparing the ladder and ADC(2) energies per particle, in nuclear matter.

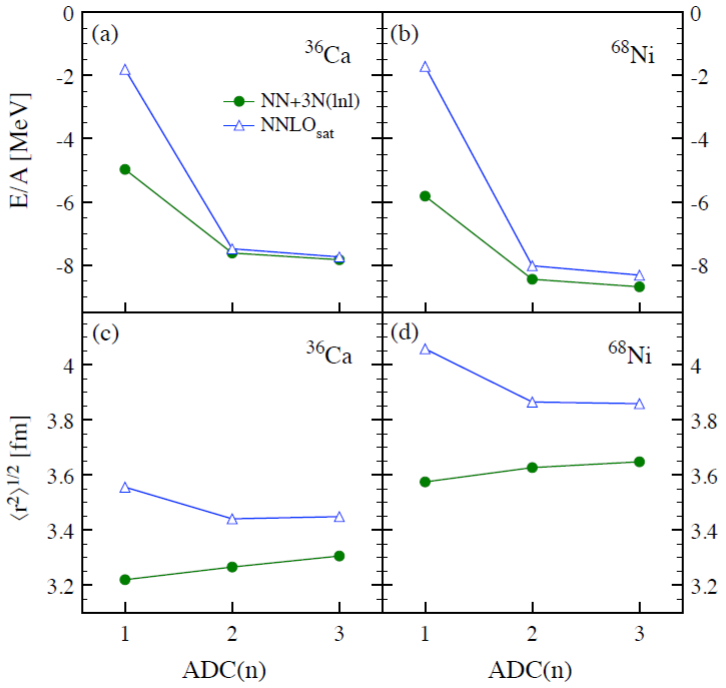

Figure 2.8: Ground state energies (top) and charge radii (down) for the ^{36}Ca and ^{68}Ni nuclei at different orders in the ADC(n) approximation scheme for two different chiral interactions, the "soft" $NN+3N(lnl)$ and the "harder" $NNLO_{sat}$. Taken from Ref. [25].

Chapter 3

Method

In electronic DFT, there exists a well established methodology to construct an energy density functional (EDF) from infinite matter results [10, 16]. In nuclear physics, this approach is less explored, although it may allow to ground the EDFs used in mean field methods in ab initio calculations [17, 73, 74]. In this Chapter, we discuss how a nuclear energy functional based on the equation of state of nuclear matter can be built using the Local Density Approximation (LDA).
Sec. 3.1 motivates this work. Sec. 3.2 introduces the basic properties of infinite nuclear matter. Sec. 3.3 presents the model functions used to interpolate the numerical calculations of the nuclear matter benchmark equations of state. Sec. 3.4 describes the resulting LDA energy functionals.

3.1 Motivation

Nuclear self-consistent mean field models (Ch. 1) have gradually evolved in an approach close to that of the Density Functional Theory (DFT) of electronic and atomic systems [10–12]. The Hohenberg-Kohn theorems [12, 75] state that the expectation values of all observables on the ground state of an interacting many-particle system can be expressed as *functionals* of the density, or more generally of the densities, of the investigated system, e.g. spin-up and spin-down densities, or in nuclear physics spin and isospin densities. Of paramount importance is the energy density functional (EDF), i.e. the expectation value of the Hamiltonian, whose minimization allows to determine the true ground state of the system. Unfortunately, the energy functional is not known exactly, but, both in condensed matter and in nuclear physics, accurate approximations have been developed [11, 30], making DFT a widely used and very successful tool [76].
In condensed matter, there exists a well-established methodology to construct the EDF "ab initio" from the theory of the homogeneous electron gas (HEG) [10]. The simplest, yet already quite accurate, approximation level is the Local Spin Density Approximation (LSDA), where at each point the exchange-correlation energy $E_{xc}^{LSDA}\left[\rho^{\uparrow},\rho^{\downarrow}\right]$ is assumed to be the same as in a HEG with that density [12]. Critical to the success of the LSDA is that virtually exact Quantum Monte Carlo calculations of the HEG correlation energy are available, as well as accurate interpolation formulas as a function of the density [10]. We also mention that at high densities the Random Phase Approximation provides an exact expression for the HEG correlation energy [12, 67]. Then, a ladder of ever more sophisticated functionals, such as the Generalized Gradient Approximation (GGA), the Meta-GGA and so on, can be constructed by introducing combinations of the gradients of

the densities on top of the LSDA [10, 16]. This "reductionist" approach, pursued mostly by Perdew and collaborators, relies as little as possible on fits to empirical quantities, privileging the use of exact relations and first principle calculations to constrain the EDF [11, 16]. Its main advantage over an "empiricist" approach is that the "ab initio" EDFs guarantee a more uniform accuracy in a wide range of systems [11, 16]. On the other hand, many empirical (also called "hybrid") functionals, tailored for specific domains of application, have been developed and are currently widely used [11].
In nuclear physics, the empirical point of view has mostly been pursued: as discussed in Sec. 1.3, the general structure of the functional is first postulated, then the several parameters it contains are fitted simultaneously on a set of observable quantities, tipically binding energies and charge radii of selected nuclei, and also some infinite matter pseudo-observables [13, 14]. This pragmatic approach has proved quite successful, in particular for the study of ground state and excited state properties of finite nuclei [7, 8, 27]. However, the absence of a guiding principle for systematically developing more accurate functionals, such as the DFT's "Jacob's ladder" of approximations [16] or the perturbative expansion of effective field theories, as well as a bias on the chosen data set, are serious drawbacks. They constitute a limitation, in particular, to the reliability of EDFs predictions concerning systems for which few or no observations are available [15], such as neutron stars, superheavy nuclei or nuclei close to the neutron drip lines [7].
The parallel developments in ab initio theory have been of inspiration to several works that try to push forward the EDF/DFT philosophy. Ref. [15, 74] explore connections with the formalism of effective field theories. In Ref. [73], a method to derive the coupling constants of a Skyrme EDF from an ab initio Hamiltonian has been proposed. Other works [17, 18, 31, 77] make use of ab initio results, in particular infinite matter calculations, to constrain the volume term of the nuclear EDF; then, corrective terms to describe the surface and spin-orbit effects are added on a phenomenological ground and fitted on finite nuclei observables [13].
Although the ab initio results are not yet exact, as they still depend on the microscopic interaction and on the many-body method [19, 21, 22], the availability of first principle calculations of the nuclear matter EoS provides an interesting opportunity for nuclear DFT since, as noticed in Ref. [17], it may allow to replicate the same method used in electronic DFT. In this thesis, we explore the nuclear EDFs obtained in the Local Density approximation (LDA) from the nuclear matter calculations performed with two methods and two different microscopic interactions: the state of the art $NNLO_{sat}$ interaction with the Self-consistent Green's function method [20, 23] (Ch. 4), and the phenomenological interaction $AV4' + UIX_c$ with the Auxiliary Field Diffusion Monte Carlo method [3, 24] (Ch. 5). Using two methods and two interactions, indeed, allows to better understand the potentialities and the limitations of the LDA functionals.
The choice of the potentials is motivated by the following considerations. From the one hand, $NNLO_{sat}$ is the state of the art interaction for finite nuclei calculations, while at the same time it predicts an infinite matter saturation point compatible with the empirical constraints [20, 23, 25]. On the other hand, the $AV4' + UIX_c$ potential is a very simple interaction that, in spite of its simplicity, provides fair results in finite nuclei [24]. It is therefore interesting to test it in infinite matter too; also, its reduced computational weight allows to explore a wider range of densities with the AFDMC method than what is possible with more complicated interactions. Both neutron matter and symmetric matter, which is generally more difficult for AFDMC, are studied.

3.2 Infinite nuclear matter

Nuclear matter is an infinite and uniform system of nucleons interacting through strong interactions only [9, 19, 50]. In spite of being a theoretical construction, nuclear matter is a useful model for several existing systems. Neutron matter, for example, is approximately realized in the interior of neutron stars and studying its properties is an interesting topic at the intersection of astrophysics and nuclear physics [44], while low-density neutron matter has a significant impact on neutron-rich nuclei [19].
Nuclear interactions strongly depend on the isospin composition of the system. Pure neutron matter cannot be bound by strong interactions; neutron stars are compact objects due to the effect of gravitational attraction [78]. On the other hand, symmetric nuclear matter admits an equilibrium state, called the saturation point (see below) and its properties around the saturation density ($\rho_{sat} \approx 0.16\,\mathrm{fm}^{-3}$) can be investigated with the help of laboratory data on finite nuclei [9].
The fundamental quantity that describes nuclear matter is the nuclear Equation of State (EoS), which at zero temperature corresponds to the energy per nucleon as a function of the number densities of neutrons and protons [9] (App. B.1). We adopt the following convention for the nuclear EoS. The number density is named ρ and is equal to the sum of neutron (ρ_n) and proton (ρ_p) densities. The asymmetry parameter β is defined as $\beta = \frac{\rho_n - \rho_p}{\rho}$. It varies between 0 and 1, with $\beta = 0$ corresponding to symmetric nuclear matter (SM) and $\beta = 1$ to pure neutron matter (NM). The energy per nucleon is called $e = E/A$. The equation of state (EoS) is the functional relation $e = e(\rho, \beta)$. In symmetric matter, the EoS has a minimum at the saturation density ($\rho_{sat} \approx 0.16\,\mathrm{fm}^{-3}$). The saturation energy $E_{sat} = e(\rho_{sat})$ is generally thought to be equal to the volume term of the empirical mass formula, $a_V = -16\,\mathrm{MeV}$ [1].
The density dependence of an EoS can be conveniently characterized by a set of coefficients, called empirical parameters [9, 80]. They are defined by an expansion of the EoS around the saturation point in powers of the parameter $x = \frac{\rho - \rho_{sat}}{3\rho_{sat}}$. The empirical parameters, although not directly observable, can be estimated with the help of a theoretical model by means of experiments that study density oscillations in nuclei or in heavy-ion collisions [9, 80]. Thus a (model-dependent) link between the properties of finite nuclei, e.g. nuclear resonances, and of nuclear matter can be established (see below).
The expansion of the symmetric matter EoS defines the empirical parameters in the isoscalar channel [80]:

$$e(\rho, \beta = 0) = E_{sat} + \frac{1}{2} K_{sat} x^2 + O(x^3) \tag{3.2.1}$$

E_{sat} is the already mentioned saturation energy; K_{sat} is called incompressibility of symmetric matter at saturation. More explicitly:

$$E_{sat} = e(\rho = \rho_{sat}) \tag{3.2.2}$$

$$\left.\frac{\partial e}{\partial \rho}\right|_{\rho=\rho_{sat},\beta=0} = 0 \tag{3.2.3}$$

$$K_{sat} = 9\rho_{sat}^2 \left.\frac{\partial^2 e}{\partial \rho^2}\right|_{\rho=\rho_{sat},\beta=0} \tag{3.2.4}$$

[1] Such assumption is however disputed in Ref. [79], where it is suggested that the saturation energy may be about -13 or -14 MeV.

Eq. 3.2.3 defines the saturation density as the minimum point of the EoS.
In finite nuclei, the isospin asymmetry parameter is a small number and it turns out useful to expand the energy per particle with respect to the asymmetry β:

$$e(\rho,\beta) = e(\rho,0) + e_{sym}(\rho)\beta^2 + O(\beta^4) \tag{3.2.5}$$

Odd powers vanish due to the isospin symmetry. At densities close to the saturation, an expansion up to second order in β is quite accurate [9]. The quantity $e_{sym}(\rho)$ is called symmetry energy and is defined in general as [9]:

$$e_{sym}(\rho) = \frac{1}{2}\frac{\partial^2 e}{\partial \beta^2}\bigg|_{\beta=0} \tag{3.2.6}$$

If the quadratic approximation is valid, then:

$$e_{sym}(\rho) \approx e(\rho,1) - e(\rho,0) \tag{3.2.7}$$

i.e. the symmetry energy is given by the difference of the energies per nucleon in NM and SM. An expansion of the symmetry energy with respect to $x = \frac{\rho-\rho_{sat}}{3\rho_{sat}}$ defines the empirical parameters in the isovector channel [80]:

$$e_{sym} = E_{sym} + L_{sym}x + \frac{1}{2}K_{sym}x^2 + O(x^3) \tag{3.2.8}$$

E_{sym} is the symmetry energy at saturation. L_{sym} is called slope parameter, K_{sym} is the incompressibility (or curvature) of the symmetry energy at saturation. They are given by the following formulae:

$$E_{sym} = e_{sym}(\rho = \rho_{sat}) \tag{3.2.9}$$

$$L_{sym} = 3\rho_{sat}\frac{\partial e_{sym}}{\partial \rho}\bigg|_{\rho=\rho_{sat}} \tag{3.2.10}$$

$$K_{sym} = 9\rho_{sat}^2\frac{\partial^2 e_{sym}}{\partial \rho^2}\bigg|_{\rho=\rho_{sat}} \tag{3.2.11}$$

The parameters ρ_{sat}, E_{sat}, E_{sym} and K_{sat} are relatively well constrained [80]. ρ_{sat} and E_{sat} are extrapolated from the semi-empirical mass formula or deduced from theoretical calculations [80]. The symmetry energy E_{sym} is correlated to the excitation energy of the isovector giant dipole resonance (IVGDR) and to the neutron skin thickness, while K_{sat} is related to the energy of the isoscalar giant monopole resonance (ISGMR) [9]. The slope L is linked to E_{sym} as well [9]. The other empirical parameters are still poorly known. See Tab. 3.2.1.

In infinite matter, a local EDF (Sec. 1.3) assumes the simple form:

$$\mathcal{E} = \mathcal{E}_{kin} + \mathcal{E}_{loc} \tag{3.2.12}$$

$\mathcal{E}$ is function of the number densities alone, since the kinetic energy density is related to ρ_q by Eq. 1.3.22. Moreover, since the densities are uniform, the energy per particle $e = E/A$ is simply related to the energy density by:

$$e = \frac{E}{A} = \frac{E}{V}\frac{V}{A} = \frac{\mathcal{E}}{\rho} \tag{3.2.13}$$

	$\rho_{sat}\,(\mathrm{fm}^{-3})$	$E_{sat}\,(\mathrm{MeV})$	$K_{sat}\,(\mathrm{MeV})$	$E_{sym}\,(\mathrm{MeV})$	$L_{sym}\,(\mathrm{MeV})$	$K_{sym}\,(\mathrm{MeV})$
Average	0.1543	-16.03	251	33.30	76.6	-3
σ_{tot}	0.0054	0.20	29	2.65	29.2	132

Table 3.2.1: Estimates of the empirical parameters from an analysis of the results of phenomenological approaches. Taken from Ref. [80].

with V being the fictitious volume of the system. Likewise, the kinetic energy per particle is defined as $t = \frac{\mathcal{E}_{kin}}{\rho}$ and the potential energy per particle as $v = \frac{\mathcal{E}_{loc}}{\rho}$, so that the energy per particle is assumed to be:

$$e(\rho, \beta) = t(\rho, \beta) + v(\rho, \beta) \tag{3.2.14}$$

$t(\rho, \beta)$ represents the kinetic energy per particle of a free non-relativistic Fermi gas [80]:

$$t(\rho, \beta) = \frac{t_{sat}}{2}\left[(1+\beta)^{\frac{5}{3}} + (1-\beta)^{\frac{5}{3}}\right]\left(\frac{\rho}{\rho_{sat}}\right)^{\frac{2}{3}} \tag{3.2.15}$$

where

$$t_{sat} = \frac{3\hbar^2}{10m}\left(\frac{3\pi^2}{2}\right)^{\frac{2}{3}}\rho_{sat}^{\frac{2}{3}} \approx 22\,\mathrm{MeV} \tag{3.2.16}$$

t_{sat} is the kinetic energy per particle of symmetric matter at saturation density, $t_{sat} = t(\rho = \rho_{sat}, \beta = 0)$. The potential energy per particle $v(\rho, \beta)$ follows immediately from the energy density $\mathcal{E}_{loc}$:

$$v(\rho, \beta) = \frac{\mathcal{E}_{loc}(\rho, \beta)}{\rho} \tag{3.2.17}$$

Both ab initio method, e.g. SCGF [20, 72], AFDMC [3, 19] and Brükner Hartree-Fock (BHF) [22, 58], and mean field methods [9, 80] have been used to study the nuclear matter EoS. However, the EoS is still only partially known. The main contribution to the large error bars is due to choice of the nuclear interaction [9, 20, 42, 81, 82], but in ab initio theory, the choice of the many-body method also contributes to the spreading [22, 46] (Fig. 3.1). As a general rule, the uncertainty on the EoS grows as the density increases [19, 20, 42]. In this work, we will assume the Hamiltonian exact and consider only the uncertainties associated to the theoretical calculation.

3.3 Model equations of state

Several different parametrizations of the EoS of nuclear matter have been proposed in the literature. For example, standard Skyrme energy functionals 1.3.3 produce an EoS of the form:

$$e(\rho, \beta = 0, 1) = a\rho^{2/3} + b\rho + c\rho^{5/3} + d\rho^{1+\alpha} \tag{3.3.1}$$

The actual coefficients are reported in Ref. [14]. A reasonable expectation is that also the ab initio EoS may be reasonably approximated with a few terms. The analytic expression used to fit the EoS is important in extrapolations to neutron stars or to finite nuclei [77]. For example, in Ref. [19] the QMC results for neutron matter are well interpolated by the

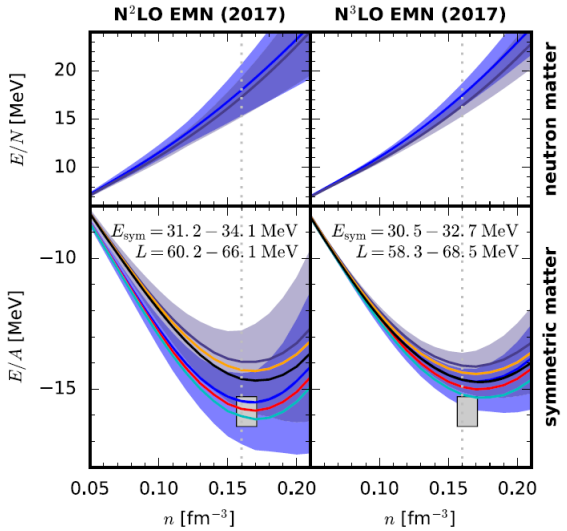

(a) EoS in NM (top) and SM (bottom) based on chiral interactions at N2LO (first column) and N3LO (second column). Taken from Ref. [42].

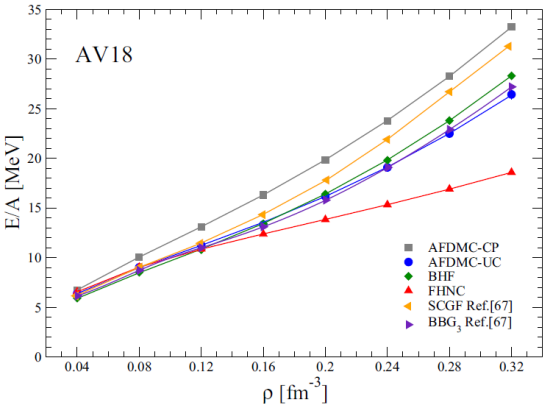

(b) Neutron matter EoS obtained with the $AV18$ NN interaction by means of several different many-body methods. Taken from Ref. [22].

Figure 3.1: Left: neutron and symmetric matter EoS with different chiral interactions and theoretical uncertainties [42]. Right: neutron matter EoS with different many-body methods [22].

function $e(\rho) = a\left(\frac{\rho}{\rho_{sat}}\right)^{\alpha} + b\left(\frac{\rho}{\rho_{sat}}\right)^{\beta}$ with a, b, α, β fitting parameters. In other works, the EoS is split into the sum of a kinetic (free Fermi gas) term $t(\rho, \beta)$ and a potential term $v(\rho, \beta)$, then $v(\rho, \beta)$ is postulated to be quadratic in the isospin asymmetry and, at fixed β, it is expressed as a polynomial of the total density ρ [80] or of the Fermi momentum $k_F \propto \rho^{\frac{1}{3}}$ [77]. In Ref. [18], a k_F-expansion is conjugated with a quartic dependence on β. The coefficients are fixed either by relating them to the empirical parameters or by fitting the theoretical data points.

In this work, we split the EoS as the sum of the free Fermi gas kinetic energy per particle $t(\rho, \beta)$ 3.2.15 and a potential term $v(\rho, \beta)$:

$$e(\rho, \beta) = t(\rho, \beta) + v(\rho, \beta) \tag{3.3.2}$$

This separation will be helpful in the construction of the nuclear EDF. Then, we assume that $v(\rho, \beta)$ depends quadratically on the isospin asymmetry, since this has been shown to be a reasonable approximation around saturation density even for large asymmetries [9]. Finally, we assume that the potential energy per particle can be expressed as a polynomial of k_F or $\rho^{\frac{1}{3}}$: this ansatz is suggested by the importance of the Fermi momentum in the description of infinite systems of fermions as well as by its greater flexibility with respect to e.g. an expansion in integer powers of ρ. Also, it is in keeping with the necessity of introducing fractional powers of ρ in order to achieve a proper saturation in EDF models [30]. Thus $v(\rho, \beta)$ will be written in general as:

$$v(\rho, \beta) = \sum_{\gamma} c_{\gamma}(\beta)\rho^{\gamma} \tag{3.3.3}$$

The theoretical EoS of both neutron and symmetric matter will be used to determine the potential term. The assumed quadratic isospin dependence implies that at any interme-

diate asymmetry β the coefficients $c_\gamma(\beta)$ are given by:

$$c_\gamma(\beta) = c_\gamma(0) + \left[c_\gamma(\beta = 1) - c_\gamma(\beta = 0)\right]\beta^2 \tag{3.3.4}$$

We introduce the following notation: $c_{\gamma,0} \equiv c_\gamma(\beta = 0)$ and $c_{\gamma,1} \equiv c_\gamma(\beta = 1) - c_\gamma(\beta = 0)$. As a consequence, we can write:

$$c_\gamma(\beta) = c_{\gamma,0} + c_{\gamma,1}\beta^2 \tag{3.3.5}$$

$c_\gamma(0)$ and $c_\gamma(1)$ are the coefficients characterizing symmetric matter and neutron matter respectively. We do not choose a priori which powers γ should enter the model EoS, but explore a wide set of polynomial of k_F with a variable number of terms. Each model is fit to symmetric and neutron matter data separately, in order to fix the parameters $c_{\gamma,0}$ and $c_{\gamma,1}$. Then, the χ^2 will be used as a quality measure to choose the best model [83]. For a given model function with a given set of exponents $\{\gamma\}$, the optimal values of the parameters $c_\gamma(0)$ and $c_\gamma(1)$ are determined fitting separately the EoS of symmetric and neutron matter respectively. The input EoS are the sets of data points $\{(\rho_i, e_i(\beta = 0))\}$ and $\{(\rho_i, e_i(\beta = 1))\}$. The optimization is based on the standard χ^2 minimization [83], performed numerically using the Python library LMFIT [84]. This amounts to minimizing the cost functions:

$$\chi^2\big(\{c_\gamma(\beta = 0)\}\big) = \sum_i \left(\frac{e(\rho_i, 0) - e_i(\beta = 0)}{\sigma_i}\right)^2 \tag{3.3.6}$$

$$\chi^2\big(\{c_\gamma(\beta = 1)\}\big) = \sum_i \left(\frac{e(\rho_i, 1) - e_i(\beta = 1)}{\sigma_i}\right)^2 \tag{3.3.7}$$

We have highlighted the dependence of the χ^2 on the coefficients c_γ. σ_i stands for the uncertainty or statistical weight on the i-th energy value. Only few many-body methods directly provide an estimate of the uncertainty, e.g. QMC, while many others do not. In the latter case, one must resort to more or less empirical consideration in order to assign a reasonable theoretical error on each datum [85]. See Ch. 4 for a discussion of the problem in the case of the SCGF method.

3.4 LDA energy functional

DFT provides the simplest way to define an energy functional grounded on the ab initio EoS of nuclear matter through the Local Density Approximation (LDA) [10, 86]. In LDA, one assumes that the same expression of the potential energy density valid in infinite matter holds for non-uniform densities $\rho_q(\mathbf{r})$ too. This is an approximation for slowly varying density distributions, so that each small region of a generic (finite or infinite) system can be treated as a piece of bulk matter [10]. In the nuclear case, this means that the potential energy density $\mathcal{E}_{loc}(\mathbf{r})$ 3.2.12 can be approximated as:

$$\mathcal{E}_{loc}\left[\rho(\mathbf{r}), \beta(\mathbf{r})\right] = \rho(\mathbf{r}) v\left[\rho(\mathbf{r}), \beta(\mathbf{r})\right] \tag{3.4.1}$$

and more explicitly:

$$\mathcal{E}_{loc}\left[\rho(\mathbf{r}), \beta(\mathbf{r})\right] = \sum_\gamma c_\gamma\left(\beta(\mathbf{r})\right)\rho^{\gamma+1}(\mathbf{r}) = \sum_\gamma \left[c_{\gamma,0} + c_{\gamma,1}\beta(\mathbf{r})^2\right]\rho^{\gamma+1}(\mathbf{r}) \tag{3.4.2}$$

The total binding energy, including the Coulomb contribution 1.3.6, is given by:

$$E_{LDA} = E_{kin} + E_{loc} + E_{Coul} \tag{3.4.3}$$

Its expression is different from the standard Skyrme functionals, as it has a richer dependence on the number density, while the effective mass coincides with the bare mass, $m_q^*(\mathbf{r}) = m$, due to the lack of $\rho\tau$ terms. Obviously, it does not contain surface contributions. Thus, the mean field equations are simpler than 1.3.19, and read:

$$\left[-\frac{\hbar^2}{2m}\Delta + U_q(\mathbf{x}) + U_{Coul}(\mathbf{r})\delta_{q,p}\right]\phi_j(\mathbf{x}) = \epsilon_j\phi_j(\mathbf{x}) \tag{3.4.4}$$

The expression of the nuclear mean field $U_q(\mathbf{r})$ is derived in the Sec. C.1:

$$U_q(\mathbf{r}) = \sum_\gamma \Big[\,(\gamma+1)\,c_{\gamma,0} + 2\beta\,(\tau_z-\beta)\,c_{\gamma,1} + (\gamma+1)c_{\gamma,1}\beta^2\Big]\rho^\gamma \tag{3.4.5}$$

where $\tau_z = +1$ for neutron and $\tau_z = -1$ for protons. The Coulomb term in Slater approximation is given by Eq. 1.3.18. We have solved the equations with the skyrme_rpa code [32], that allows to solve the HF equations in spherical symmetry using Skyrme effective interactions. We have suitably modified the code in order to use the non-standard EDF here presented. In Sec. C.2 and C.3, the expression for the rearrangement energy is derived and a preliminary numerical test is shown.
The LDA EDF 3.4.3 is based on nuclear matter calculations only and does not contain any information on finite nuclei. By construction it reproduces well the underlying EoS, thus, if the latter is compatible with the empirical constraints, the EDF will be too. This feature is not trivial, as for example only a restricted number of Skyrme models is compatible with nuclear matter constraints [81]. On the other hand, we do not know how it will perform in nuclei. In electronic DFT, for example, the LDA performs surprisingly well, given its simplicity [10]. In our case, we expect that it may be more accurate in heavier nuclei than in lighter ones, since the surface contributions get relatively less relevant as the mass number increases [26].

Chapter 4

Nuclear energy functionals based on the $NNLO_{sat}$ interaction

The $NNLO_{sat}$ [23] is a state-of-the-art chiral interaction, whose popularity stems from the fact that is perhaps the only chiral potential that allows to reproduce binding energies and radii well up to medium-mass nuclei and, at the same time, it is compatible with the empirical nuclear matter saturation point [25]. In the present work, the equations of state (EoS) of symmetric and neutron matter, computed with the self-consistent Green's function method, are used as input to determine a local nuclear energy density functional (EDF) following the method discussed in Chapter 3.
This Chapter is organized as follows. Sec. 4.1 introduces the $NNLO_{sat}$ interaction. Sec. 4.2 describes how the theoretical EoS have been fitted. Sec. 4.3 presents the predictions obtained with the resulting EDF in finite nuclei. In Sec. 4.4, the $NNLO_{sat}$ EDF is compared with an existing Skyrme functional, SkP [87]. Sec. 4.5 summarizes the results.

4.1 Introduction

The $NNLO_{sat}$ [23] by Ekström *et al.* is a very popular chiral interaction, whose peculiarity is that NN and NNN forces are simultaneously optimized on a data set that includes few-nucleon observables as well as properties of selected light nuclei such as carbon and oxygen isotopes. This choice, although being in a sense a violation of the strict EFT paradigm, allows to reach a good description of nuclei up to medium masses, while at the same time the predicted saturation point is relatively close to the empirical region (Fig. 4.1). The $NNLO_{sat}$ interaction is so popular because it is probably the only chiral potential that reproduces both charge radii and binding energies accurately even in heavier nuclei than those on which it has been fitted [25] (Fig. 2.4) [1].
In order to derive the EDF, we take as a starting point the EoS of neutron and symmetric matter obtained with the SCGF method (Sec. 2.4) in Ref. [20]. The SCGF equations are solved at finite temperature using the ladder approximation for the self-energy. The limit $T = 0$ is taken at the end. The finite temperature formalism allows to perform fully self-consistent and thermodynamically consistent calculations [72]. The EoS have been

[1] Recent works show that, however, the energy per particle in neutron matter and the symmetry energy are underestimated [20]. Also, the agreement of $NNLO_{sat}$ with experimental nucleon-nucleon phase shifts is less accurate than that of other interactions [43]. Moreover, it strives to reproduce spectroscopic properties in the *sd* shell below $N = 20$ [25]. Some of these limitations may be related to the fact that $NNLO_{sat}$ is only next-to-next-to-leading order in the chiral expansion [33].

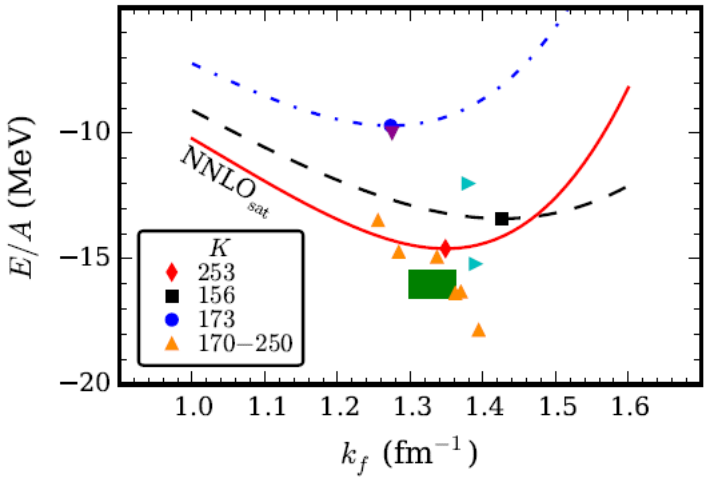

Figure 4.1: Equation of state for symmetric nuclear matter from chiral interactions. Results for $NNLO_{sat}$ are shown in red. Green box: empirical saturation point. Taken from Ref. [23].

computed for densities up to $2\rho_{sat}$, with a step of 0.1 fm^{-3}, and are shown in Fig. 4.2. A first issue to address is that the SCGF method provides no error bars. In order to determine the optimal model EoS with the χ^2 method, however, it is necessary to have an estimate of the uncertainty or weight on each data point (ρ_i, e_i). On an empirical ground, we propose to assign an error that is proportional to the kinetic energy of the free Fermi gas $t(\rho, \beta)$ 3.2.15 at the same density [77]. The motivation is the following: it is known that many-body methods tend to perform worse at higher densities, because stronger correlations develop as the density is increased [39] [2]. Moreover, in light of an application to nuclei, the information on the low-density region is more relevant, thus we want to assign a lower weight to higher density points. This suggests that it may be a good strategy to assign errors σ_i that increase with the density. Instead of using an arbitrary function of ρ, a quite natural choice is then to set the weight proportional to the Fermi gas kinetic energy [77]. A sensible error bar should be a small fraction of the kinetic energy per particle $t(\rho, \beta)$ as $t(\rho, \beta)$ is $\approx 20\,\mathrm{MeV/A}$ at saturation density and $\approx 30\,\mathrm{MeV/A}$ at $2\rho_{sat}$, it may be more to the point to consider uncertainties of around $t/100$, i.e. of a few hundreds of keV/A, compatible to a rough estimates of the theoretical errors on SCGF calculations [20, 39] (Sec. 2.4). Therefore, we will assign weights:

$$\sigma_i = t(\rho_i, \beta)/100 \tag{4.1.1}$$

We note that rescaling all the errors σ_i by a constant factor does not alter the minimum of the χ^2 functions and thus it does not influence the value of the model parameters. However, a sensible estimate of the order of magnitude of uncertainties is important when evaluating the fit quality and comparing different models [85] (Sec. 3.3).

4.2 Fitting the equations of state

In this Section, we present an analysis of the fitting procedure relative to the $NNLO_{sat}$ EoS. We have considered a set of several model functions of the form $e(\rho, \beta) = t(\rho, \beta) +$

[2] At higher densities there is also more disagreement between different many-body methods, see e.g. Ref. [22].

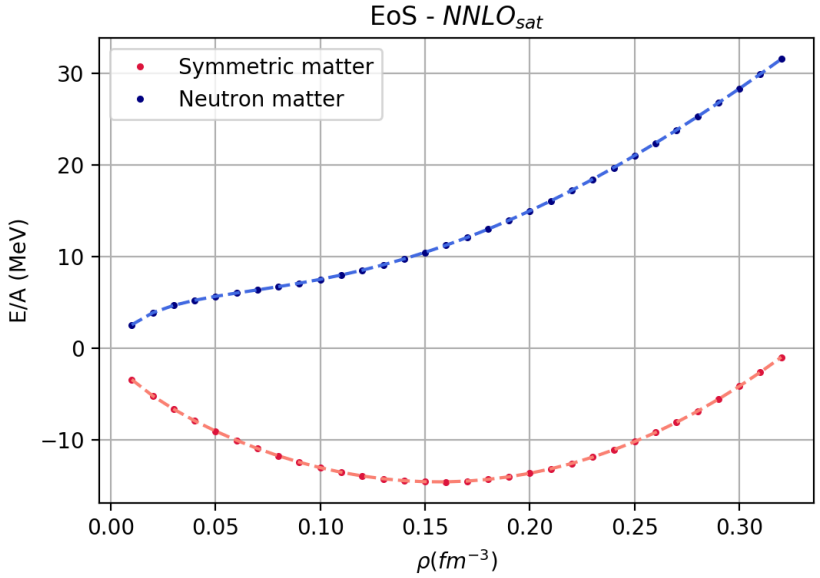

Figure 4.2: Equation of state of symmetric and pure neutron matter obtained with a SCGF calculation using the $NNLO_{sat}$ interaction [20]. Lines are a guide to the eye.

$v(\rho, \beta)$, where $v(\rho, \beta)$ at fixed asymmetry β is a polynomial of the Fermi momentum, or of $\rho^{1/3}$. Each model function has been fitted independently on symmetric matter and neutron matter. See Sec. 3.3 and, in particular, Eqs. 3.3.3 and 3.3.5. We identify each model EoS by the k_F powers it contains. For example, $(2, 3, 4)$ stands for the model with potential $v(\rho, \beta) = c_{\frac{2}{3}}(\beta)\rho^{2/3} + c_1(\beta)\rho + c_{\frac{4}{3}}(\beta)\rho^{4/3}$. The comparison of the different models, which include a different number of terms and different powers of the density, will be based on the reduced χ^2 criterion, but will also involve looking at some predictions related to the model EoS, such as the empirical parameters and binding energies and radii of a few selected doubly magic nuclei.
We have considered all the possible models made of combinations of 2, 3 or 4 powers of k_F between k_F and k_F^6. Each of them has been fitted on the SM and NM EoS and its χ^2 has be computed. The LMFIT library [84] has been employed to perform the fits. Tab. 4.2.1 shows only the models which reproduce the data with $\chi^2_{red} < 2$ in both SM and NM. It appears that 3 terms are necessary to reproduce the data well and 4 are sufficient, the latter leading to very small χ^2_{red}. In this exploratory phase, we prefer to analyze as simple model functions as possible and thus we concentrate on the two 3-parameter models, $(1, 3, 5)$ and $(2, 5, 6)$. Their coefficients are reported in Tab. 4.2.2.

Fig. 4.3 shows the fit residuals $\Delta e = e_{calculated} - e_{input}$ in both SM and NM for the two model EoS of interest (solid lines). The chosen errors 4.1.1 on the input data points are also shown (solid lines). The model EoS are accurate in reproducing the data up to intermediate densities. The discrepancy gets more pronounced at higher densities, which are however comparatively less important for finite nuclei.
It is also interesting to compare the predictions for the empirical parameters (Sec. 3.2 and App. B). From Tab. 4.2.3, it looks that while the saturation density, the saturation energy and symmetry energy are almost independent on the parametrization, the higher-order parameters, which are related to the derivatives of the EoS, are more sensitive to the model function. One would expect that such model-dependence disappears if more terms are included in the fit.

Model	χ^2_{red} (SM)	χ^2_{red} (NM)
(1,3,5)	0.756	1.584
(2,5,6)	1.891	1.285
(1,2,3,4)	1.683	0.035
(1,2,3,5)	0.711	0.149
(1,2,3,6)	0.167	0.415
(1,2,4,5)	0.340	0.334
(1,2,4,6)	0.062	0.641
(1,2,5,6)	0.009	0.903
(1,3,4,5)	0.631	0.302
(1,3,4,6)	0.402	0.470
(1,3,5,6)	0.539	0.491
(1,4,5,6)	1.818	0.204
(2,3,4,5)	0.056	0.440
(2,3,4,6)	0.000	0.623
(2,3,5,6)	0.021	0.686
(2,4,5,6)	0.067	0.577

Table 4.2.1: Reduced χ^2 (χ^2_{red}) relative to the fit to symmetric matter (SM) and neutron matter (NM) EoS (from SCGF calculations with $NNLO_{sat}$ interaction) of the polynomial models enumerated in the first column. Only models having $\chi^2_{red} < 2$ in both SM and NM are shown.

Model	$c_{\frac{1}{3},\frac{2}{3}}(0)$	$c_{1,\frac{5}{3}}(0)$	$c_{\frac{5}{3},2}(0)$	$c_{\frac{1}{3},\frac{2}{3}}(1)$	$c_{1,\frac{5}{3}}(1)$	$c_{\frac{5}{3},2}(1)$
(1, 3, 5)	-18.420	-321.702	526.549	-1.786	-256.643	392.976
(2, 5, 6)	-139.256	-30.649	370.635	-25.766	-164.165	397.578

Table 4.2.2: Coefficients of model functions $(1, 3, 5)$ and $(2, 5, 6)$ determined by a fit to the input $NNLO_{sat}$ EoS. Each coefficient c_γ has dimension [MeV fm$^{3\gamma}$].

Model	ρ_{sat} (fm^{-3})	$E_{sat}\,(MeV)$	$K_{sat}\,(MeV)$	$E_{sym}\,(MeV)$	$L_{sym}\,(MeV)$	$K_{sym}\,(MeV)$
(1,3,5)	0.1516	-14.5700	203.9553	24.8240	33.3689	-99.0119
(2,5,6)	0.1520	-14.5034	196.4594	24.4458	28.6569	-71.8420

Table 4.2.3: Empirical parameters predicted by the model EoS $(1, 3, 5)$ and $(2, 5, 6)$.

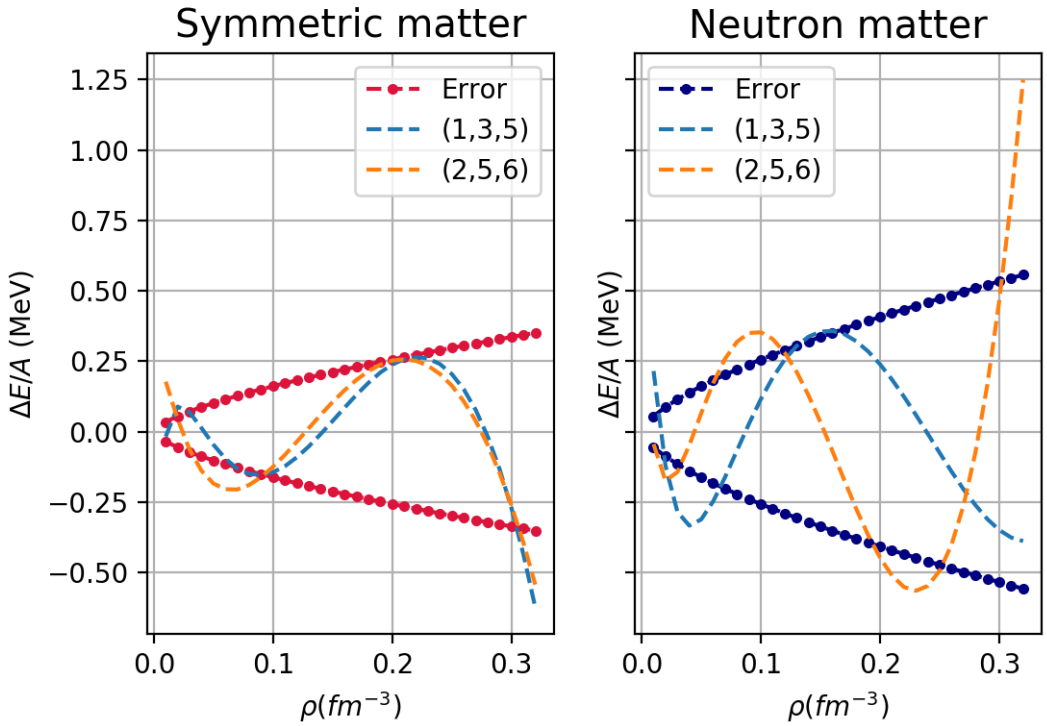

Figure 4.3: Dashed: fit residuals $\Delta e = e_{calculated} - e_{input}$ in SM and NM for the two model EoS $(1, 3, 5)$ and $(2, 5, 6)$. The dots lines denote the error σ_i 4.1.1 on the input points.

As a next step, we test the LDA energy functionals that are obtained from the two model EoS by following the method described in Chapter 3. The Hartree-Fock equations are solved with the skyrme_rpa code [32] under the assumption of spherical symmetry. We study a set of selected doubly magic nuclei (^{16}O, ^{40}Ca, ^{48}Ca, ^{90}Zr, ^{132}Sn, ^{208}Pb) and compare the predicted values for binding energies per nucleon E/A and charge radii r_{ch} with the experimental values (Tab. 4.2.4 and 4.2.5). These EDFs are very simple, thus we cannot expect a very precise agreement with the experimental values or with the available SCGF calculations in finite nuclei. Anyway, charge radii are quite well reproduced; also, the two models give very similar radii (up to a few 10^{-2} fm). Binding energies are farther from experiment, but it is encouraging that the order of magnitude of E/A is correct; also, except for the light ^{16}O nucleus, the discrepancy does not exceed 2 MeV per nucleon (around 20%) in the worst case, that of ^{40}Ca. The LDA EDFs work increasingly better as the mass number increases, with fair results especially for ^{132}Sn and ^{208}Pb. This is coherent with our intuition, as surface contributions, which are absent in the LDA, should have a stronger impact on lighter nuclei than on heavier nuclei [26].
In general, both models overbind the nuclei, as it is expected by LDA EDFs that lack surface terms. On the other hand, charge radii are close to the experimental values. Indeed, if the saturation density is close to the empirical value $\rho_{sat} \approx 0.16\,\mathrm{fm}^{-3}$, then one can expect that the predicted radii be close to the experimental ones [88]. Finally, we observe that both the EDFs considered give similar results, with $(2, 5, 6)$ being perhaps slightly better in predicting radii. Thus, from now on we will thoroughly study only the $(2, 5, 6)$ model.

$E/A\,(MeV)$	^{16}O	^{40}Ca	^{48}Ca	^{90}Zr	^{132}Sn	^{208}Pb
Exp	-7.98	-8.55	-8.67	-8.71	-8.35	-7.87
(1, 3, 5)	-11.20	-10.40	-9.89	-9.41	-8.77	-8.05
(2, 5, 6)	-11.17	-10.36	-9.85	-9.36	-8.73	-8.00

Table 4.2.4: Binding energies. Experimental values are taken from Ref. [89].

$r_{ch}\,(fm)$	^{16}O	^{40}Ca	^{48}Ca	^{90}Zr	^{132}Sn	^{208}Pb
Exp	2.699	3.4776	3.4771	4.2694	4.7093	5.5012
(1, 3, 5)	2.46	3.32	3.48	4.27	4.61	5.73
(2, 5, 6)	2.54	3.32	3.44	4.22	4.75	5.55

Table 4.2.5: Charge radii. Experimental values are taken from Ref. [90].

4.3 Results in finite nuclei

In this Section, we report an analysis of the results obtained in finite nuclei with the functional named $(2,5,6)$, described above in Sec. 4.2. Moreover, we present a comparison of $(2,5,6)$ with the SCGF calculations based on $NNLO_{sat}$ and with the Skyrme functional SkP [87]. SkP is an accurate EDF with effective mass ratio equal to 1 in nuclear matter and close to 1 in finite nuclei; it is thus easier to compare with our LDA EDF, which, lacking $\rho\tau$ terms, has effective mass exactly equal to the bare mass (Ch. 1). We examined even-even nuclei, with a focus on magic nuclei. $(2,5,6)$ and SkP are employed in a Hartree-Fock code [32] under the assumption of spherical symmetry. At this early stage, we do not include pairing terms and we limit our study to nuclei that show a clear shell closure. HF calculations can access the whole nuclear chart; actually, they are generally more reliable in medium-heavy nuclei. SCGF, instead, is computationally intensive and here results performed with the ADC(3) approximation (Sec. 4.1) for nuclei only up to ^{54}Ca are reported [25].

In Fig. 4.4, the binding energies per nucleon for a sample of nuclei between ^{12}O and ^{208}Pb are shown. While SkP and SCGF produce binding energies very close to the experiment, $(2,5,6)$ clearly overbinds all nuclei. The relative discrepancy of the three methods with respect to experiment (from Ref. [89]), shown in Fig. 4.5 as the ratio $(E_k - E_{exp})/|E_{exp}|$ with k standing for the three theoretical methods, makes evident, though, a trend in which the discrepancy decreases as the mass number is increased. This in line with our expectation that surface terms, lacking in the LDA functional $(2,5,6)$, are less relevant in heavier nuclei than in lighter ones; also, it is interesting that the relative discrepancy is no more than about 20% in nuclei with $A \geqslant 34$.

As a second relevant observable, charge radii are compared with the experimental values, taken from Ref. [90], for doubly magic nuclei. The absolute (Fig. 4.6) and relative discrepancies (Fig. 4.7) show that the $NNLO_{sat}$ interaction used in the SCGF method gives extremely accurate predictions for the charge radii; SkP agrees with the experiment well, too, and does so in a very wide mass range. The HF results with the $(2,5,6)$ functional are, perhaps surprisingly, only slightly worse than SkP's, although with opposite sign (smaller nuclei) up to ^{90}Zr. This fact is worth investigating; for now, we remind that $(2,5,6)$ has been constrained on the $NNLO_{sat}$ EoS and, as $NNLO_{sat}$ produces a realistic saturation point in symmetric matter and accurate radii in nuclei [23], there may be a

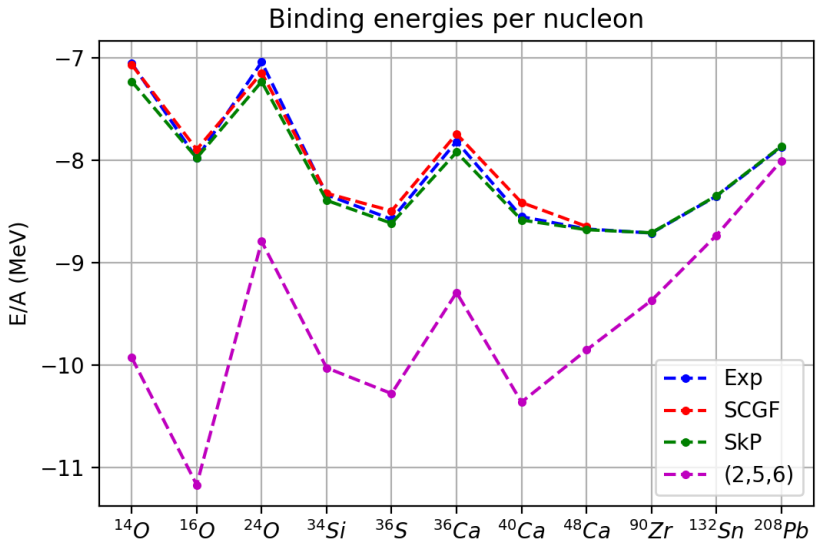

Figure 4.4: Binding energies per nucleon for a sample of even-even nuclei. Experimental values are shown together with HF calculations with the SkP and $(2, 5, 6)$ functionals, as well as SCGF calculations based on the $NNLO_{sat}$ interaction.

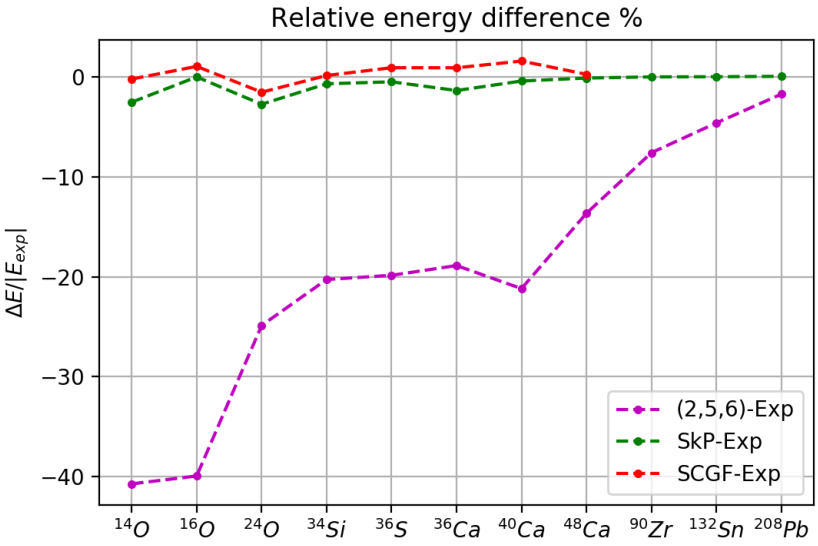

Figure 4.5: Relative discrepancy (%) of theoretical binding energies with respect to the experimental values.

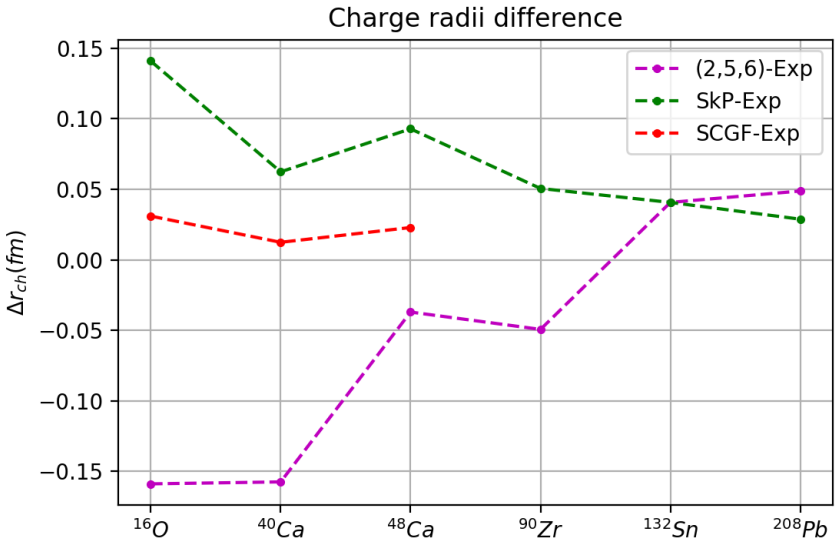

Figure 4.6: Discrepancy between theoretical and experimental values of the charge radii of a set of doubly magic nuclei. Experimental radii are taken from Ref. [90].

link between realistic saturation properties and an accurate reproduction of the nuclear radii. See e.g. Ref. [58].
Then, we show proton and number densities for two magic nuclei, ^{48}Ca (Fig. 4.8) as an example of medium mass nucleus and ^{132}Sn (Fig. 4.9) as a representative heavier mass nucleus. For ^{48}Ca, HF calculations with the functionals SkP and $(2,5,6)$ are reported alongside SCGF results with $NNLO_{sat}$, while for ^{132}Sn only HF results are available. In ^{48}Ca there is a close agreement between SkP and SCGF densities; $(2,5,6)$ densities, on the other hand, show wider oscillations especially in the interior, while the discrepancy is smaller on the surface. The $(2,5,6)$ functional is constructed in such a way as to reproduce well the $NNLO_{sat}$ EoS, but this is not sufficient to obtain a close agreement with $NNLO_{sat}$ results also in finite nuclei: one has to go beyond the local density approximation and include non local terms in order to improve the functional. We suggest that gradient terms such as $|\nabla\rho|^2$ in the EDF may penalize variations in the densities and help smoothing their oscillations. Also, the densities of the ^{132}Sn nucleus show that, compared to SkP, $(2,5,6)$ produces more pronounced spatial variations in the density; naively, one may have expected that differences in the density profiles would reduce in heavier nuclei, but that is not necessary the case.

4.4 Comparing SkP and (2,5,6)

In order to shed light on the role of the non-local or gradient terms, we carry out a comparison between the SkP [87] and the $(2,5,6)$ EDFs. In particular, we consider the trends of the different contributions to the total energy - kinetic, Coulomb, local and non-local (for SkP) energies (see Eq. 1.3.23) - for a set of even-even nuclei. In Fig. 4.10, the kinetic energy per particle E_{kin}/A as a function of the mass number A is shown for calculation with SkP and $(2,5,6)$. The dashed curves represent power laws of the form cA^{γ} fitted on the ^{48}Ca, ^{90}Zr, ^{132}Sn and ^{208}Pb results relative to SkP and $(2,5,6)$. They represent qualitatively the behaviour of the energy per particle with respect to A in

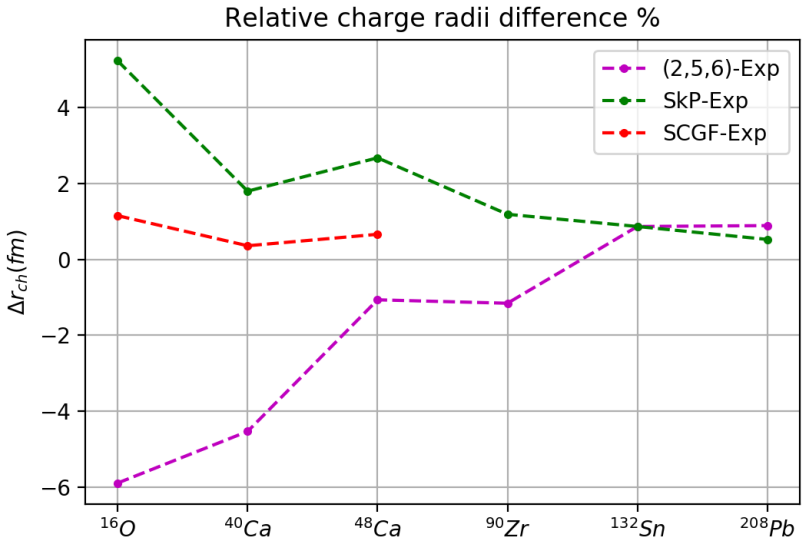

Figure 4.7: Relative discrepancy (%) between theoretical and experimental values of the charge radii of a set of doubly magic nuclei.

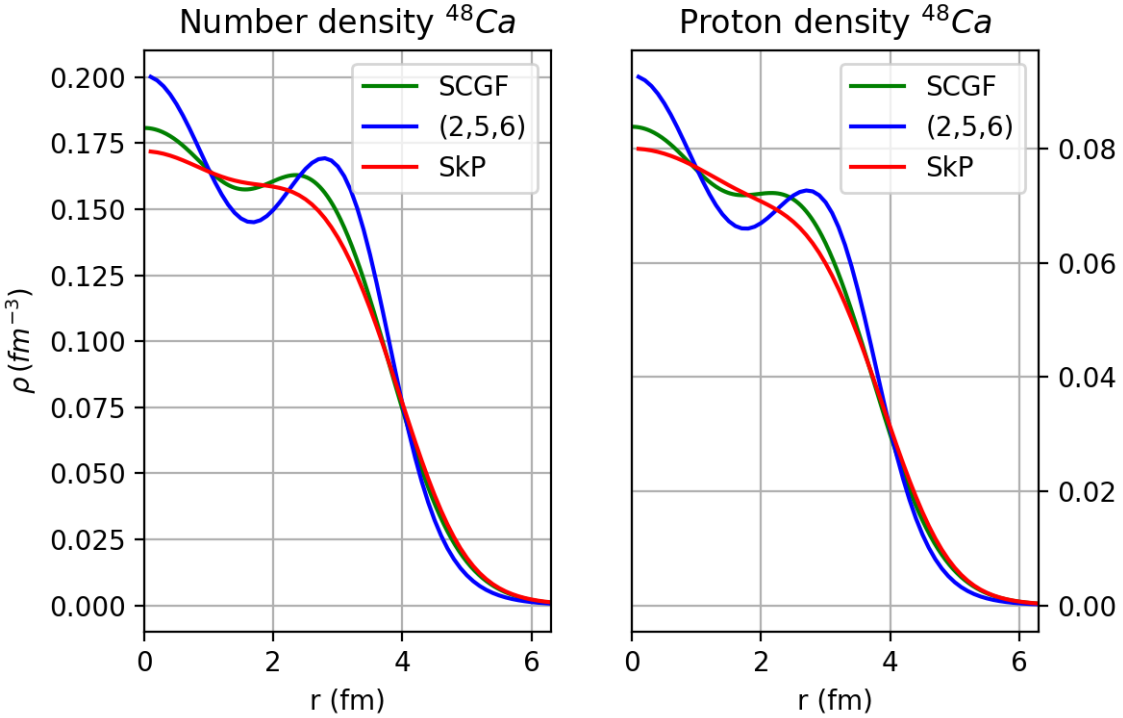

Figure 4.8: Number (left) and proton (right) densities of ^{48}Ca determined with the SkP and $(2, 5, 6)$ energy functionals and with the SCGF method with $NNLO_{sat}$ interaction.

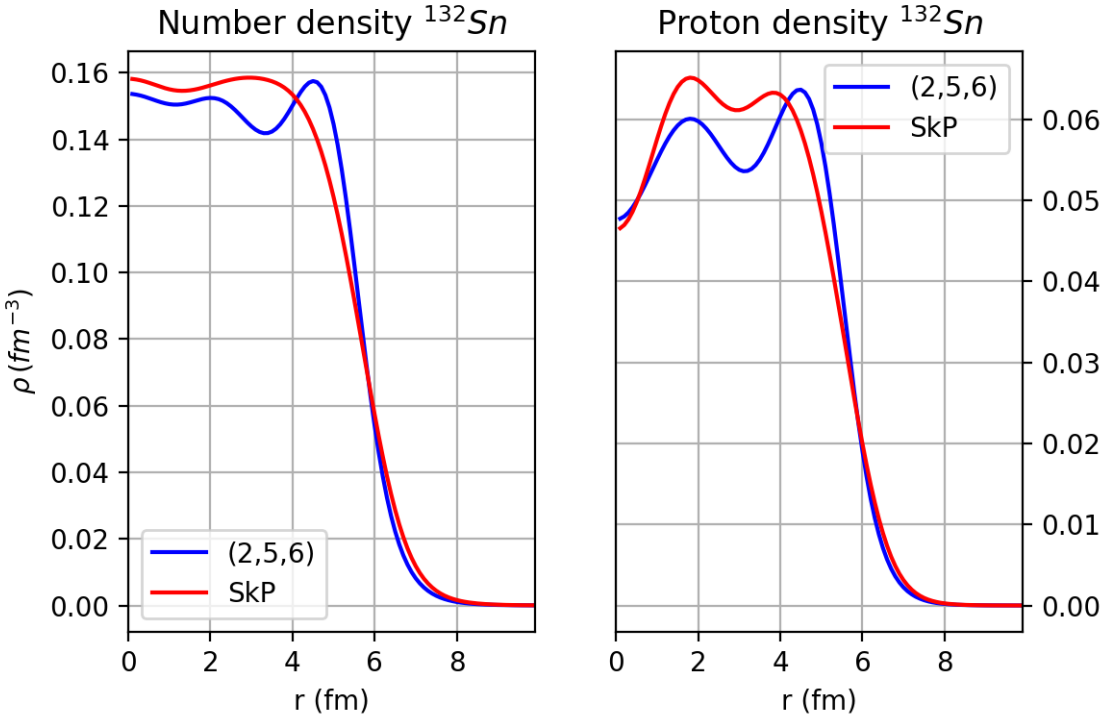

Figure 4.9: Number (left) and proton (right) densities of ^{132}Sn determined with the SkP and $(2,5,6)$ energy functionals.

medium-heavy nuclei. It is easy to see that $(2,5,6)$ predicts higher kinetic energies that SkP, with the difference slightly shrinking as A increases.
In Fig. 4.11, the Coulomb energy per particle E_{Coul}/A is shown as a function of $Z^2A^{-4/3}$. From the mass formula we expect a linear trend [6], and this is quite well verified. Also, SkP and $(2,5,6)$ give very similar results, despite the fact that the proton densities show some differences, as one can see in the right panels of Fig. 4.8 and 4.9. The charge radii are also somewhat different (Fig. 4.6).
In the left panel of Fig. 4.12, the local energy per nucleon E_{loc}/A as a function of the mass number A is reported. We defined the local energy in Eq. 1.3.24 as the the sum of the contribution to the total energy due to the ρ and $\tau\rho$ terms of a general local functional 1.3.9. We expect E_{loc} to approximately correspond to the volume term of the mass formula [26]. Thus, E_{loc}/A should be roughly constant, at least for sufficiently heavy nuclei. The dashed curves represent power laws of the form cA^{γ} fitted on ^{48}Ca, ^{90}Zr, ^{132}Sn and ^{208}Pb. The exponents, written in the legend, are small for both SkP and $(2,5,6)$ (0.05 and 0.1), suggesting that E_{loc}/A has actually a mild dependence on A. (Lighter nuclei are much more spread out.) $(2,5,6)$ consistently predicts smaller local energies than SkP, leading in turn to $(2,5,6)$ predicting smaller total energies: as seen in Fig. 4.4, $(2,5,6)$ overbinds all nuclei. The right side of Fig. 4.12 shows the non-local energy contribution, i.e. the sum of the contribution to the total energy due to the $\Delta\rho$ and spin-orbit terms of a Skyrme EDF (Eqs. 1.3.25, 1.3.23). $E_{non-loc}/A$ is a positive quantity and is smaller in heavier nuclei than in lighter ones. Both these properties are characteristic of surface terms, although the scaling with A (dashed line) does not look like the one we would expect from the mass formula, according to which $E_{surface} \sim A^{2/3}$ and $E_{surface}/A \sim A^{-1/3}$.
We have seen that SkP reproduces experimental binding energies well, while $(2,5,6)$ produces overbound nuclei. $(2,5,6)$, compared to SkP, yields higher kinetic energies and

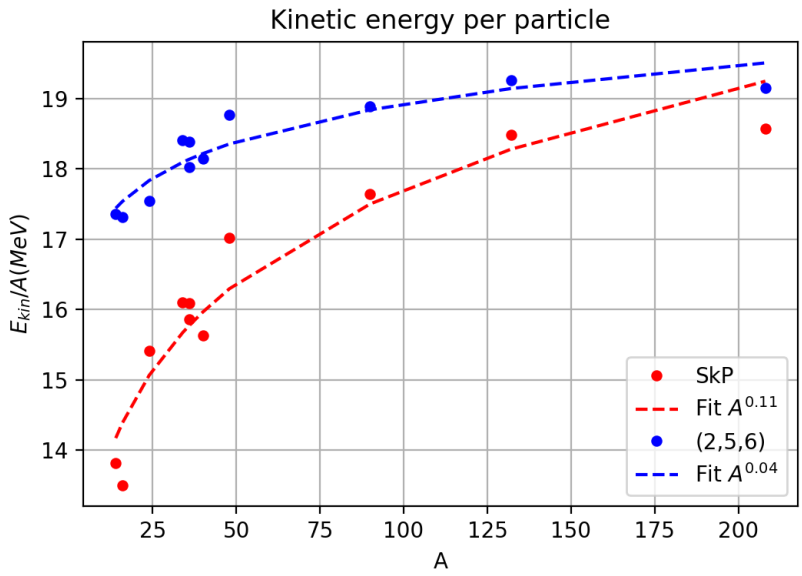

Figure 4.10: Kinetic energy per particle E_{kin}/A as a function of the mass number A for a set of even-even nuclei. HF results with SkP and $(2,5,6)$ functionals are shown Dashed lines are power law fits to SkP and $(2,5,6)$ data for ^{48}Ca, ^{90}Zr, ^{132}Sn and ^{208}Pb.

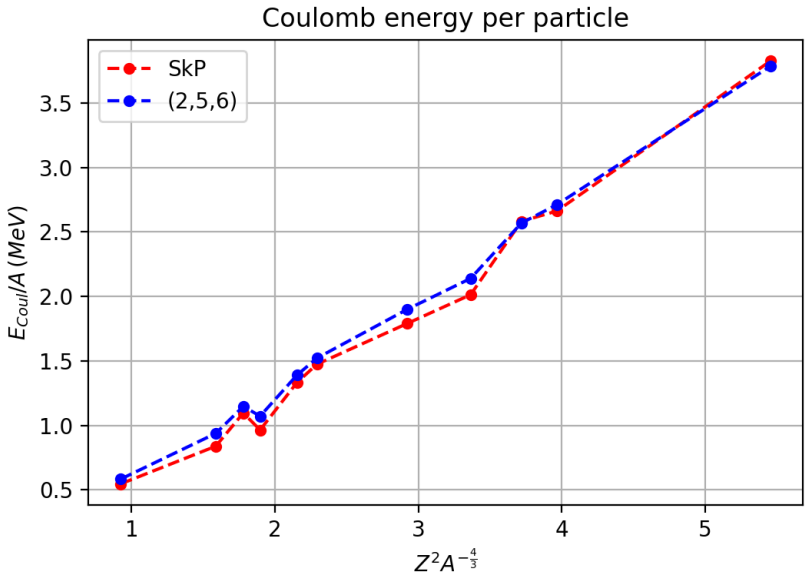

Figure 4.11: Coulomb energy per particle E_{Coul}/A as a function of $Z^2A^{-4/3}$.

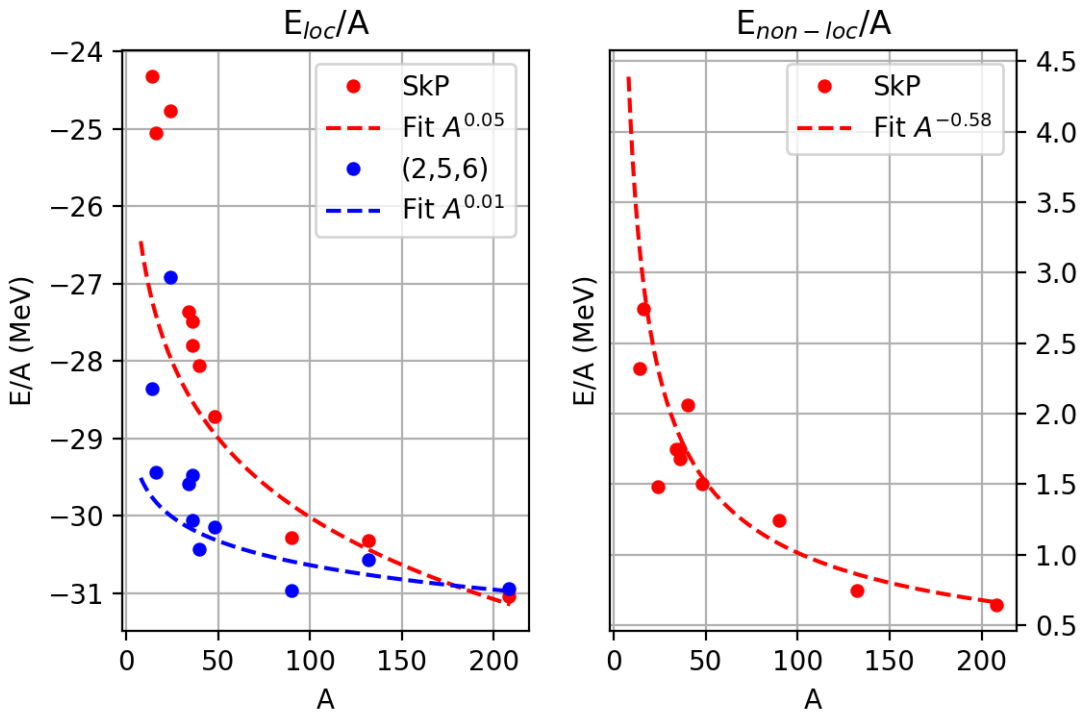

Figure 4.12: Local energy per nucleon (left) and non-local energy per nucleon (right) as a function of the mass number for a set of even-even nuclei. See Eq. 1.3.24, 1.3.25 for definitions. Results obtained in Hartree-Fock approximation with the energy functionals SkP and (2,5,6) are shown. Dashed lines are power law fits to ^{48}Ca, ^{90}Zr, ^{132}Sn and ^{208}Pb data points.

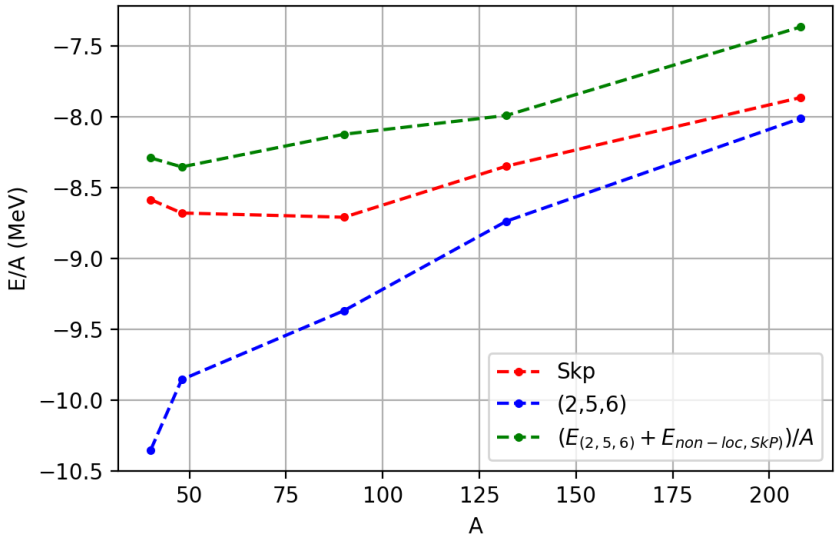

Figure 4.13: Non-local energy per nucleon from calculations with the SkP functional (blue) and with $(2,5,6)$ (red). In green, the sum of the $(2,5,6)$ binding energy per nucleon and the SkP non-local energy per nucleon is shown. See text for details.

lower local energy contributions. As a simple numerical experiment. we add to the $(2,5,6)$ binding energy the SkP non-local energy. In Fig. 4.13, we compare this quantity, $\frac{E_{(2,5,6)}+E_{non-loc,SkP}}{A}$ (green line), to the binding energies per nucleon obtained with SkP (red) and (2,5,6) (blue). In this way, we can see that simply adding the non-local energy contribution of SkP to the LDA functional $(2,5,6)$ leads to underbound nuclei. The energy surplus is approximately 0.5 MeV per nucleon and it does not vary much with the mass number. We suggest expect that the optimal gradient terms on top of $(2,5,6)$ should be somewhat smaller than those of SkP.

4.5 Conclusion

We have applied the method described in Ch. 3 to derive a LDA EDF based on the $NNLO_{sat}$ interaction [23]. We have made use of the EoS obtained with the SCGF method in Ref. [20]. A good fit to the EoS of both NM and SM is provided by the three-parameters model named $(2, 5, 6)$, whose potential energy per particle 3.3.3 has the form $c_{2/3}\rho^{2/3} + c_{5/3}\rho^{5/3} + c_2\rho^2$. From this model EoS an EDF has been constructed and thoroughly analyzed, comparing it with the $NNLO_{sat}$ results in finite nuclei [25] and with the well-known Skyrme interaction SkP [87]. Due to the simplicity of the LDA scheme, and in particular to the lack of gradient terms in the energy functional, we cannot expect a very close agreement to experiment. Nonetheless, the $(2, 5, 6)$ EDF reproduces the charge radii with an accuracy close to that of SkP, although far from the impressive performance of the $NNLO_{sat}$ interaction itself. As far as the binding energies are concerned, the LDA EDF is far from the results of the two other interactions, but is is interesting to observe that, while all nuclei are overbound, the discrepancy with the experiment steadily reduces as the mass number is increased: for example, for ^{40}Ca it is about 20%, while in ^{132}Sn and ^{208}Pb it lowers to less than 10%. This is in keeping with the expectation that the surface contributions to the binding energy should be less relevant in heavier nuclei than in lighter ones.

The $(2, 5, 6)$ EDF produces density profiles that are quite similar to those predicted by $NNLO_{sat}$, although the former show wider oscillations that may be smoothed out if gradient terms were introduced. Lastly, in finite nuclei, the $(2, 5, 6)$ EDF predicts higher kinetic energies and lower (local) potential contributions with respect to the SkP interaction.

All considered, the LDA EDF based on the $NNLO_{sat}$ interaction looks a promising "first rug" [16] in the ladder of approximate functionals.

Chapter 5

Nuclear energy functionals based on the $AV4' + UIX_c$ interaction

In this Chapter, we show the results obtained by means of the Auxiliary Field Diffusion Monte Carlo (AFDMC) ab initio method [3] with the phenomenological $AV4' + UIX_c$ potential [48, 51], made up with the nucleon-nucleon interaction Argonne 4 ($AV4'$) plus the the central part of the three-nucleon Urbana IX potential (UIX_c). The $AV4' + UIX_c$ potential, although very simple, provides fair results in finite nuclei [24] and it is thus interesting to test it further on both nuclei and nuclear matter. The equations of state of infinite matter are then used to constrain an energy density functional, following the methodology presented in Ch. 3. This chapter runs in parallel to Ch. 4.
Sec. 5.1 introduces the $AV4' + UIX_c$ interaction. Sec. 5.2 shows the nuclear matter AFDMC calculations and the EDFs we determine from these input EoS. Sec. 5.3 shows the AFDMC results for a set of finite nuclei and a detailed comparison with the performance of the nuclear energy functional. Sec. 5.4 summarizes the results.

5.1 Introduction

The Argonne potentials constitute a family of phenomenological nucleon-nucleon interactions [37, 48] (Sec. 2.2). The $AV18$ interaction is a sophisticated and accurate model made of 18 operators, but due to its complexity requires very large computational resources. Argonne potentials with a simplified operator structure have been devised [48] and have found application in infinite matter calculations, see Ref. [22, 46]. These AVn' potentials contain a subset of n operators of the full $AV18$ interaction, of which they are not simply a truncation, since they are refitted in order to reproduce as many two-nucleon properties as possible [46].
Despite being accurate on NN observables, two-body interactions predict underbound light nuclei and overestimate the saturation density of symmetric matter [50]. It is therefore necessary to introduce three-nucleon interactions to provide a (partial) solution to these issues [58, 91]. The Argonne potential are often combined with phenomenological 3N interactions of the Urbana family [4]. The popular Urbana IX (UIX), for example, contains two contribution: the two-pion exchange Fujita-Miyazawa term and a phenomenological short-range repulsive central term [51]. The UIX potential has two free parameters that are fitted to reproduce the observed ^{3}H binding energy and the empirical saturation density. The three-body potential depends on the chosen NN potential, although in practice the same coefficients as those used with $AV18$ are often employed.

In this Chapter, we consider the particularly simple $AV4'$ NN interaction, complemented by the central term of the phenomenological Urbana IX three-body interaction (UIX_c) [49, 51]. In spite of its simplicity, the $AV4' + UIX_c$ potential has been shown to produce fairly reasonable results in nuclei, with a discrepancy of about 10% with respect to experimental binding energies [24]. It is therefore interesting to test it also in infinite matter. $AV4'$ is computationally light, so that it allows to study a wider range of densities with the AFDMC method than what is possible with more complicated interactions.

The $AV4'$ potential includes only four operators [46]:

$$O_{ij}^{p=1,..,4} = [1, \sigma_i \cdot \sigma_j] \otimes [1, \tau_i \cdot \tau_j] \tag{5.1.1}$$

and lacks the tensor and spin-orbit terms (Sec. 2.2). The central part of the Urbana IX potential, called UIX_c, is a repulsive spin-isospin independent term V^R and is given by [51]:

$$V^R = \sum_{cyclic} V_{ijk}^R = U_0 \sum_{cyclic} T^2(m_\pi r_{ij}) T^2(m_\pi r_{jk}) \tag{5.1.2}$$

where:

$$\begin{aligned} \xi(x) &= 1 - e^{-cx^2} \\ Y(x) &= \frac{e^{-x}}{x} \xi(x) \\ T(x) &= \left(1 + \frac{3}{x} + \frac{3}{x^2}\right) Y(x) \xi(x) \end{aligned} \tag{5.1.3}$$

The $\xi(x)$ are short-range cutoff functions; in the UIX interaction, $c = 2.1\text{fm}^{-2}$. For the U_0 parameter, we use the value $U_0 = 0.0048$ MeV that allows to reproduce the empirical saturation point with the $AV18$ NN interaction [24, 51].

We have performed Auxiliary Field Diffusion Monte Carlo (AFDMC) calculations (Sec. 2.3) in symmetric and neutron matter and in a selected number of nuclei up to ^{90}Zr. The relatively light computational weight of the $AV4' + UIX_c$ potential, indeed, allows to easily study medium-mass nuclei that are out of reach of fully realistic interactions. Our calculations extend the results of Ref. [24] for finite nuclei. The nuclear matter EoS are new; in the literature only calculations with the $AV4'$ alone are available [46]. The resulting EDFs will be compared to the Monte Carlo predictions for finite nuclei and with experiment.

5.2 Equations of state

We have performed AFDMC calculations in infinite matter with the $AV4'$ NN interactions plus the central part of the 3N UIX phenomenological potential (UIX_c). The equations of state are shown in Fig. 5.1 and Tab. 5.2.1 for several densities up to $0.40\,\text{fm}^{-3}$. In the table, the Monte Carlo statistical errors are shown as well. We have used $A = 28$ nucleons in SM and $A = 14$ neutrons in NM. For such a simple potential, the results are already quite reliable when a limited number of particles is used in the simulation box. See Ref. [2], Tab. 8.1, for the "magic numbers" of nucleons in momentum space shells.
The three-nucleon potential has a repulsive effect and is responsible for the saturation of the symmetric matter EoS, which happens at a large density, $\rho_{sat} \approx 0.25\,\text{fm}^{-3}$, quite far from the empirical saturation density $0.16\,\text{fm}^{-3}$. By contrast, the EoS of Ref. [46],

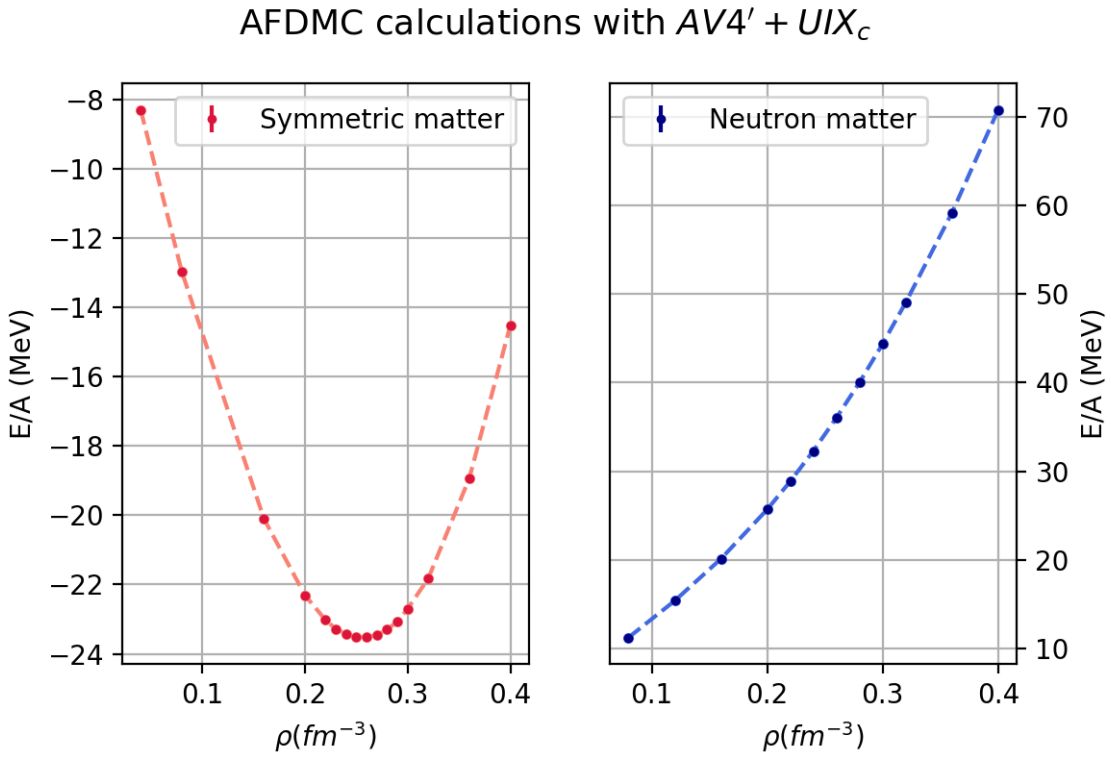

Figure 5.1: Equations of state of symmetric and neutron matter. Calculations are performed with the AFDMC method with the $AV4' + UIX_c$ interaction. Lines are a guide to the eye.

$\rho\,(\mathrm{fm}^{-3})$	SM	NM
0.08	-12.97(8)	11.240(3)
0.12		15.382(4)
0.16	-20.103(5)	20.110(7)
0.20	-22.309(7)	25.67(1)
0.22	-23.024(8)	28.85(1)
0.23	-23.279(8)	
0.24	-23.425(8)	32.28(1)
0.25	-23.521(7)	
0.26	-23.51(1)	36.03(2)
0.27	-23.462(7)	
0.28	-23.30(1)	40.02(2)
0.29	-23.07(1)	
0.30	-22.70(1)	44.36(2)
0.32	-21.83(1)	49.10(3)
0.36	-18.94(1)	59.14(3)
0.40	-14.53(4)	70.74(4)

Table 5.2.1: AFDMC calculations of the energy per particle in symmetric (SM) and neutron (NM) matter with the $AV4' + UIX_c$ potential.

Model	χ^2_{red} (SM)	χ^2_{red} (NM)
(2,3,4,6)	2.571	1.523
(1,2,3,4,5)	1.965	1.460
(1,2,3,4,6)	2.096	1.527
(1,2,3,5,6)	2.293	1.533
(1,2,4,5,6)	2.351	1.520
(1,3,4,5,6)	2.568	1.523
(2,3,4,5,6)	2.185	1.499

Table 5.2.2: Reduced χ^2 (χ^2_{red}) relative to the fit to symmetric matter (SM) and neutron matter (NM) EoS (from AFDMC calculations with the $AV4' + UIX_c$ interaction) of the polynomial models enumerated in the first column. Only models having $\chi^2_{red} < 3$ in both SM and NM are shown.

Model	$c_{\frac{2}{3}}(0)$	$c_1(0)$	$c_{\frac{4}{3}}(0)$	$c_2(0)$	$c_{\frac{2}{3}}(0)$	$c_1(1)$	$c_{\frac{4}{3}}(1)$	$c_2(1)$
(2,3,4,6)	-240.107	572.720	-968.168	820.807	-64.897	102.900	-311.145	574.232

Table 5.2.3: Coefficients of the $(2, 3, 4, 6)$ model determined by fitting the $AV4' + UIX_c$ EoS. Each coefficient c_γ has dimension [MeV fm$^{3\gamma}$].

obtained with the $AV4'$ potential alone, does not saturate. The reduced computational load of the $AV4'$ interaction allows to study a larger number of densities than what is possible by QMC calculations with more sophisticated potentials. In particular, the region around the saturation point can be better explored.
The EoS of NM and SM have been fitted independently with a set of model functions, as described in Sec. 3.3 and 4.2. The analysis follows that of Ch. 4, but, at variance with the SCGF case, here it is not necessary to make assumptions on the uncertainties, as the Monte Carlo calculations provide statistical error bars. In Tab. 5.2.2 the reduced χ^2 are shown for the models that reproduce both the EoS with $\chi^2_{red} < 3$. The four-parameter model $(2, 3, 4, 6)$ interpolates the data points with a quality comparable to that of the five-parameter models. As in Ch. 4, we opt for studying the simplest model. Thus in the following we will analyze only the $(2, 3, 4, 6)$ EDF, whose parameters are reported in Tab. 5.2.3.

We have checked that the choice of the specific function among those in Tab. 5.2.2 has a quite limited impact on the results in finite nuclei, although it significantly affects the value of the higher-order empirical parameters. See also Sec. 4.2). For example, K_{sat} and K_{sym}, which are related to the second derivatives of the EoS, are very sensitive to the analytic form of the equations of state.
Fig. 5.2 shows the fit residuals relative to the $(2, 3, 4, 6)$ parametrization, while in Tab. 5.2.4 its empirical coefficients are presented. As anticipated, the saturation point is located at a very large density, $\rho_{sat} \approx 0.26\,\text{fm}^{-3}$, and a very low energy, $E_{sat} \approx -24\,\text{MeV}$. Both values are far from the empirical saturation region. The other coefficients likewise are not compatible with the experimental constraints. Thus, the $AV4' + UIX_c$ potential, although quite reasonable, despite its simplicity, in finite nuclei [24] (Fig. 5.3), is not apt for an accurate description of nuclear matter. We mention here that refitting the central repulsive three-body term, which depends on a single parameter, may allow the EoS to saturate at a density closer to the empirical saturation density; however, the increased

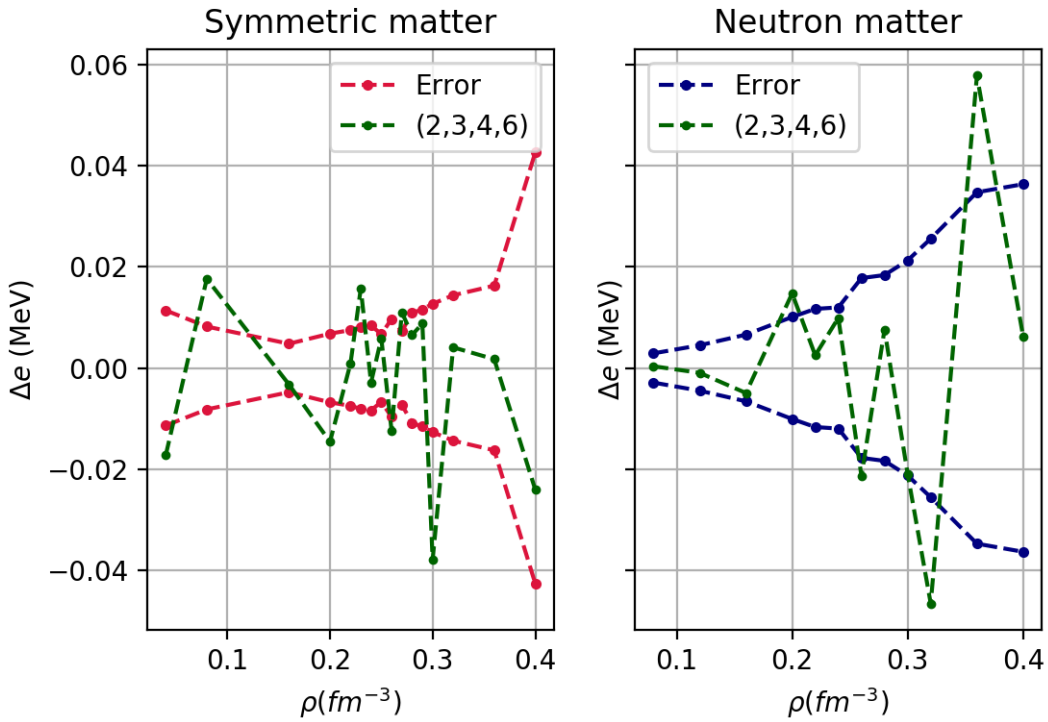

Figure 5.2: Solid lines: fit residuals $\Delta e = e_{calculated} - e_{input}$ in SM and NM. The dashed-dot lines denote the Monte Carlo statistical error σ_i on the input points.

Model	ρ_{sat} (fm^{-3})	E_{sat} (MeV)	K_{sat} (MeV)	E_{sym} (MeV)	L_{sym} (MeV)	K_{sym} (MeV)
(2,3,4,6)	0.2560	-23.5297	472.0717	57.8151	144.3220	-38.5784

Table 5.2.4: Empirical parameters predicted by the model EoS $(2, 3, 4, 6)$.

repulsion would probably lead to excessively underbound nuclei.

5.3 Results in finite nuclei

We have performed AFDMC calculations for several closed-subshell nuclei (in the shell model basis [1]) with the $AV4' + UIX_c$ potential, both with and without the Coulomb potential. We have used as a benchmark the binding energies for $AV4' + UIX_c$ without Coulomb reported in Ref. [24]. We have found a very good agreement (Tab. 5.3.1).
For completeness, we also report the results obtained including the Coulomb interaction: in Fig. 5.3, the experimental binding energies per nucleon and the charge radii are compared with those obtained with Quantum Monte Carlo (QMC). The charge radii are obtained from the proton radii with the empirical formula $r_{ch}^2 = r_p^2 + (0.8\,\text{fm})^2$ [7].

From the model EoS presented in Sec. 5.2 a nuclear EDF is derived as in Sec. 3.3 and tested on finite nuclei. The results are compared with the AFDMC results. All these results refer to calculations performed *without* the Coulomb interaction. What is relevant is to understand to what extent the LDA energy functionals can reproduce in finite nuclei the outcome of the interaction on which the EDFs are based. Fig. 5.4 compares the

[1] A useful tool is `http://calistry.org/calculate/shellModel`.

Nucleus	$AV4' + UIX_c$	Ref. [24]
^{4}He	-25.88(4)	-26.63(2)
^{16}O	-120.5(1)	-119.9(2)
^{40}Ca	-383.2(2)	-383.3(3)
^{48}Ca	-414.0(4)	-413.2(3)
^{90}Zr	-979.2(7)	

Table 5.3.1: AFDMC binding energies for a set of nuclei with the $AV4'+UIX_c$ interaction. We compare our results with those of Ref. [24].

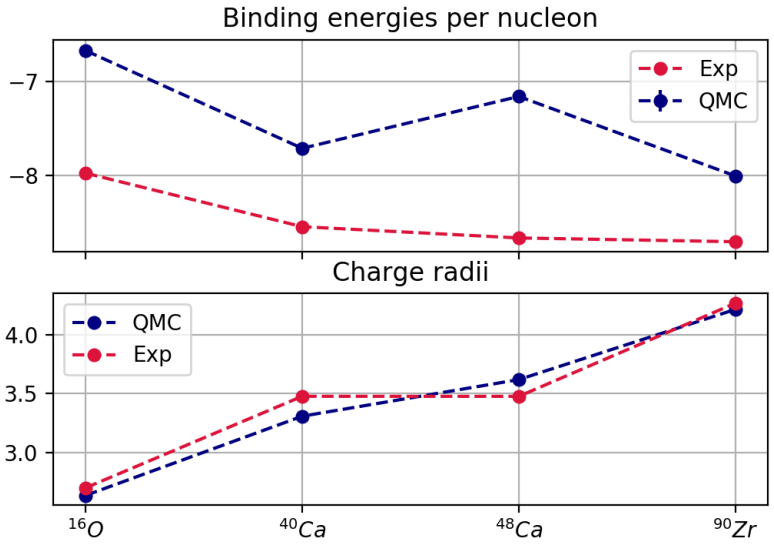

Figure 5.3: Binding energies of a set of magic nuclei. Results from AFDMC calculations with $AV4' + UIX_c$ interaction plus Coulomb potential as well as experimental results are shown. Charge radii are computed from the proton radii with the empirical formula $r_{ch}^2 = r_p^2 + (0.8\,\mathrm{fm})^2$.

QMC and EDF binding energies per nucleon, while Fig. 5.5 shows neutron and proton radii separately. The outcome is puzzling, as both the HF binding energies and radii are strongly underestimated with respect to the QMC results. The binding energies, in particular, are by no means realistic (on average, $E/A \approx -19$ MeV). The densities for the ^{48}Ca and ^{90}Zr nuclei are shown in Fig. 5.6 and 5.7, respectively. The $(2, 3, 4, 6)$ densities differ considerably from the QMC densities: the surface is much steeper and the density profile much more compact, leading to sensibly smaller radii. The central density is also somewhat overestimated.

We try to suggest a possible explanation of the different behaviour of the LDA scheme in the two cases, $NNLO_{sat}$ and $AV4' + UIX_c$. The Argonne potentials belong to a family of "hard" phenomenological interactions, characterized by a very large momentum cutoff and a strong repulsive core at short distances, while the $NNLO_{sat}$ interaction is a relatively "soft" chiral potential [56, 92] (Sec. 2.2). The hard core may induce correlations that necessarily require the introduction of non-local terms 1.3.25 in the nuclear EDF in order to be simulated by DFT calculations. In chiral interactions such as $NNLO_{sat}$, the effects of the repulsive core are milder and thus the LDA may be more appropriate. By

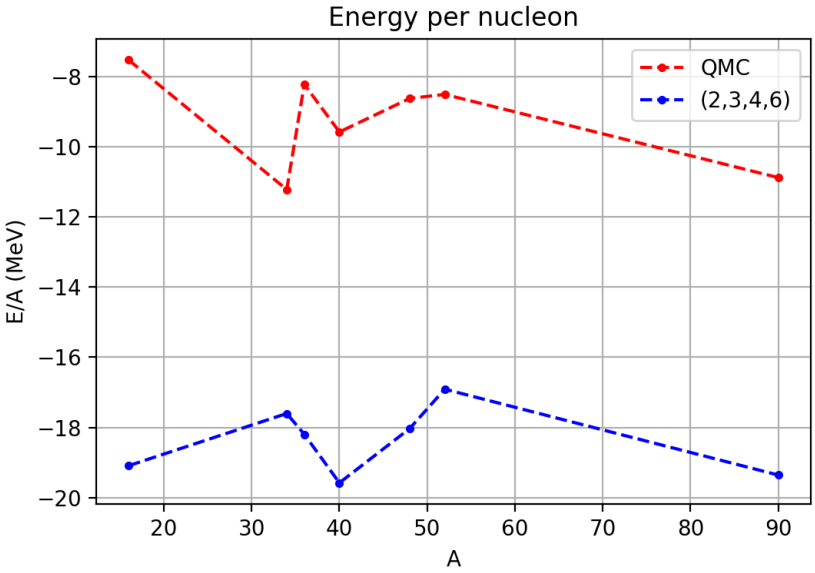

Figure 5.4: Binding energies per nucleon for a sample of even-even nuclei. The QMC results are shown alongside the HF results obtained with the EDF. See text for details.

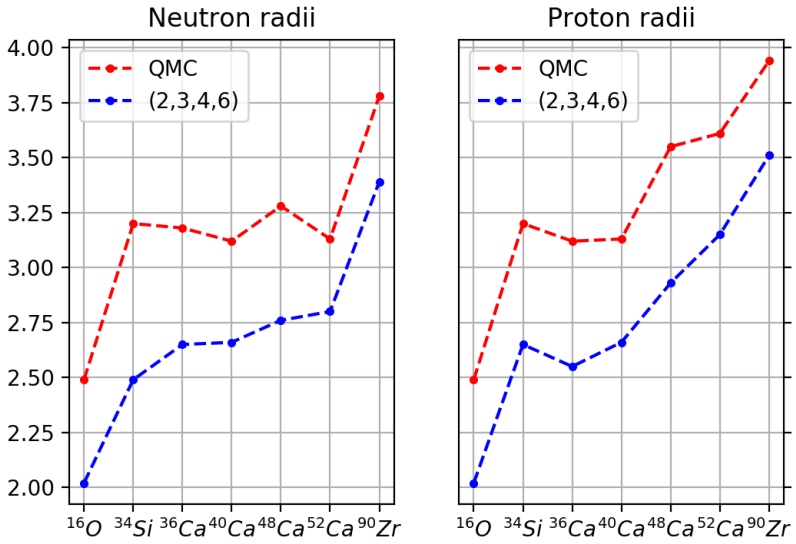

Figure 5.5: Proton and neutron radii for a sample of even-even nuclei. The QMC results are shown alongside the HF results obtained with the EDF.

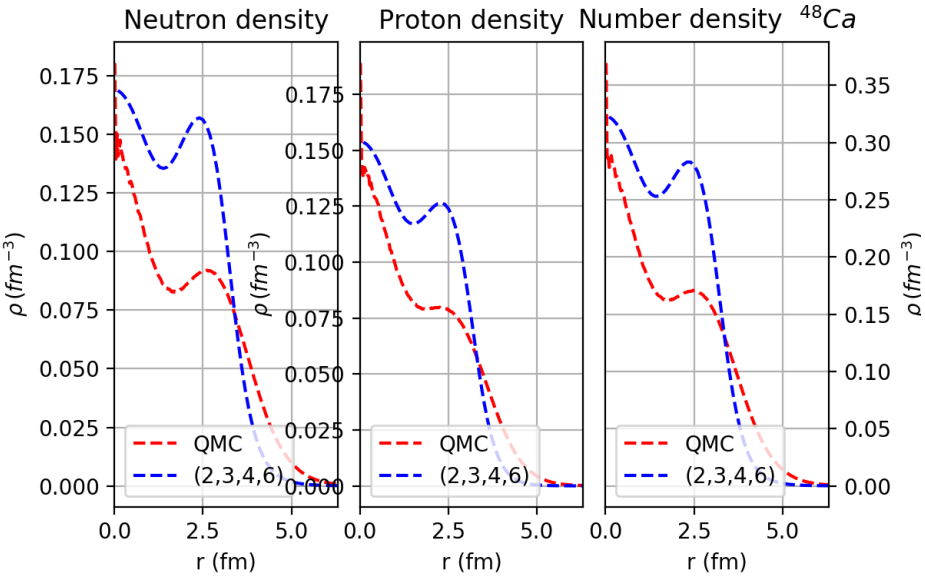

Figure 5.6: Neutron, proton and number densities for the ^{48}Ca nucleus obtained with QMC calculations and with the EDF.

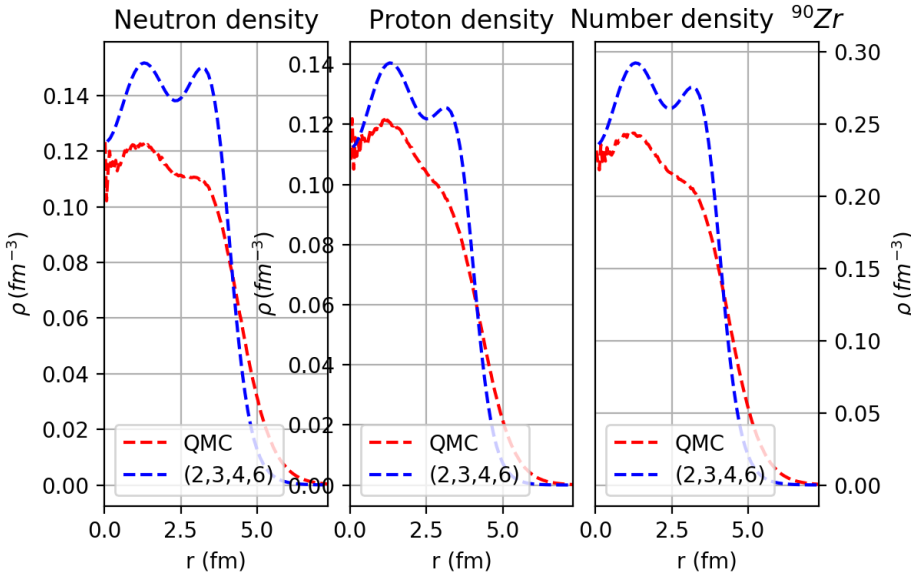

Figure 5.7: Neutron, proton and number densities for the ^{90}Zr nucleus obtained with QMC calculations and with the EDF.

comparing Fig. 5.6 and 4.8, for example, it is apparent that the $AV4' + UIX_c$ interaction produces a much more rapidly varying density profile than $NNLO_{sat}$ (or the SkP EDF), so that the hypothesis behind the LDA [86] (Sec. 3.3) may not be valid.
In order to further explore this possibility, it would be interesting to construct LDA EDFs based on more sophisticated Argonne potential, e.g. $AV6'$ or $AV8'$, or on other soft chiral potentials, and test them on finite nuclei. The study of other Argonne interactions is potentially very important, as it would allow to understand if there exists a relation between the saturation density, that significantly differs between $AV4' + UIX_c$ and the other Argonne+Urbana forces, and the behaviour of the LDA EDFs in finite nuclei.
Also, studying the energy density profile ($\mathcal{E}(r)$ or $4\pi r^2\,\mathcal{E}(r)$) may help understand the weight of bulk vs. surface in the distribution of the binding energy [79], in both the EDF and ab initio results.

5.4 Conclusions

We have performed AFDMC calculations of symmetric and neutron matter and of a set of closed-subshell nuclei with the $AV4' + UIX_c$ interaction and we have noticed that, on the one hand, this potential, in spite of its simplicity, predicts reasonable radii and binding energies in finite nuclei (Fig. 5.3), as already reported in Ref. [24]; on the other hand, it gives rise to clearly unrealistic nuclear matter EoS, with a very high saturation density ($\rho_{sat} \approx 0.26\,\mathrm{fm}^{-3}$) and a low saturation energy ($E_{sat} \approx -24\,\mathrm{MeV}$). This is an instance of the general difficulty of finding a three-body force that allows to reproduce the empirical saturation point and at the same time performs well in finite nuclei [91]. In this case, this issue is particularly evident, due to he simple structure of the $AV4' + UIX_c$ interaction.
In passing, we mention that in infinite matter the AFDMC statistical uncertainties show an increasing trend as the density increases (Fig. 5.2). This is feature common to different many-body methods.
The $AV4'+UIX_c$ EoS have been fitted with polynomial functions of the Fermi momentum k_F. The $(2, 3, 4, 6)$ parametrization has been used to derive a LDA EDF following the method exposed in Ch. 3, which has then been applied to finite nuclei. The comparison of the EDF with the AFDMC results shows extremely large differences: the LDA functional reproduces the $AV4' + UIX_c$ interaction in infinite matter, but not in finite nuclei, that are clearly overbound. Also, the EDF predicts too small radii and rather sharp density profiles. The Local Density Approximation is, in contrast to the $NNLO_{sat}$ case (Ch. 4), clearly inadequate.
A possible explanation of the very different behaviour of the LDA in the two cases (EDFs based on $NNLO_{sat}$ or on $AV4' + UIX_c$) takes into account the fact that the Argonne potentials belong to a family of "hard" phenomenological interactions, characterized by a very large momentum cutoff and a strong repulsive core at short distances, while the $NNLO_{sat}$ interaction is a relatively soft chiral potential [56, 58]. The hard core may induce short-range correlations that are cannot be properly mimicked by the LDA and that require instead the introduction of density gradients. This hypothesis may be further investigated by studying other interactions, e.g. more sophisticated Argonne potentials, and quantities such as the energy density distribution [79].

Chapter 6

Conclusions

In this work, we have explored the possibility of constructing energy density functionals based on ab initio calculations of nuclear matter. We have proposed to interpolate the theoretical EoS of neutron matter and symmetric matter with polynomial functions of the Fermi momentum k_F. Then, we have discussed how a nuclear EDF can be obtained from the nuclear matter results by means of the Local Density Approximation (LDA). We have performed AFDMC calculations with the phenomenological $AV4' + UIX_c$ potential in both nuclear matter and finite nuclei and constructed LDA functionals based on the resulting EoS, as well as on the SCGF EoS obtained in Ref. [20] with the $NNLO_{sat}$ interaction.
In the case of the $NNLO_{sat}$ interaction, the LDA provides quite reasonable results, with a fair reproduction of the charge radii and binding energies. The latter get increasingly closer to experiment as the mass number increases, suggesting that the surface terms, that are absent in the LDA EDF, have a weaker effect in heavier nuclei. In this case, the LDA functional looks like a promising starting point to build more complex and accurate ab initio-motivated nuclear EDFs.
In the case of the $AV4' + UIX_c$ potential, on the other hand, the LDA functional fails to reproduce the Monte Carlo results: it predicts strongly overbound nuclei and at the same time gibes rise to much smaller radii and steeper density profiles. It seems that in this case the LDA ansatz fails to capture the correlations of the microscopic interaction. A hypothesis (Sec. 5.3) is that the very different behaviour in the two cases may be due to the phenomenological $AV4'$ interaction being very hard (large momentum cut-off): the strongly repulsive character at short distances may induce correlations in the many-nucleon wave function that cannot be mimicked by an energy functional that is purely local in the densities. Further work is necessary to prove or disprove this possible explanation. To what extent the introduction of gradient terms in the EDF may improve the outcomes is another interesting open question.
In conclusion, the method discussed in this work to define nuclear EDFs grounded in ab initio EoS suggests that the information contained in nuclear matter is not sufficient to accurately reproduce finite nuclei observables. Gradient and spin-orbit contributions are a necessary element of the nuclear energy functionals. The Local Density Approximation is however, at least for the $NNLO_{sat}$ case, a promising starting point for further explorations and improvements.

There are several possible developments to this thesis. First of all, it would be interesting to study LDA functionals based on different microscopic interaction, e.g. a more sophisticated Argonne potential, such as $AV6'$ or $AV8'$, or a very soft chiral interaction.

This would help to gauge the importance of the hard/soft character of a given potential on the EDF results. Also, it would allow to understand the correlation, if any, between the saturation density of symmetric matter and the behaviour of the EDFs in finite nuclei.
A longer-term goal is to obtain accurate ab initio-based EDFs. The general philosophy of a "step by step" improvement, relying as much as possible on ab initio calculations, can be pushed forward in several respects. In order to constrain the gradient terms (in particular the isovector gradient term), one could study the neutron drops, i.e. neutron matter trapped in a potential well, as suggested by Ref. [93, 94]. An alternative is to study semi-infinite systems (slabs), in analogy to what has been done in condensed matter physics. AFDMC and SCGF are both powerful methods; further useful information may be drawn from a comparison between them.
Lastly, Bayesian techniques may be used to improve the fitting procedure and test the sensibility of the EDFs to variations in the EoS parameters [95].

Appendix A

Derivation of the Hartree-Fock equations

In this Section, we provide a derivation of the basic equations of the Hartree-Fock method. The core of the Hartree-Fock (HF) method lies in the independent-particle picture: one assumes that each particle of a system of A fermions can be described as an independent particle moving in an average potential generated by the interactions with all the other $A-1$ fermions. In nuclear physics, the success of the shell model in explaining qualitatively several properties of the nuclei suggests that an average potential exists [26]. Thus, the starting point amounts to considering an A-particle system with Hamiltonian $H = T+V$, with V a two-body interaction, and assuming the existence of the average Hamiltonian:

$$H^{HF} = \sum_{i=1}^{A} h(i) \tag{A.0.1}$$

We call $|HF\rangle$ the ground state of H^{HF}, with energy $E^{HF} = \langle HF| H |HF\rangle$. The variational principle implies that E^{HF} is an upper limit for the true ground state energy of H. The ground state of H^{HF} is the Slater determinant:

$$|HF\rangle = |\Phi(1...A)\rangle = \prod_{k=1}^{A} c_k^\dagger |0\rangle \tag{A.0.2}$$

where $|0\rangle$ is the vacuum state and $c_k^\dagger$ is the creation operator for an eigenstate k of the single-particle Hamiltonian h. In the coordinate space representation, the one-particle wave functions, $\phi_k(i) = \langle \mathbf{r}_i s_i t_i | k\rangle$, satisfy:

$$h(i)\phi_k(i) = \epsilon_k \phi_k(i) \qquad i = (\mathbf{r}_i, s_i, t_i) \tag{A.0.3}$$

In this representation, the ground state is given by $\phi(1...A) = \det\{\phi_k(i)\}$. $|HF\rangle$ is an approximation to the true ground state wave function.
The strategy is now to calculate the expectation value of H on $|HF\rangle$ and then to minimize it in order to determine the optimal orbitals and HF potential. We roughly follow the derivation of Ref. [26]. In second quantization, the Hamiltonian operator looks like:

$$H = T + V = \sum_{12} t_{12} c_1^\dagger c_2 + \frac{1}{4} \sum_{1234} \bar{v}_{12,34} c_1^\dagger c_2^\dagger c_4 c_3 \tag{A.0.4}$$

where $t_{12} = \langle a| t |2\rangle$ and $\bar{v}_{12,34} = \langle 12| v |34\rangle - \langle 12| v |43\rangle$ are the antisymmetrized matrix elements of the potential. The sums are extended over a generic basis of single-particle states.

It is useful to introduce the density matrix $\rho_{12} = \langle HF| c_2^\dagger c_1 |HF\rangle$. $E^{HF} = \langle HF| H |HF\rangle$ is easier to calculate if we make use of Wick's theorem (see e.g. [67]):

$$\begin{aligned}\langle HF| c_1^\dagger c_2^\dagger c_4 c_3 |HF\rangle &= \langle HF| c_1^\dagger c_3 |HF\rangle \langle HF| c_2^\dagger c_4 |HF\rangle - \langle HF| c_1^\dagger c_4 |HF\rangle \langle HF| c_2^\dagger c_4 |HF\rangle \\ &= \rho_{31}\rho_{42} - \rho_{41}\rho_{32}\end{aligned} \tag{A.0.5}$$

As $\bar{v}_{12,34} = \bar{v}_{12,43}$, the expectation value of the potential finally reads:

$$\langle HF| V |HF\rangle = \frac{1}{2} \sum_{1234} \bar{v}_{1234}\rho_{31}\rho_{42} \tag{A.0.6}$$

Thus the HF energy is:

$$E^{HF}[\rho] = \sum_{12} t_{12}\rho_{21} + \frac{1}{2} \sum_{1234} \rho_{31}\bar{v}_{1234}\rho_{42} \tag{A.0.7}$$

The dependence of E^{HF} on the single-particle density has been highlighted. Its variation is given by:

$$\delta E = E[\rho + \delta\rho] - E[\rho] = \sum_{ij} h_{ij}\delta\rho_{ji} \tag{A.0.8}$$

where the matrix h is defined as:

$$h_{ij} = \frac{\partial E^{HF}[\rho]}{\partial \rho_{ji}} \tag{A.0.9}$$

Inserting Eq. A.0.7, it is easy to show that:

$$h_{ij} = t_{ij} + \sum_{12} \bar{v}_{i1,j2}\rho_{21} \tag{A.0.10}$$

This means that h is a single-particle operator given by the sum of the kinetic energy t and of the *self-consistent field* Γ:

$$\Gamma_{ij}[\rho] = \sum_{12} \bar{v}_{i1,j2}\rho_{21} \tag{A.0.11}$$

Ref. [26] shows that the vanishing of the variation, $\delta E = 0$, implies $[h, \rho] = [t + \Gamma[\rho], \rho] = 0$, thus h and ρ can be diagonalized simultaneously. The Hartree-Fock basis is that in which the two operators are indeed diagonal, leading to the eigenvalue problem for h:

$$h_{ij} = t_{ij} + \sum_{l=1}^{A} \bar{v}_{il,jl} = \epsilon_i \delta_{ij} \tag{A.0.12}$$

while $\rho_{ii} = 1$ for $i \leqslant A$ and $= 0$ otherwise. Eq. A.0.12 is a pretty general form of the HF equations and, although it may look unfamiliar, as in many applications the coordinate space representation is used, it is very compact and will help in deriving a few interesting relations. Also, already at this stage it is clear that HF equations most be solved in an iterative fashion, since the mean field $\Gamma[\rho]$ at the same time determines and is determined by the solution of the HF equations.
Let us start from Eq. A.0.7: in the HF basis, ρ is diagonal, leading to:

$$E^{HF}[\rho] = \sum_i t_i + \frac{1}{2} \sum_{ij} \bar{v}_{ij,ij} \tag{A.0.13}$$

Then, we make use of the mean field equations: setting $i = j$ in Eq. A.0.12 and summing over i, then plugging into the previous expression for E^{HF}, one obtains the following formula for the HF energy:

$$E^{HF} = \frac{1}{2}\sum_i (t_i + \epsilon_i) \tag{A.0.14}$$

In the case the potential depends on the density, $V = V[\rho]$, Eqs. A.0.14 and A.0.10 need to be generalized. Since $E^{HF} = \langle HF| T + V[\rho] |HF\rangle$, the single-particle Hamiltonian is given by:

$$h_{ij} = \frac{\partial E^{HF}[\rho]}{\partial \rho_{ji}} = t_{ij} + \sum_{12} \bar{v}_{i1,j2}\rho_{21} + \langle HF| \frac{\delta v}{\delta \rho_{ji}} \tag{A.0.15}$$

It is easy to show [26] that the total energy includes an additional contribution E_{rea}, called rearrangement energy:

$$E = \frac{1}{2}\left(T + \sum_k \epsilon_k\right) + E_{rea} \tag{A.0.16}$$

where:

$$E_{rea} = -\frac{1}{2}\sum_{ij} \langle HF| \frac{\delta v}{\delta \rho_{ji}} |HF\rangle \rho_{ij} \tag{A.0.17}$$

Appendix B

Relation to empirical parameters

In this Chapter, we investigate how the model EoS presented in Sec. 3.3 are related to the empirical parameters of nuclear matter. In Sec. B.1 we remind some basic concepts of thermodynamics. Then, in Sec. B.2 we derive the expression of the empirical parameters from the polynomial model EoS, while in Sec. B.3 we go in the other direction and show how the model coefficients can be deduced from the knowledge of the empirical parameters.

B.1 Thermodynamics

In this section, we briefly review some elements of thermodynamics and statistical mechanics. The fundamental principle of thermodynamics is the equation which defines the relation between the internal energy E of a given system with the extensive quantities entropy S, volume V and number of particles N_i for every species i of particles:

$$dE = T\,dS - P\,dV + \sum_i \mu_i\,dN_i \tag{B.1.1}$$

The intensive quantities are thus defined: T is the temperature, P the pressure and μ_i the chemical potentials. The internal energy must be considered as a function $E = E(S, V, N_i)$ of the extensive quantities.
Euler relations for homogeneous functions [67] yield the finite expression for $E(S, V, N_i)$:

$$E = TS - PV + \sum_i \mu_i N_i \tag{B.1.2}$$

If the energy is known, e.g. from a quantum-mechanical ground state calculation or a statistical mechanics approach, then Eq.B.1.1 and B.1.2 connects it to macroscopic quantities. If one writes known the general expression for the differential of $E(S, V, N_i)$ and compares to Eq. B.1.1, then it follows that:

$$T = \left(\frac{\partial E}{\partial S}\right)_{V,N_i} \tag{B.1.3}$$

$$P = -\left(\frac{\partial E}{\partial V}\right)_{S,N_i} \tag{B.1.4}$$

$$\mu_i = \left(\frac{\partial E}{\partial N_i}\right)_{S,V,\{N_j\}_{j\neq i}} \tag{B.1.5}$$

As common rule in thermodynamics, we keep note of the variables which are kept fixed when deriving. It is useful to write the pressure as a function of the number density $\rho = \frac{N}{V}$ and of the energy per particle $e = \frac{E}{N}$. First, we derive a simple identity, which relates the derivatives with respect to V and to ρ at fixed number of particles N:

$$\frac{\partial}{\partial V} = \frac{\partial \rho}{\partial V}\frac{\partial}{\partial \rho} = -\frac{N}{V^2}\frac{\partial}{\partial \rho} = -\frac{\rho}{V}\frac{\partial}{\partial \rho} \tag{B.1.6}$$

Then, $E = eN$, thus:

$$P = -\frac{\partial E}{\partial V} = -N\frac{\partial e}{\partial V} = (-N)\left(-\frac{\rho}{V}\frac{\partial}{\partial \rho}\right)e = \rho^2\frac{\partial e}{\partial \rho} \tag{B.1.7}$$

Next, we introduce the compressibility:

$$\chi = -\frac{1}{V}\left(\frac{\partial P}{\partial V}\right)^{-1}_{S,N} \tag{B.1.8}$$

A change of variable from V to $\rho = N/V$, keeping the number of particles fixed, leads, due to the identity $\frac{\partial}{\partial V} = -\frac{\rho}{V}\frac{\partial}{\partial \rho}$, to $\chi = \frac{1}{\rho}\left(\frac{\partial P}{\partial \rho}\right)^{-1}$, or, inserting Eq. B.1.7:

$$\frac{1}{\chi} = \rho^3\frac{\partial^2 e}{\partial \rho^2} \tag{B.1.9}$$

B.2 Calculation of the empirical parameters

In this Section, we derive the explicit expression that derive the model EoS of Sec. 3.3 to the empirical parameters of nuclear matter [80] (Sec. 3.2). We start from:

$$\begin{aligned} e(\rho,\beta) &= t(\rho,\beta) + v(\rho,\beta) \\ v(\rho,\beta) &= \sum_\gamma c_\gamma(\beta)\rho^\gamma \\ c_\gamma(\beta) &= c_{\gamma,0} + c_{\gamma,1}\beta^2 \end{aligned} \tag{B.2.1}$$

where

$$\begin{aligned} t(\rho,\beta) &= \frac{t_{sat}}{2}\left[(1+\beta)^{\frac{5}{3}} + (1-\beta)^{\frac{5}{3}}\right]\left(\frac{\rho}{\rho_{sat}}\right)^{\frac{2}{3}} \\ t_{sat} &= t(\rho_{sat},0) = \frac{3\hbar^2}{10m}\left(\frac{3\pi^2}{2}\right)^{\frac{2}{3}}\rho_{sat}^{\frac{2}{3}} \end{aligned} \tag{B.2.2}$$

We assume that the EoS is known; then the saturation density is promptly obtained by minimizing the energy per particle in symmetric matter, $e(\rho, 0)$.
We split the discussion of the parameters in the saturation (or isoscalar) channel (ρ_{sat}, E_{sat} and K_{sat}) form that of the coefficients in the symmetry (or isovector) channel (E_{sym}, L_{sym}, and K_{sym}).

Isoscalar channel The first and second derivatives of t and v with respect to the density are given by:

$$\frac{\partial t}{\partial \rho} = \frac{2}{3}\frac{t}{\rho} \qquad \frac{\partial^2 t}{\partial \rho^2} = -\frac{2}{9}\frac{t}{\rho^2} \tag{B.2.3}$$

$$\frac{\partial v}{\partial \rho} = \sum_\gamma \gamma c_\gamma(\beta)\rho^{\gamma-1} \qquad \frac{\partial^2 v}{\partial \rho^2} = \sum_\gamma \gamma(\gamma-1)c_\gamma(\beta)\rho^{\gamma-2} \tag{B.2.4}$$

The saturation density is determined by the condition:

$$\left.\frac{\partial e}{\partial \rho}\right|_{\rho=\rho_{sat},\beta=0} = 0 \tag{B.2.5}$$

while saturation energy and incompressibility satisfy:

$$\begin{aligned} E_{sat} &= e(\rho=\rho_{sat},\beta=0) \\ K_{sat} &= 9\rho_{sat}^2 \left.\frac{\partial^2 e}{\partial \rho^2}\right|_{\rho=\rho_{sat},\beta=0} \end{aligned} \tag{B.2.6}$$

Isovector channel The symmetry energy $e_{sym}(\rho)$ 3.2.6 implies that:

$$e_{sym}(\rho) = \frac{1}{2}\left.\frac{\partial^2 e}{\partial \beta^2}\right|_{\beta=0} \equiv t_{sym}(\rho) + v_{sym}(\rho) \tag{B.2.7}$$

where:

$$t_{sym}(\rho) \equiv \frac{1}{2}\left.\frac{\partial^2 t}{\partial \beta^2}\right|_{\beta=0} = \frac{5}{9}t_{sat}\left(\frac{\rho}{\rho_{sat}}\right)^{\frac{2}{3}} \tag{B.2.8}$$

$$v_{sym}(\rho) \equiv \frac{1}{2}\left.\frac{\partial^2 v}{\partial \beta^2}\right|_{\beta=0} = \sum_\gamma c_{\gamma,1}\rho^\gamma \tag{B.2.9}$$

While the potential term is quadratic in β, the kinetic term is not. The formula $e_{sym}(\rho) \approx e(\rho,1) - e(\rho,0)$, however, provides quite an accurate estimate of the symmetry energy. The derivatives of the symmetry energies are:

$$\begin{aligned} \frac{\partial t_{sym}}{\partial \rho} &= \frac{2}{3}\frac{t_{sym}}{\rho} & \frac{\partial^2 t_{sym}}{\partial \rho^2} &= -\frac{2}{9}\frac{t_{sym}}{\rho^2} \\ \frac{\partial v_{sym}}{\partial \rho} &= \sum_\gamma \gamma c_{\gamma,1}\rho^{\gamma-1} & \frac{\partial^2 v_{sym}}{\partial \rho^2} &= \sum_\gamma \gamma(\gamma-1)c_{\gamma,1}\rho^{\gamma-2} \end{aligned} \tag{B.2.10}$$

At the saturation point:

$$t_{sym}(\rho_{sat}) = \frac{5}{9}t_{sat} \qquad \left.\frac{\partial t_{sym}}{\partial \rho}\right|_{\rho_{sat}} = \frac{10}{27}\frac{t_{sat}}{\rho_{sat}} \qquad \left.\frac{\partial^2 t_{sym}}{\partial \rho^2}\right|_{\rho_{sat}} = -\frac{10}{81}\frac{t_{sat}}{\rho_{sat}^2} \tag{B.2.11}$$

Then, the empirical coefficients satisfy the following expressions:

$$E_{sym} = e_{sym}(\rho_{sat}) = \frac{5}{9}t_{sat} + \sum_\gamma c_{\gamma,1}\rho_{sat}^\gamma \tag{B.2.12}$$

$$L_{sym} = 3\rho_{sat}\left.\frac{\partial e_{sym}}{\partial \rho}\right|_{\rho_{sat}} = \frac{10}{9}t_{sat} + 3\sum_\gamma \gamma c_{\gamma,1}\rho_{sat}^\gamma \tag{B.2.13}$$

$$K_{sym} = 9\rho_{sat}^2\left.\frac{\partial^2 e_{sym}}{\partial \rho^2}\right|_{\rho_{sat}} = -\frac{10}{9}t_{sat} + 9\sum_\gamma \gamma(\gamma-1)c_{\gamma,1}\rho_{sat}^\gamma \tag{B.2.14}$$

B.3 From empirical parameters to the model EoS

The relations exposed in the previous section can also be read in another way: the model coefficients c_γ and c_γ^{sym} can be deduced from the empirical parameters, once the exponents γ have been chosen. The relations depend on the number of terms included in the potential B.2.1; a detailed discussion is carried for $N = 3$ terms and results for $N = 2$ are reported. The $N = 3$ potential energy per particle is written as:

$$v(\rho, \beta) = c_\lambda(\beta)\rho^\lambda + c_\mu(\beta)\rho^\mu + c_\nu(\beta)\rho^\nu \tag{B.3.1}$$

where the coefficients $c_\gamma(\beta)$ have the usual form 3.3.5

$$c_\gamma(\beta) = c_{\gamma,0} + c_{\gamma,1}\beta^2 \tag{B.3.2}$$

It is not necessary to impose any other restriction on the coefficients or on the exponents λ, μ and ν, which are assumed to be general. What is going to be shown is that the six model coefficients ($c_{\gamma,0}$, $c_{\gamma,1}$) are in a one-to-one correspondence with six empirical parameters: ρ_{sat}, E_{sat}, E_{sym}, L_{sym}, K_{sat} and K_{sym}.

Isoscalar channel The empirical parameters ρ_{sat}, E_{sat} and K_{sat} can be computed from their definitions 3.2.3, 3.2.2 and 3.2.4. First and second derivatives of t and v are:

$$\frac{\partial t}{\partial \rho} = \frac{2}{3}\frac{t}{\rho} \qquad \frac{\partial^2 t}{\partial \rho^2} = -\frac{2}{9}\frac{t}{\rho^2} \tag{B.3.3}$$

$$\frac{\partial v}{\partial \rho} = \sum_\gamma \gamma c_\gamma(\beta)\rho^{\gamma-1} \qquad \frac{\partial^2 v}{\partial \rho^2} = \sum_\gamma \gamma(\gamma-1)c_\gamma(\beta)\rho^{\gamma-2} \tag{B.3.4}$$

Applying this formulae to the potential B.3.1, and using $t(\rho_{sat}, 0) = t_{sat}$, $\frac{\partial e}{\partial \rho} = \frac{2}{3}\frac{t_{sat}}{\rho_{sat}}$ and $\frac{\partial^2 e}{\partial \rho^2} = -\frac{2}{9}\frac{t_{sat}}{\rho_{sat}^2}$, with t_{sat} given by 3.2.16, then the following equations are obtained:

$$c_{\lambda,0}\rho_{sat}^\lambda + c_{\mu,0}\rho_{sat}^\mu + c_{\nu,0}\rho_{sat}^\nu + t_{sat} = E_{sat} \tag{B.3.5}$$

$$\lambda c_{\lambda,0}\rho_{sat}^\lambda + \mu c_{\mu,0}\rho_{sat}^\mu + \nu c_{\nu,0}\rho_{sat}^\nu + \frac{2}{3}t_{sat} = 0 \tag{B.3.6}$$

$$\lambda(\lambda-1)c_{\lambda,0}\rho_{sat}^\lambda + \mu(\mu-1)c_{\mu,0}\rho_{sat}^\mu + \nu(\nu-1)c_{\nu,0}\rho_{sat}^\nu - \frac{2}{9}t_{sat} = \frac{K_{sat}}{9} \tag{B.3.7}$$

Isovector channel Specializing Eqs. B.2.12. B.2.13 and B.2.14 to the $N = 3$ case:

$$c_{\lambda,1}\rho_{sat}^\lambda + c_{\mu,1}\rho_{sat}^\mu + c_{\nu,1}\rho_{sat}^\nu + \frac{5}{9}t_{sat} = E_{sym} \tag{B.3.8}$$

$$\lambda c_{\lambda,1}\rho_{sat}^\lambda + \mu c_{\mu,1}\rho_{sat}^\mu + \nu c_{\nu,1}\rho_{sat}^\nu + \frac{10}{27}t_{sat} = \frac{L_{sym}}{3} \tag{B.3.9}$$

$$\lambda(\lambda-1)c_{\lambda,1}\rho_{sat}^\lambda + \mu(\mu-1)c_{\mu,1}\rho_{sat}^\mu + \nu(\nu-1)c_{\nu,1}\rho_{sat}^\nu - \frac{10}{81}t_{sat} = \frac{K_{sym}}{9} \tag{B.3.10}$$

For a given set of exponents γ, the equations B.3.5-B.3.7 and B.3.8-B.3.10 can be read in two ways:

- If the model coefficients $\{c_{\gamma,0}\}$, $\{c_{\gamma,1}\}$ are known, for example if they have been determined by fitting a set of data points, then the relations above allow to calculate analytically the empirical parameters;
- viceversa, if one wants to determine the coefficients of the model EoS from some known values of the empirical quantities, then the equations above can be seen as linear systems which can be easily solved numerically.

The first method is followed in this work. As for the second method, which is used e.g. in Ref. [80], it is convenient to rearrange the six equation in matrix form as:

$$Ax_{sat} = b_{sat} \qquad Ax_{sym} = b_{sym} \tag{B.3.11}$$

where the matrix A and the vectors $x_{sat/sym}$ and $b_{sat/sym}$ are given by:

$$A = \begin{pmatrix} \rho_{sat}^{\lambda} & \rho_{sat}^{\mu} & \rho_{sat}^{\nu} \\ \lambda\rho_{sat}^{\lambda} & \mu\rho_{sat}^{\mu} & \nu\rho_{sat}^{\nu} \\ \lambda(\lambda-1)\rho_{sat}^{\lambda} & \mu(\mu-1)\rho_{sat}^{\mu} & \nu(\nu-1)\rho_{sat}^{\nu} \end{pmatrix} \tag{B.3.12}$$

$$x_{sat} = \begin{pmatrix} c_{\lambda,0} \\ c_{\mu,0} \\ c_{\nu,0} \end{pmatrix} \qquad b_{sat} = \begin{pmatrix} E_{sat} - t_{sat} \\ 0 \\ \frac{K_{sat}+2t_{sat}}{9} \end{pmatrix} \tag{B.3.13}$$

$$x_{sym} = \begin{pmatrix} c_{\lambda,1} \\ c_{\mu,1} \\ c_{\nu,1} \end{pmatrix} \qquad b_{sat} = \begin{pmatrix} E_{sym} - \frac{5}{9}t_{sat} \\ \frac{L_{sym}}{3} - \frac{10}{27}t_{sat} \\ \frac{K_{sym}}{9} + \frac{10}{81}t_{sat} \end{pmatrix} \tag{B.3.14}$$

Case N=2 In case of a 2-terms potential

$$v(\rho,\beta) = c_{\lambda}(\beta)\rho^{\lambda} + c_{\mu}\rho^{\mu} \tag{B.3.15}$$

a link between the four model coefficients $c_{\lambda,0/1}$ and $c_{\mu,0/1}$ and the four empirical parameters ρ_{sat}, E_{sat}, E_{sym} and L_{sym} is easily established. With the same matrix notation as before, the four equations are written as:

$$Ax_{sat} = b_{sat} \qquad Ax_{sym} = b_{sym} \tag{B.3.16}$$

where:

$$A = \begin{pmatrix} \rho_{sat}^{\lambda} & \rho_{sat}^{\mu} \\ \lambda\rho_{sat}^{\lambda} & \mu\rho_{sat}^{\mu} \end{pmatrix} \tag{B.3.17}$$

$$x_{sat} = \begin{pmatrix} c_{\lambda,0} \\ c_{\mu,0} \end{pmatrix} \qquad b_{sat} = \begin{pmatrix} E_{sat} - t_{sat} \\ 0 \end{pmatrix} \tag{B.3.18}$$

$$x_{sym} = \begin{pmatrix} c_{\lambda,1} \\ c_{\mu,1} \end{pmatrix} \qquad b_{sat} = \begin{pmatrix} E_{sym} - \frac{5}{9}t_{sat} \\ \frac{L_{sym}}{3} - \frac{10}{27}t_{sat} \end{pmatrix} \tag{B.3.19}$$

Example Consider the following potential:

$$v(\rho,\beta) = c_1(\beta)\rho + c_2(\beta)\rho^2 \tag{B.3.20}$$

Set $\rho_{sat} = 0.16\, fm^{-3}$, $E_{sat} = -16\, MeV$, $E_{sym} = 31.5\, MeV$ and $L_{sym} = 60\, MeV$. Then the numerical solution of B.3.16 gives:

$$c_{1,0} = -384.23 \qquad c_{1,1} = 166.40 \qquad c_{2,0} = 912.86 \qquad c_{2,1} = -289.30 \tag{B.3.21}$$

We have not written explicitly the dimension of the coefficients. In general, $[c_{\gamma}] = MeV\, fm^{3\gamma}$.

Appendix C

Mean field and rearrangement energy for the LDA functional

In this Appendix, we complement the discussion of the LDA nuclear energy functional exposed in Ch. 3. In Sec. C.1 the expression of the mean field potential $U_q(\mathbf{r})$ is derived. In Sec. C.2 the rearrangement energy contribution is calculated. In Sec. C.3 a numerical test is reported.

C.1 Derivation of the mean field potential

We derive the mean field potential $U_q(\mathbf{r})$ for the local energy functional introduced in Sec. 3.4. By definition:

$$U_q(\mathbf{r}) = \frac{\delta E_{pot}}{\delta \rho_q(\mathbf{r})} \qquad q = n, p \tag{C.1.1}$$

Since:

$$E\left[\tau, \rho, \beta\right] = E_{kin}\left[\tau\right] + E_{loc}\left[\rho, \beta\right] + E_{Coul}\left[\rho_p\right] \tag{C.1.2}$$

where:

$$\begin{aligned} E_{kin}\left[\tau(\mathbf{r})\right] &= \int d\mathbf{r}\, \mathcal{E}_{kin}(\mathbf{r}) \\ E_{loc}\left[\rho(\mathbf{r}), \beta(\mathbf{r})\right] &= \int d\mathbf{r}\, \mathcal{E}_{loc}(\mathbf{r}) \end{aligned} \tag{C.1.3}$$

and

$$\mathcal{E}_{loc}(\mathbf{r}) = \sum_{\gamma} c_\gamma \left(\beta(\mathbf{r})\right) \rho^{\gamma+1}(\mathbf{r}) = \sum_{\gamma} \left(c_{\gamma,0} + c_{\gamma,1}\beta^2(\mathbf{r})\right) \rho^{\gamma+1}(\mathbf{r}) \tag{C.1.4}$$

while the Coulomb energy is shown in Eq. 1.3.6, then:

$$U_q(\mathbf{r}) = \frac{\partial \mathcal{E}_{loc}}{\partial \rho_q} = \frac{\partial \mathcal{E}_{loc}}{\partial \rho}\frac{\partial \rho}{\partial \rho_q} + \frac{\partial \mathcal{E}_{loc}}{\partial \beta}\frac{\partial \beta}{\partial \rho} = \frac{\partial \mathcal{E}_{loc}}{\partial \rho} + \frac{\partial \beta}{\partial \rho_q}\frac{\partial \mathcal{E}_{loc}}{\partial \beta} \tag{C.1.5}$$

The chain rule has been used. We remind that $\rho = \rho_n + \rho_p$ and $\beta = \frac{\rho_n - \rho_p}{\rho}$ and move on to calculate the three different pieces.

$$\frac{\partial \beta}{\partial \rho_q} = \frac{1}{\rho}\frac{\partial}{\partial \rho_q}\left(\rho_n - \rho_p\right) + \left(\rho_n - \rho_p\right)\left(-\frac{1}{\rho^2}\right)\frac{\partial \rho}{\partial \rho_q} = \frac{\tau_z}{\rho} - \frac{\beta}{\rho} = \frac{\tau_z - \beta}{\rho} \tag{C.1.6}$$

where $\tau_z = +1$ for neutrons and $\tau_z = -1$ for protons.

$$\frac{\partial \mathcal{E}_{loc}}{\partial \rho} = \sum_{\gamma} \left(\gamma + 1\right) c_\gamma(\beta) \rho^\gamma \tag{C.1.7}$$

As usual, $c_\gamma(\beta) = c_{\gamma,0} + c_{\gamma,1}\beta^2$. Then:

$$\frac{\partial \mathcal{E}_{loc}}{\partial \beta} = \sum_\gamma \frac{\partial c_\gamma(\beta)}{\partial \beta}\rho^\gamma = 2\beta \sum_\gamma c_{\gamma,1}\rho^{\gamma+1} \tag{C.1.8}$$

Putting the different terms together, one obtains:

$$U_q = \sum_\gamma (\gamma+1)c_\gamma(\beta)\rho^\gamma + (\tau_z - \beta)\,2\beta \sum_\gamma c_{\gamma,1}\rho^\gamma = \sum_\gamma \Big[\,(\gamma+1)\,c_\gamma(\beta)\rho^\gamma + 2\beta\,(\tau_z-\beta)\,c_{\gamma,1}\Big]\rho^\gamma \tag{C.1.9}$$

Finally:

$$U_q(\mathbf{r}) = \sum_\gamma \Big[\,(\gamma+1)\,c_{\gamma,0} + 2\beta\,(\tau_z-\beta)\,c_{\gamma,1} + (\gamma+1)c_{\gamma,1}\beta^2\Big]\rho^\gamma \tag{C.1.10}$$

C.2 Rearrangement energy

The total energy in the Hartree-Fock method with density independent interaction is given by the formula A.0.14:

$$E = \frac{1}{2}\left(T + \sum_k \epsilon_k\right) \tag{C.2.1}$$

where T is the kinetic energy and ϵ_k are the energy eigenvalues. However, when dealing with density *dependent* interactions, a correction term, called *rearrangement energy*, must be added:

$$E = \frac{1}{2}\left(T + \sum_k \epsilon_k\right) + E_{rea} \tag{C.2.2}$$

While Ref. [26] gives a general definition of rearrangement energy (Eq. A.0.17, here we'll employ a more practical expression. Below one finds a detailed calculations of E_{rea} for the local functional of Sec. 3.4. The equality of the energies obtained in two different ways - direct integration versus Hartree-Fock formula C.2.2 - is very strong hint of the correctness of the numerical implementation of the Hartree-Fock method.

Local functional The local functional 1.3.24 is defined as:

$$\mathcal{E} = \frac{\hbar^2}{2m}\tau + \mathcal{E}_{loc}(\mathbf{r}) \tag{C.2.3}$$

where:

$$\mathcal{E}_{loc} = \mathcal{E}_{loc}\Big[\rho(\mathbf{r}), \beta(\mathbf{r})\Big] = \sum_\gamma c_\gamma(\beta)\rho^{\gamma+1} \tag{C.2.4}$$

with $c_\gamma(\beta) = c_{\gamma,0} + c_{\gamma,1}\beta^2$. The energy is a functional $E = E\big[\rho, \beta, \tau\big]$. The effective mass is equal to the bare mass and we have included no spin orbit or surface terms. The mean field potential U_q is given by Eq. C.1.10. Now, the rearrangement energy is defined as:

$$E_{rea} = \int d\mathbf{r}\,\mathcal{E}_{loc}(\mathbf{r}) - \frac{1}{2}\sum_q \int d\mathbf{r} U_q(\mathbf{r})\rho_q(\mathbf{r}) \tag{C.2.5}$$

	^{40}Ca	^{48}Ca	^{90}Zr	^{132}Sn	^{208}Pb
E(int)	-414.455	-472.945	-843.223	-1152.721	-1664.800
E(HF)	-414.458	-472.944	-843.223	-1152.713	-1664.788

Table C.2.1: Energies computed with Eq. C.2.2 ($E(HF)$) and by integration of the energy density ($E(int)$) using the local interaction $(2, 5, 6)$ (see text).The agreement of the two estimates of the total energy is remarkable.

Then:

$$\sum_q U_q \rho_q = U_n \rho_n + U_p \rho_p = \left[U_n(1+\beta) + U_p(1-\beta)\right] \frac{\rho}{2} = \left[(U_n + U_p) + (U_n - U_p)\,\beta\right] \frac{\rho}{2} \tag{C.2.6}$$

We calculate $U_n + U_p$ and $U_n - U_p$ separately.

$$U_n + U_p = 2 \sum_\gamma \left[(\gamma+1)\, c_{\gamma,0} - 2\beta^2 c_{\gamma,1} + (\gamma+1)\,\beta^2 c_{\gamma,1}\right] \rho^\gamma = 2 \sum_\gamma \left[(\gamma+1)\, c_{\gamma,0} + (\gamma-1)\,\beta^2 c_{\gamma,1}\right] \rho^\gamma \tag{C.2.7}$$

The τ_z terms in U_q vanish in the sum, as $\tau_z = 1$ for neutrons and $\tau_z = -1$ for protons. Since:

$$U_n - U_p = \sum_\gamma 4\beta c_{\gamma,1} \rho^\gamma \tag{C.2.8}$$

then:

$$\sum_q U_q \rho_q = \frac{\rho}{2}\, 2 \sum_\gamma \left[(\gamma+1)\, c_{\gamma,0} + (\gamma+1)\,\beta^2 c_{\gamma,1}\right] \rho^{\gamma+1} \tag{C.2.9}$$

Plugging into the definitions of E_{rea}:

$$E_{rea} = \int d\mathbf{r} \sum_\gamma \left(c_{\gamma,0} + \beta^2 c_{\gamma,1}\right) \rho^{\gamma+1} - \left(\frac{1+\gamma}{2}\right) \left(c_{\gamma,0} + \beta^2 c_{\gamma,1}\right) \rho^{\gamma+1} \tag{C.2.10}$$

and finally:

$$E_{rea} = \int d\mathbf{r} \sum_\gamma \left(\frac{1-\gamma}{2}\right) \left(c_{\gamma,0} + \beta^2 c_{\gamma,1}\right) \rho^{\gamma+1} \tag{C.2.11}$$

Tab. C.2.1 shows a very good agreement between total energies computed with Eq. C.2.2 ($E(HF)$ in the table) and by direct integration ($E(int)$), $E = \int d\mathbf{r}\, \mathcal{E}$, using the interaction $(2, 5, 6)$ described in Ch. 4 and Tab. 4.2.2.

C.3 Test with a $t_0 - t_3$ Skyrme interaction

As a test for the correctness of the energy-density functional introduced in Ch. 3, we consider an especially simple Skyrme functional and show that it can be mapped to a local functional 1.3.24. We then check that the calculation with such simple functional and with the thus defined local functional yield the same results.
The energy density of the Skyrme functional is given by:

$$\mathcal{E}_{kin} = \frac{\hbar^2}{2m} \tau \tag{C.3.1}$$

$$\mathcal{E} = \mathcal{E}_{kin} + \mathcal{H}_0 + \mathcal{H}_3 \tag{C.3.2}$$

where

$$\mathcal{H}_0 = \frac{t_0}{4}\Big(2\rho^2 - (\rho_n^2 + \rho_p^2)\Big) \tag{C.3.3}$$

$$\mathcal{H}_3 = \frac{t_3}{24}\rho^{\frac{1}{6}}\Big(2\rho^2 - (\rho_n^2 + \rho_p^2)\Big) \tag{C.3.4}$$

with $t_0 = -2931.7$ and $t_3 = 18709$. Comparing with the general expression of Skyrme functionals [14], we can see that it is very simple, as it depends only on proton and neutron densities, but does not contain gradient and spin orbit terms. We will call it a $t_0 - t_3$ functional. We want to show that this energy density can be expressed in the form:

$$\mathcal{E} = \mathcal{E}_{kin} + \mathcal{E}_{loc} \tag{C.3.5}$$

$$\mathcal{E}_{loc}(\rho,\beta) = \sum_\gamma c_\gamma(\beta)\rho^{\gamma+1} = \sum_\gamma \Big(c_{\gamma,0} + c_{\gamma,1}\beta^2\Big)\rho^{\gamma+1} \tag{C.3.6}$$

It is convenient to express $\mathcal{H}_0$ and $\mathcal{H}_3$ as a function of the total density $\rho = \rho_n + \rho_p$ and the asymmetry $\beta = \frac{\rho_n - \rho_p}{\rho}$. As $\rho_n = \frac{1+\beta}{2}\rho$ and $\rho_p = \frac{1-\beta}{2}\rho$, it follows that:

$$\rho_n^2 + \rho_p^2 = \frac{\rho^2}{2}\left(1 + \beta^2\right) \tag{C.3.7}$$

and then:

$$\rho^2 - \left(\rho_n^2 + \rho_p^2\right) = \frac{\rho^2}{2}\left(3 - \beta^2\right) \tag{C.3.8}$$

Finally:

$$\mathcal{H}_0 = \frac{t_0}{8}\left(3 - \beta^2\right)\rho^2 \tag{C.3.9}$$

$$\mathcal{H}_3 = \frac{t_3}{48}\left(3 - \beta^2\right)\rho^{\frac{13}{6}} \tag{C.3.10}$$

Comparing with Eq. C.3.6, we see that $t_0 - t_3$ has the form:

$$\mathcal{E}_{loc}(\rho,\beta) = \mathcal{H}_0 + \mathcal{H}_3 = c_1(\beta)\rho^2 + c_{7/6}(\beta)\rho^{\frac{13}{6}} \tag{C.3.11}$$

The coefficients are reported in C.3.1:

γ	c_0	c_1	$c(\beta = 1)$
1	$\frac{3}{8}t_0$	$-\frac{t_0}{8}$	$\frac{t_0}{4}$
$\frac{7}{6}$	$\frac{3}{48}t_3$	$-\frac{t_3}{48}$	$\frac{t_3}{24}$

Table C.3.1: Parameters of the $t_0 - t_3$ Skyrme functional, expressed in the form Eq. C.3.6.

Last, we report a sample of results that show that the local functional with the potential term C.3.11 is actually equivalent to the $t_0 - t_3$ functional (Tab. C.3.2 and C.3.3). Results are reported with 5 decimal digits and show a perfect agreement between the two energy functionals.

Binding energy (MeV)	^{40}Ca	^{48}Ca	^{90}Zr	^{132}Sn	^{208}Pb
$t_0 - t_3$ functional	-456.16986	-523.88383	-940.61031	-1301.71945	-1898.21477
Local functional	-456.16986	-523.88383	-940.61031	-1301.71945	-1898.21477

Table C.3.2: Total binding energies for a sample of doubly magic nuclei, calculated with the $t_0 - t_3$ Skyrme functional and with the local functional defined by Eqs. C.3.11 and C.3.5. Results are reported with 5 decimal digits.

Charge radius (fm)	^{40}Ca	^{48}Ca	^{90}Zr	^{132}Sn	^{208}Pb
$t_0 - t_3$ functional	3.22176	3.34199	4.10581	4.62990	5.40684
Local functional	3.22176	3.34199	4.10581	4.62989	5.40684

Table C.3.3: Charge radii for a sample of doubly magic nuclei, calculated with the $t_0 - t_3$ Skyrme functional and with the local functional defined by Eqs. C.3.11 and C.3.5. Results are reported with 5 decimal digits.

Bibliography

[1] Winfried Leidemann and Giuseppina Orlandini. "Modern ab initio approaches and applications in few-nucleon physics with A⩾4". In: *Progress in Particle and Nuclear Physics* 68 (2013), pp. 158–214. ISSN: 0146-6410. DOI: https://doi.org/10.1016/j.ppnp.2012.09.001. URL: http://www.sciencedirect.com/science/article/pii/S014664101200110X.

[2] Morten Hjorth-Jensen, Maria Lombardo, and U. van Kolck. *An Advanced Course in Computational Nuclear Physics: Bridging the Scales from Quarks to Neutron Stars*. Jan. 2017. ISBN: 978-3-319-53335-3. DOI: 10.1007/978-3-319-53336-0.

[3] Stefano Gandolfi et al. "Atomic Nuclei From Quantum Monte Carlo Calculations With Chiral EFT Interactions". In: *Frontiers in Physics* 8 (Apr. 2020). DOI: 10.3389/fphy.2020.00117.

[4] J.E. Lynn et al. "Quantum Monte Carlo Methods in Nuclear Physics: Recent Advances". In: *Annual Review of Nuclear and Particle Science* 69.1 (2019), pp. 279–305. DOI: 10.1146/annurev-nucl-101918-023600. eprint: https://doi.org/10.1146/annurev-nucl-101918-023600. URL: https://doi.org/10.1146/annurev-nucl-101918-023600.

[5] Vittorio Somà. *Self-consistent Green's function theory for atomic nuclei*. 2020. arXiv: 2003.11321 [nucl-th].

[6] Michael Bender, Paul-Henri Heenen, and Paul-Gerhard Reinhard. "Self-consistent mean-field models for nuclear structure". In: *Rev. Mod. Phys.* 75 (2003), pp. 121–180. DOI: 10.1103/RevModPhys.75.121.

[7] G. Colò. "Nuclear density functional theory". In: *Advances in Physics: X* 5.1 (2020), p. 1740061. DOI: 10.1080/23746149.2020.1740061. eprint: https://doi.org/10.1080/23746149.2020.1740061. URL: https://doi.org/10.1080/23746149.2020.1740061.

[8] Takashi Nakatsukasa et al. "Time-dependent density-functional description of nuclear dynamics". In: *Rev. Mod. Phys.* 88 (4 Nov. 2016), p. 045004. DOI: 10.1103/RevModPhys.88.045004. URL: https://link.aps.org/doi/10.1103/RevModPhys.88.045004.

[9] X. Roca-Maza and N. Paar. "Nuclear equation of state from ground and collective excited state properties of nuclei". In: *Progress in Particle and Nuclear Physics* 101 (2018), pp. 96–176. ISSN: 0146-6410. DOI: https://doi.org/10.1016/j.ppnp.2018.04.001. URL: http://www.sciencedirect.com/science/article/pii/S0146641018300334.

[10] Richard M. Martin. *Electronic Structure: Basic Theory and Practical Methods*. Cambridge University Press, 2004. DOI: 10.1017/CBO9780511805769.

[11] R. O. Jones. "Density functional theory: Its origins, rise to prominence, and future". In: *REVIEWS OF MODERN PHYSICS* 87.3 (AUG 25 2015), 897–923. ISSN: 0034-6861. DOI: {10.1103/RevModPhys.87.897}.

[12] Robert G. Parr and Weitao Yang. *Density-Functional Theory of Atoms and Molecules (International Series of Monographs on Chemistry)*. Oxford University Press, USA, 1994. ISBN: 0195092767.

[13] Nicolas Schunck, ed. 2053-2563. IOP Publishing, 2019. ISBN: 978-0-7503-1422-0. DOI: 10.1088/2053-2563/aae0ed. URL: http://dx.doi.org/10.1088/2053-2563/aae0ed.

[14] E. Chabanat et al. "A Skyrme parametrization from subnuclear to neutron star densities". In: *Nuclear Physics A* 627.4 (1997), pp. 710–746. ISSN: 0375-9474. DOI: https://doi.org/10.1016/S0375-9474(97)00596-4. URL: http://www.sciencedirect.com/science/article/pii/S0375947497005964.

[15] Marcella Grasso. "Effective density functionals beyond mean field". In: *Progress in Particle and Nuclear Physics* 106 (2019), pp. 256–311. ISSN: 0146-6410. DOI: https://doi.org/10.1016/j.ppnp.2019.02.002. URL: http://www.sciencedirect.com/science/article/pii/S0146641019300043.

[16] John P. Perdew and Karla Schmidt. "Jacob's ladder of density functional approximations for the exchange-correlation energy". In: *AIP Conference Proceedings* 577.1 (2001), pp. 1–20. DOI: 10.1063/1.1390175. eprint: https://aip.scitation.org/doi/pdf/10.1063/1.1390175. URL: https://aip.scitation.org/doi/abs/10.1063/1.1390175.

[17] M. Baldo, P. Schuck, and X. Viñas. "Kohn–Sham density functional inspired approach to nuclear binding". In: *Physics Letters B* 663.5 (2008), pp. 390–394. ISSN: 0370-2693. DOI: https://doi.org/10.1016/j.physletb.2008.04.013. URL: http://www.sciencedirect.com/science/article/pii/S0370269308004383.

[18] Aurel Bulgac et al. "Minimal nuclear energy density functional". In: *Phys. Rev. C* 97 (4 Apr. 2018), p. 044313. DOI: 10.1103/PhysRevC.97.044313. URL: https://link.aps.org/doi/10.1103/PhysRevC.97.044313.

[19] Stefano Gandolfi, Alexandros Gezerlis, and J. Carlson. "Neutron Matter from Low to High Density". In: *Annual Review of Nuclear and Particle Science* 65.1 (2015), pp. 303–328. DOI: 10.1146/annurev-nucl-102014-021957. eprint: https://doi.org/10.1146/annurev-nucl-102014-021957. URL: https://doi.org/10.1146/annurev-nucl-102014-021957.

[20] Arianna Carbone. "Setting nonperturbative uncertainties on finite-temperature properties of neutron matter". In: *Phys. Rev. Research* 2 (2 May 2020), p. 023227. DOI: 10.1103/PhysRevResearch.2.023227. URL: https://link.aps.org/doi/10.1103/PhysRevResearch.2.023227.

[21] Francesca Sammarruca and Randy Millerson. "Nuclear Forces in the Medium: Insight From the Equation of State". In: *Frontiers in Physics* 7 (2019), p. 213. ISSN: 2296-424X. DOI: 10.3389/fphy.2019.00213. URL: https://www.frontiersin.org/article/10.3389/fphy.2019.00213.

[22] M. Piarulli et al. "Benchmark calculations of pure neutron matter with realistic nucleon-nucleon interactions". In: *Phys. Rev. C* 101 (4 Apr. 2020), p. 045801. DOI: 10.1103/PhysRevC.101.045801. URL: https://link.aps.org/doi/10.1103/PhysRevC.101.045801.

[23] A. Ekström et al. "Accurate nuclear radii and binding energies from a chiral interaction". In: *Phys. Rev. C* 91 (5 May 2015), p. 051301. DOI: 10.1103/PhysRevC.91.051301. URL: https://link.aps.org/doi/10.1103/PhysRevC.91.051301.

[24] Diego Lonardoni and Francesco Pederiva. *Medium-mass hypernuclei and the nucleon-isospin dependence of the three-body hyperon-nucleon-nucleon force*. 2017. arXiv: 1711.07521 [nucl-th].

[25] V Soma et al. "Novel chiral Hamiltonian and observables in light and medium-mass nuclei". In: *PHYSICAL REVIEW C* 101.1 (JAN 22 2020). ISSN: 2469-9985. DOI: {10.1103/PhysRevC.101.014318}.

[26] P. Ring and P. Schuck. *The nuclear many-body problem*. New York: Springer-Verlag, 1980.

[27] Jacek Dobaczewski. "Current Developments in Nuclear Density Functional Methods". In: *Journal of Physics: Conference Series* 312 (Sept. 2010). DOI: 10.1088/1742-6596/312/9/092002.

[28] D. Vautherin and D. M. Brink. "Hartree-Fock Calculations with Skyrme's Interaction. I. Spherical Nuclei". In: *Phys. Rev. C* 5 (3 Mar. 1972), pp. 626–647. DOI: 10.1103/PhysRevC.5.626. URL: https://link.aps.org/doi/10.1103/PhysRevC.5.626.

[29] J. Dobaczewski and J. Dudek. "Time-odd components in the mean field of rotating superdeformed nuclei". In: *Phys. Rev. C* 52 (4 Oct. 1995), pp. 1827–1839. DOI: 10.1103/PhysRevC.52.1827. URL: https://link.aps.org/doi/10.1103/PhysRevC.52.1827.

[30] G. Colo. "Density Functional Theory (DFT) for atomic nuclei: a simple introduction". In: (July 2018).

[31] M. Baldo et al. "New Kohn-Sham density functional based on microscopic nuclear and neutron matter equations of state". In: *Phys. Rev. C* 87 (6 June 2013), p. 064305. DOI: 10.1103/PhysRevC.87.064305. URL: https://link.aps.org/doi/10.1103/PhysRevC.87.064305.

[32] Gianluca Colò et al. "Self-consistent RPA calculations with Skyrme-type interactions: The skyrme$_r$*paprogram*". In: *Computer Physics Communications* 184.1 (2013), pp. 142–161. ISSN: 0010-4655. DOI: https://doi.org/10.1016/j.cpc.2012.07.016. URL: http://www.sciencedirect.com/science/article/pii/S0010465512002627.

[33] R. Machleidt and F. Sammarruca. "Can chiral EFT give us satisfaction?" English. In: *EUROPEAN PHYSICAL JOURNAL A* 56.3 (MAR 24 2020). ISSN: 1434-6001. DOI: {10.1140/epja/s10050-020-00101-3}.

[34] J. Carlson et al. "Quantum Monte Carlo methods for nuclear physics". English (US). In: *Reviews of Modern Physics* 87.3 (Sept. 2015). ISSN: 0034-6861. DOI: 10.1103/RevModPhys.87.1067.

[35] Carlo Barbieri and Arianna Carbone. "Self-Consistent Green's Function Approaches". In: *An Advanced Course in Computational Nuclear Physics: Bridging the Scales from Quarks to Neutron Stars*. Ed. by Morten Hjorth-Jensen, Maria Paola Lombardo, and Ubirajara van Kolck. Cham: Springer International Publishing, 2017, pp. 571–644. ISBN: 978-3-319-53336-0. DOI: 10.1007/978-3-319-53336-0_11. URL: https://doi.org/10.1007/978-3-319-53336-0_11.

[36] Shihang Shen et al. "Towards an ab initio covariant density functional theory for nuclear structure". In: *Progress in Particle and Nuclear Physics* 109 (2019), p. 103713. ISSN: 0146-6410. DOI: https://doi.org/10.1016/j.ppnp.2019.103713. URL: http://www.sciencedirect.com/science/article/pii/S0146641019300481.

[37] R. B. Wiringa, V. G. J. Stoks, and R. Schiavilla. "Accurate nucleon-nucleon potential with charge-independence breaking". In: *Phys. Rev. C* 51 (1 Jan. 1995), pp. 38–51. DOI: 10.1103/PhysRevC.51.38. URL: https://link.aps.org/doi/10.1103/PhysRevC.51.38.

[38] E. Epelbaum, H.-W. Hammer, and Ulf-G. Meißner. "Modern theory of nuclear forces". In: *Rev. Mod. Phys.* 81 (4 Dec. 2009), pp. 1773–1825. DOI: 10.1103/RevModPhys.81.1773. URL: https://link.aps.org/doi/10.1103/RevModPhys.81.1773.

[39] A. Rios. "Green's functions techniques for extended nuclear systems". In: (June 2020). arXiv: 2006.10610 [nucl-th].

[40] G Hagen et al. "Coupled-cluster computations of atomic nuclei". In: *Reports on Progress in Physics* 77.9 (Sept. 2014), p. 096302. DOI: 10.1088/0034-4885/77/9/096302. URL: https://doi.org/10.1088%2F0034-4885%2F77%2F9%2F096302.

[41] Alexander Tichai, Robert Roth, and Thomas Duguet. *Many-body perturbation theories for finite nuclei*. 2020. arXiv: 2001.10433 [nucl-th].

[42] C. Drischler, K. Hebeler, and A. Schwenk. "Chiral Interactions up to Next-to-Next-to-Next-to-Leading Order and Nuclear Saturation". In: *Phys. Rev. Lett.* 122 (4 Jan. 2019), p. 042501. DOI: 10.1103/PhysRevLett.122.042501. URL: https://link.aps.org/doi/10.1103/PhysRevLett.122.042501.

[43] Christian Drischler et al. *Towards grounding nuclear physics in QCD*. 2019. arXiv: 1910.07961 [nucl-th].

[44] Felipe J. Llanes-Estrada and Eva Lope-Oter. "Hadron matter in neutron stars in view of gravitational wave observations". In: *Progress in Particle and Nuclear Physics* 109 (2019), p. 103715. ISSN: 0146-6410. DOI: https://doi.org/10.1016/j.ppnp.2019.103715. URL: http://www.sciencedirect.com/science/article/pii/S014664101930050X.

[45] Arnau Rios. "Beta decay gets the ab initio treatment". English. In: *NATURE PHYSICS* 15.5 (MAY 2019), 425–426. ISSN: 1745-2473. DOI: {10.1038/s41567-019-0483-y}.

[46] M. Baldo et al. "Comparative study of neutron and nuclear matter with simplified Argonne nucleon-nucleon potentials". In: *Phys. Rev. C* 86 (6 Dec. 2012), p. 064001. DOI: 10.1103/PhysRevC.86.064001. URL: https://link.aps.org/doi/10.1103/PhysRevC.86.064001.

[47] V. G. J. Stoks et al. "Partial-wave analysis of all nucleon-nucleon scattering data below 350 MeV". In: *Phys. Rev. C* 48 (2 Aug. 1993), pp. 792–815. DOI: 10.1103/PhysRevC.48.792. URL: https://link.aps.org/doi/10.1103/PhysRevC.48.792.

[48] R. B. Wiringa and Steven C. Pieper. "Evolution of Nuclear Spectra with Nuclear Forces". In: *Phys. Rev. Lett.* 89 (18 Oct. 2002), p. 182501. DOI: 10.1103/PhysRevLett.89.182501. URL: https://link.aps.org/doi/10.1103/PhysRevLett.89.182501.

[49] J. Carlson, V.R. Pandharipande, and R.B. Wiringa. "Three-nucleon interaction in 3-, 4- and ∞-body systems". In: *Nuclear Physics A* 401.1 (1983), pp. 59–85. ISSN: 0375-9474. DOI: https://doi.org/10.1016/0375-9474(83)90336-6. URL: http://www.sciencedirect.com/science/article/pii/0375947483903366.

[50] Alessandro Lovato. *Ab initio calculations on nuclear matter properties including the effects of three-nucleons interaction*. 2012. arXiv: 1210.0593 [nucl-th].

[51] Alessandro Lovato et al. "Density-dependent nucleon-nucleon interaction from three-nucleon forces". In: *PHYSICAL REVIEW C* 83.5 (MAY 27 2011). ISSN: 0556-2813. DOI: {10.1103/PhysRevC.83.054003}.

[52] Steven C. Pieper et al. "Realistic models of pion-exchange three-nucleon interactions". In: *Phys. Rev. C* 64 (1 June 2001), p. 014001. DOI: 10.1103/PhysRevC.64.014001. URL: https://link.aps.org/doi/10.1103/PhysRevC.64.014001.

[53] R Machleidt and F Sammarruca. "Chiral EFT based nuclear forces: achievements and challenges". In: *Physica Scripta* 91.8 (July 2016), p. 083007. DOI: 10.1088/0031-8949/91/8/083007. URL: https://doi.org/10.1088%2F0031-8949%2F91%2F8%2F083007.

[54] D. Lonardoni et al. "Auxiliary field diffusion Monte Carlo calculations of light and medium-mass nuclei with local chiral interactions". In: *Phys. Rev. C* 97 (4 Apr. 2018), p. 044318. DOI: 10.1103/PhysRevC.97.044318. URL: https://link.aps.org/doi/10.1103/PhysRevC.97.044318.

[55] Andreas Ekström. *Ab initio models of atomic nuclei: challenges and new ideas*. 2019. arXiv: 1912.02227 [nucl-th].

[56] A. Rios, A. Carbone, and A. Polls. "Comparison of nuclear Hamiltonians using spectral function sum rules". In: *Phys. Rev. C* 96 (1 July 2017), p. 014003. DOI: 10.1103/PhysRevC.96.014003. URL: https://link.aps.org/doi/10.1103/PhysRevC.96.014003.

[57] V. Lapoux et al. "Radii and Binding Energies in Oxygen Isotopes: A Challenge for Nuclear Forces". In: *Phys. Rev. Lett.* 117 (5 July 2016), p. 052501. DOI: 10.1103/PhysRevLett.117.052501. URL: https://link.aps.org/doi/10.1103/PhysRevLett.117.052501.

[58] Francesca Sammarruca and Randy Millerson. *Exploring the relationship between nuclear matter and finite nuclei with chiral two- and three-nucleon forces*. 2020. arXiv: 2005.01958 [nucl-th].

[59] D. Lonardoni et al. "Nuclear and neutron-star matter from local chiral interactions". In: *Phys. Rev. Research* 2 (2 May 2020), p. 022033. DOI: 10.1103/PhysRevResearch.2.022033. URL: https://link.aps.org/doi/10.1103/PhysRevResearch.2.022033.

[60] Thomas Hüther et al. *Family of Chiral Two- plus Three-Nucleon Interactions for Accurate Nuclear Structure Studies*. 2019. arXiv: 1911.04955 [nucl-th].

[61] W. M. C. Foulkes et al. "Quantum Monte Carlo simulations of solids". In: *Rev. Mod. Phys.* 73 (1 Jan. 2001), pp. 33–83. DOI: 10.1103/RevModPhys.73.33. URL: https://link.aps.org/doi/10.1103/RevModPhys.73.33.

[62] D. M. Ceperley and B. J. Alder. "Ground State of the Electron Gas by a Stochastic Method". In: *Phys. Rev. Lett.* 45 (7 Aug. 1980), pp. 566–569. DOI: 10.1103/PhysRevLett.45.566. URL: https://link.aps.org/doi/10.1103/PhysRevLett.45.566.

[63] Mateusz Buraczynski, Nawar Ismail, and Alexandros Gezerlis. "Nonperturbative Extraction of the Effective Mass in Neutron Matter". In: *Phys. Rev. Lett.* 122 (15 Apr. 2019), p. 152701. DOI: 10.1103/PhysRevLett.122.152701. URL: https://link.aps.org/doi/10.1103/PhysRevLett.122.152701.

[64] A. Akmal, V. R. Pandharipande, and D. G. Ravenhall. "Equation of state of nucleon matter and neutron star structure". In: *Phys. Rev. C* 58 (3 Sept. 1998), pp. 1804–1828. DOI: 10.1103/PhysRevC.58.1804. URL: https://link.aps.org/doi/10.1103/PhysRevC.58.1804.

[65] Diego Lonardoni. *From Hypernuclei to Hypermatter: a Quantum Monte Carlo Study of Strangeness in Nuclear Structure and Nuclear Astrophysics*. 2013. arXiv: 1311.6672 [nucl-th].

[66] Francesco Pederiva, Alessandro Roggero, and Kevin Schmidt. "Variational and diffusion monte carlo approaches to the nuclear few- and many-body problem". English (US). In: *Lecture Notes in Physics*. Vol. 936. Lecture Notes in Physics. Germany: Springer Verlag, 2017, pp. 401–476. DOI: 10.1007/978-3-319-53336-0_9.

[67] A. L. Fetter and J. D. Walecka. *Quantum Theory of Many-Particle Systems*. Boston: McGraw-Hill, 1971.

[68] P. Arthuis et al. *Ab initio computation of charge densities for Sn and Xe isotopes*. 2020. arXiv: 2002.02214 [nucl-th].

[69] Carlo Barbieri, Francesco Raimondi, and Christopher McIlroy. "Recent Applications of Self-Consistent Green's Function Theory to Nuclei". In: *Journal of Physics: Conference Series* 966 (Feb. 2018), p. 012015. DOI: 10.1088/1742-6596/966/1/012015. URL: https://doi.org/10.1088%2F1742-6596%2F966%2F1%2F012015.

[70] V. Somà, C. Barbieri, and T. Duguet. "Ab initio Gorkov-Green's function calculations of open-shell nuclei". In: *Phys. Rev. C* 87 (1 Jan. 2013), p. 011303. DOI: 10.1103/PhysRevC.87.011303. URL: https://link.aps.org/doi/10.1103/PhysRevC.87.011303.

[71] C Barbieri. "Many-body Propagator Theory with Three-Body Interactions: a Path to Exotic Open Shell Isotopes". In: *Journal of Physics: Conference Series* 529 (Aug. 2014), p. 012005. DOI: 10.1088/1742-6596/529/1/012005. URL: https://doi.org/10.1088%2F1742-6596%2F529%2F1%2F012005.

[72] Arianna Carbone, Arnau Rios, and Artur Polls. "Correlated density-dependent chiral forces for infinite-matter calculations within the Green's function approach". In: *Phys. Rev. C* 90 (5 Nov. 2014), p. 054322. DOI: 10.1103/PhysRevC.90.054322. URL: https://link.aps.org/doi/10.1103/PhysRevC.90.054322.

[73] G. Salvioni et al. *Model nuclear energy density functionals derived from ab initio calculations*. 2020. arXiv: 2002.01903 [nucl-th].

[74] R. J. Furnstahl. *Turning the nuclear energy density functional method into a proper effective field theory: reflections*. 2019. arXiv: 1906.00833 [nucl-th].

[75] P. Hohenberg and W. Kohn. "Inhomogeneous Electron Gas". In: *Phys. Rev.* 136 (3B Nov. 1964), B864–B871. DOI: 10.1103/PhysRev.136.B864. URL: https://link.aps.org/doi/10.1103/PhysRev.136.B864.

[76] W. Kohn. "Nobel Lecture: Electronic structure of matter—wave functions and density functionals". In: *Rev. Mod. Phys.* 71 (5 Oct. 1999), pp. 1253–1266. DOI: 10.1103/RevModPhys.71.1253. URL: https://link.aps.org/doi/10.1103/RevModPhys.71.1253.

[77] Panagiota Papakonstantinou et al. "Density dependence of the nuclear energy-density functional". In: *Phys. Rev. C* 97 (1 Jan. 2018), p. 014312. DOI: 10.1103/PhysRevC.97.014312. URL: https://link.aps.org/doi/10.1103/PhysRevC.97.014312.

[78] Pierre M. Pizzochero. *Exploring fundamental physics with neutron stars*. 2016. arXiv: 1609.07587 [astro-ph.HE].

[79] M. C. Atkinson et al. *Revisiting the relation between the binding energy of finite nuclei and the equation of state of infinite nuclear matter*. 2020. arXiv: 2001.07231 [nucl-th].

[80] Jérôme Margueron, Rudiney Hoffmann Casali, and Francesca Gulminelli. "Equation of state for dense nucleonic matter from metamodeling. I. Foundational aspects". In: *Phys. Rev. C* 97 (2 Feb. 2018), p. 025805. DOI: 10.1103/PhysRevC.97.025805. URL: https://link.aps.org/doi/.

[81] M. Dutra et al. "Skyrme interaction and nuclear matter constraints". In: *Phys. Rev. C* 85 (3 Mar. 2012), p. 035201. DOI: 10.1103/PhysRevC.85.035201. URL: https://link.aps.org/doi/10.1103/PhysRevC.85.035201.

[82] J. W. Holt and N. Kaiser. "Equation of state of nuclear and neutron matter at third-order in perturbation theory from chiral effective field theory". In: *Phys. Rev. C* 95 (3 Mar. 2017), p. 034326. DOI: 10.1103/PhysRevC.95.034326. URL: https://link.aps.org/doi/10.1103/PhysRevC.95.034326.

[83] René Andrae, Tim Schulze-Hartung, and Peter Melchior. "Dos and don'ts of reduced chi-squared". In: 2010.

[84] Matthew Newville et al. *LMFIT: Non-Linear Least-Square Minimization and Curve-Fitting for Python*. Version 0.8.0. Sept. 2014. DOI: 10.5281/zenodo.11813. URL: https://doi.org/10.5281/zenodo.11813.

[85] J Dobaczewski, W Nazarewicz, and P-G Reinhard. "Error estimates of theoretical models: a guide". In: *Journal of Physics G: Nuclear and Particle Physics* 41.7 (May 2014), p. 074001. DOI: 10.1088/0954-3899/41/7/074001. URL: https://doi.org/10.1088%2F0954-3899%2F41%2F7%2F074001.

[86] J.R. Stone and P.-G. Reinhard. "The Skyrme interaction in finite nuclei and nuclear matter". In: *Progress in Particle and Nuclear Physics* 58.2 (Apr. 2007), pp. 587–657. ISSN: 0146-6410. DOI: 10.1016/j.ppnp.2006.07.001. URL: http://dx.doi.org/10.1016/j.ppnp.2006.07.001.

[87] J. Dobaczewski, H. Flocard, and J. Treiner. "Hartree-Fock-Bogolyubov description of nuclei near the neutron-drip line". In: *Nuclear Physics A* 422.1 (1984), pp. 103–139. ISSN: 0375-9474. DOI: https://doi.org/10.1016/0375-9474(84)90433-0. URL: http://www.sciencedirect.com/science/article/pii/0375947484904330.

[88] J. Simonis et al. "Saturation with chiral interactions and consequences for finite nuclei". In: *Phys. Rev. C* 96 (1 July 2017), p. 014303. DOI: 10.1103/PhysRevC.96.014303. URL: https://link.aps.org/doi/10.1103/PhysRevC.96.014303.

[89] Meng Wang et al. "The AME2016 atomic mass evaluation (II). Tables, graphs and references". In: *Chinese Physics C* 41.3 (Mar. 2017), p. 030003. DOI: 10.1088/1674-1137/41/3/030003. URL: https://doi.org/10.1088%2F1674-1137%2F41%2F3%2F030003.

[90] I. Angeli and K.P. Marinova. "Table of experimental nuclear ground state charge radii: An update". In: *Atomic Data and Nuclear Data Tables* 99.1 (2013), pp. 69–95. ISSN: 0092-640X. DOI: https://doi.org/10.1016/j.adt.2011.12.006. URL: http://www.sciencedirect.com/science/article/pii/S0092640X12000265.

[91] Domenico Logoteta et al. "Comparative study of three-nucleon force models in nuclear matter". In: *Phys. Rev. C* 91 (6 June 2015), p. 064001. DOI: 10.1103/PhysRevC.91.064001. URL: https://link.aps.org/doi/10.1103/PhysRevC.91.064001.

[92] A. Rios, A. Polls, and W. H. Dickhoff. "Density and isospin-asymmetry dependence of high-momentum components". In: *PHYSICAL REVIEW C* 89.4 (APR 4 2014). ISSN: 0556-2813. DOI: {10.1103/PhysRevC.89.044303}.

[93] S. Gandolfi, J. Carlson, and Steven C. Pieper. "Cold Neutrons Trapped in External Fields". In: *Phys. Rev. Lett.* 106 (1 Jan. 2011), p. 012501. DOI: 10.1103/PhysRevLett.106.012501. URL: https://link.aps.org/doi/10.1103/PhysRevLett.106.012501.

[94] Mateusz Buraczynski, Nawar Ismail, and Alexandros Gezerlis. *Neutron matter at the interface(s): from interactions to ab initio and from there to phenomenology.* 2019. arXiv: 1906.01674 [nucl-th].

[95] Udo von Toussaint. "Bayesian inference in physics". In: *Rev. Mod. Phys.* 83 (3 Sept. 2011), pp. 943–999. DOI: 10.1103/RevModPhys.83.943. URL: https://link.aps.org/doi/10.1103/RevModPhys.83.943.

Ringraziamenti

Vorrei ringraziare prima di tutto il mio relatore, Prof. Gianluca Colò, e i miei correlatori, Prof. Xavier Roca-Maza e Prof. Francesco Pederiva, senza i quali questo lavoro non sarebbe stato possibile: grazie per il supporto costante lungo tutto il progetto, il tempo dedicatomi e le molte opportunità che ho ricevuto. Tra queste ultime, ricordo in particolare la possibilità di partecipare alla conferenza di Bormio e le due visite a Trento.
Un doveroso ringraziamento va anche ad Alessandro Lovato, Enrico Vigezzi e Carlo Barbieri, per l'aiuto, soprattutto sui calcoli ab initio, e numerosi suggerimenti e discussioni.
Grazie ai miei compagni di ufficio, Giancarlo, Giuseppe e Simone, e ai miei amici di Fisica e non, con i quali ho condiviso una parte significativa di questi anni. Infine, grazie ai miei genitori.